Calhoun: The NPS Institutional Archive

DSpace Repository

Theses and Dissertations | 1. Thesis and Dissertation Collection, all items

1990-12

Mixed layer dynamics in the onset of freezing

Claes, Dennis C.

Monterey, California: Naval Postgraduate School

http://hdl.handle.net/10945/27565

This publication is a work of the U.S. Government as defined in Title 17, United States Code, Section 101. Copyright protection is not available for this work in the United States.

Downloaded from NPS Archive: Calhoun

http://www.nps.edu/library

Calhoun is the Naval Postgraduate School's public access digital repository for research materials and institutional publications created by the NPS community. Calhoun is named for Professor of Mathematics Guy K. Calhoun, NPS's first appointed -- and published -- scholarly author.

Dudley Knox Library / Naval Postgraduate School
411 Dyer Road / 1 University Circle
Monterey, California USA 93943

AD-A241 787

(2)

NAVAL POSTGRADUATE SCHOOL
Monterey, California

DTIC

THESIS

MIXED LAYER DYNAMICS IN
THE ONSET OF FREEZING

by

Dennis C. Claes

December 1990

Thesis Advisor Roland W. Garwood

Approved for public release; distribution is unlimited.

91-13910

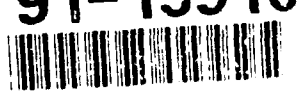

91 10 23 025

Unclassified

security classification of this page

REPORT DOCUMENTATION PAGE

1a Report Security Classification: Unclassified			1b Restrictive Markings
2a Security Classification Authority			3 Distribution Availability of Report: Approved for public release; distribution is unlimited.
2b Declassification Downgrading Schedule			
4 Performing Organization Report Number(s)			5 Monitoring Organization Report Number(s)
6a Name of Performing Organization: Naval Postgraduate School	6b Office Symbol (*if applicable*): 35		7a Name of Monitoring Organization: Naval Postgraduate School
6c Address (*city, state, and ZIP code*): Monterey, CA 93943-5000			7b Address (*city, state, and ZIP code*): Monterey, CA 93943-5000
8a Name of Funding Sponsoring Organization	8b Office Symbol (*if applicable*)		9 Procurement Instrument Identification Number
8c Address (*city, state, and ZIP code*)			10 Source of Funding Numbers: Program Element No / Project No / Task No / Work Unit Accession No

11 Title (*Include security classification*): MIXED LAYER DYNAMICS IN THE ONSET OF FREEZING

12 Personal Author(s): Dennis C. Claes

13a Type of Report	13b Time Covered	14 Date of Report (*year, month, day*)	15 Page Count
Master's Thesis	From To	December 1990	110

16 Supplementary Notation: The views expressed in this thesis are those of the author and do not reflect the official policy or position of the Department of Defense or the U.S. Government.

17 Cosati Codes			18 Subject Terms (*continue on reverse if necessary and identify by block number*)
Field	Group	Subgroup	Oceanography,Sea Ice,Mixed Layer Modeling,Freezing

19 Abstract (*continue on reverse if necessary and identify by block number*)

A two layer ocean mixed layer model is used to study the relationship between the onset of freezing and mixed layer depth, wind forcing, surface buoyancy flux, and temperature and salinity changes between the two layers. Universal non-dimensional parameters for stability and surface forcing are derived and related to the maximum freezing rate. Analytic solutions to the model are found in terms of the universal parameters and the model turbulent mixing tuning constants.

Sensitivity studies show the dependence of the freezing rate on the stability as defined by the salinity and temperature jumps, the forcing by the wind stress and the surface heat flux, and the mixed layer depth. Results show that an increase in heat flux produces a nearly linear increase in the freezing rate. Mixing energy from the wind, proportional to the wind speed cubed, results in a nearly linear decrease in freezing rate. There is a non-linear relationship between the temperature jump between layers and the freezing rate. A warming of the deeper layer decreases the freezing rate and ultimately prevents freezing. A non-linear relation was also found between the salinity jump and the freezing rate. An increase in the deeper layer salinity causes an increase in the freezing rate and leads to the maximum expected freezing rate. A nearly hyperbolic relationship between the mixed layer depth and the freezing rate was found. As the mixed layer depth increases from near zero, there is a rapid increase in the freezing rate, and then the maximum expected freezing rate is approached asymptotically.

A relationship between the forcing parameter and the stability parameter was derived which defined areas where freezing could occur. For low values of the stability parameter there is the possibility of freezing for any value of the forcing parameter. For larger values of stability there can only be freezing for small values of the forcing parameter. There is a critical value of the stability parameter above which freezing is not possible regardless of surface forcing.

20 Distribution Availability of Abstract	21 Abstract Security Classification	
☒ unclassified unlimited ☐ same as report ☐ DTIC users	Unclassified	
22a Name of Responsible Individual: Roland W. Garwood	22b Telephone (*include Area code*): (408) 646-3260	22c Office Symbol: OC,Gd

DD FORM 1473,84 MAR 83 APR edition may be used until exhausted
All other editions are obsolete

security classification of this page

Unclassified

Approved for public release; distribution is unlimited.

Mixed Layer Dynamics In
The Onset of Freezing

by

Dennis C. Claes
Lieutenant Commander, United States Navy
B.S., University of Utah, 1978

Submitted in partial fulfillment of the
requirements for the degree of

MASTER OF SCIENCE IN METEOROLOGY AND OCEANOGRAPHY

from the

NAVAL POSTGRADUATE SCHOOL
December 1990

Author:

Dennis C. Claes

Approved by: 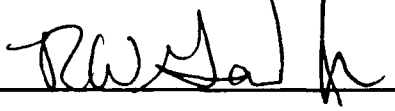

Roland W. Garwood, Thesis Advisor

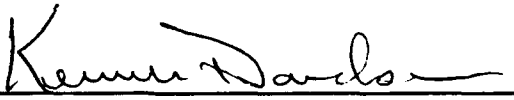

Kenneth L. Davidson, Second Reader

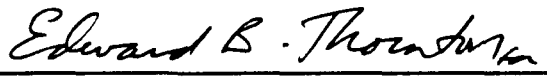

Curtis A. Collins, Chairman,
Department of Oceanography

ABSTRACT

A two layer ocean mixed layer model is used to study the relationship between the onset of freezing and mixed layer depth, wind forcing, surface buoyancy flux, and temperature and salinity changes between the two layers. Universal non-dimensional parameters for stability and surface forcing are derived and related to the maximum freezing rate. Analytic solutions to the model are found in terms of the universal parameters and the model turbulent mixing tuning constants.

Sensitivity studies show the dependence of the freezing rate on the stability as defined by the salinity and temperature jumps, the forcing by the wind stress and the surface heat flux, and the mixed layer depth. Results show that an increase in heat flux produces a nearly linear increase in the freezing rate. Mixing energy from the wind, proportional to the wind speed cubed, results in a nearly linear decrease in freezing rate. There is a non-linear relationship between the temperature jump between layers and the freezing rate. A warming of the deeper layer decreases the freezing rate and ultimately prevents freezing. A non-linear relation was also found between the salinity jump and the freezing rate. An increase in the deeper layer salinity causes an increase in the freezing rate and leads to the maximum expected freezing rate. A nearly hyperbolic relationship between the mixed layer depth and the freezing rate was found. As the mixed layer depth increases from near zero, there is a rapid increase in the freezing rate, and then the maximum expected freezing rate is approached asymptotically.

A relationship between the forcing parameter and the stability parameter was derived which defined areas where freezing could occur. For low values of the stability parameter there is the possibility of freezing for any value of the forcing parameter. For larger values of stability there can only be freezing for small values of the forcing parameter. There is a critical value of the stability parameter above which freezing is not possible regardless of surface forcing.

Accession For
NTIS GRA&I
DTIC TAB
Unannounced
Justification
By
Distribution/
Availability Codes
Dist Special
A-1

TABLE OF CONTENTS

I. INTRODUCTION 1

II. THEORY 4
A. MIXED LAYER DYNAMICS 4
1. The Oceanic Mixed Layer 4
2. Freezing Processes 9
3. Heat Fluxes in the Mixed Layer 10
a. Shortwave radiation 10
b. Longwave Radiation 11
c. Latent Heat Flux 12
d. Sensible Heat Flux 12
e. Conductive Heat Flux 13
4. Salinity Fluxes in the Mixed Layer 16
5. Salinity and Temperature Effects on Buoyancy 16
6. Entrainment 18
B. THE TURBULENT KINETIC ENERGY BUDGET 18
1. Total Turbulent Kinetic Energy Equation 18
2. Total TKE Change 19
3. Stress Terms 19
4. Buoyancy Term 20
5. Turbulent Transport Terms 20
6. Dissipation Terms 21
7. TKE Summary 21

III. THE MIXED LAYER MODEL 22
A. THE ONE-DIMENSIONAL MODEL 22
1. Model Assumptions 22
2. Vertically Integrated TKE Equation 23
a. Stress Terms 23
b. The Buoyancy Flux 24
c. Transport Terms 26

d. Dissipation Terms 26
e. Reduced TKE Equation 26
3. Buoyancy Fluxes 27
a. Surface Heat Flux 28
b. Surface Salinity Flux 28
c. Surface Buoyancy Flux 28
d. Heat Flux at the Lower Boundary 29
e. Salinity flux at the Lower Boundary 29
f. Buoyancy Flux at the Lower Boundary 30
4. Entrainment Velocity 30
B. THE THERMODYNAMIC MODEL 31
1. The Surface Heat Flux 31
2. The Freezing Temperature 34
3. The Freezing Rate 34
C. THE NUMERICAL MODEL 35
1. The Time Dependent Equations 35
2. Model Formulas 36

IV. MODEL RESULTS 42
A. MODEL INITIAL CONDITIONS AND BOUNDARY CONDITIONS . . 42
1. Model Sensitivity To Wind 45
2. Model Sensitivity To Salinity Jump 49
3. Model Sensitivity To Temperature Jump 49
4. Model Sensitivity To Mixed Layer Depth 52
5. Model Sensitivity To Surface Heat Flux 52
B. NON-DIMENSIONAL PARAMETERIZATION 53
1. Formation of Non-Dimensional Parameters 53
2. Freezing Efficiency Parameter 53
3. Forcing Ratio Parameter 54
4. Stability Ratio Parameter 55
C. MODEL SENSITIVITY TO NON-DIMENSIONAL PARAMETERS . . . 59
1. Model Sensitivity to S* Variable Changes 59
2. Model Sensitivity to F* Variable Changes 66
D. THE LIMIT OF FREEZING 68

E. FREEZING EFFICIENCY RELATIONSHIP TO FORCING AND STABILITY 70

V. SUMMARY 75
A. CONCLUSIONS 75
B. RECOMMENDATIONS 76

APPENDIX A. THE LIMIT OF FREEZING 77
A. THE MODEL EQUATIONS 77
B. THE FREEZING LIMIT SOLUTION 79

APPENDIX B. AN EXPRESSION FOR THE FREEZING RATE 81
A. THE CONDITIONS 81
B. ESSENTIAL EQUATIONS 81
C. THE DERIVATION 81
D. POINTS OF INTEREST 83

APPENDIX C. AN EXPRESSION FOR U* 85
A. BEGINNING EQUATIONS 85
B. THE DERIVATION 85
C. POINTS OF INTEREST 87

APPENDIX D. FREEZING EFFICIENCY 89
A. THE EQUATIONS 89
B. DERIVATION 89

REFERENCES 93

INITIAL DISTRIBUTION LIST 100

LIST OF TABLES

Table 1. MODEL VARIABLES 38
Table 2. MODEL VARIABLES CONTINUED 39
Table 3. MODEL VARIABLES CONTINUED 40
Table 4. MODEL CONSTANTS 41
Table 5. NORMAL VALUES AND SENSITIVITY RUN VALUES 42
Table 6. NON-DIMENSIONAL PARAMETERS 56
Table 7. VALUES FOR S* SENSITIVITY MODEL RUNS 59
Table 8. VALUES FOR F* SENSITIVITY MODEL RUNS 66

LIST OF FIGURES

Figure 1. Sample Midlatitude Temperature, Salinity, Depth Profiles 4
Figure 2. Typical Arctic Temperature And Salinity Depth Profile 5
Figure 3. Vertical Distribution of Temperature and Salinity at Six Locations 6
Figure 4. MIZEX 87 Temperature, Salinity, Density Profile 7
Figure 5. Values of α g and β g at Various Temperatures and Salinities 14
Figure 6. Values of α g And β g Near Freezing Temperatures 15
Figure 7. Heavyside Step Function And Modified Heavyside Step Function 33
Figure 8. Freezing Rate as a Function of Wind Speed, U, Only 43
Figure 9. Freezing as a Function of u * 44
Figure 10. Freezing Rate as a Function of the Salinity Jump 46
Figure 11. Freezing Rate as a Function of Salinity Jump 47
Figure 12. Freezing Rate as a Function of Temperature Jump 48
Figure 13. Freezing Rate as a Function of Mixed Layer Depth 50
Figure 14. Freezing Rate as a Function of Surface Heat Flux 51
Figure 15. Model Sensitivity to S* Variable Changes vs T 57
Figure 16. Model Sensitivity to S* Variable Changes vs S 58
Figure 17. Model Sensitivity to F* Variable Changes vs Q 60
Figure 18. Model Sensitivity to F* Variable Changes vs h 61
Figure 19. Model Sensitivity to F* Variable Changes vs h 62
Figure 20. Model Sensitivity to F* Variable Changes vs u* 63
Figure 21. Model Sensitivity to F* Variable Changes vs u* 64
Figure 22. Model Sensitivity to F* Variable Changes vs Q 65
Figure 23. The Limit of Freezing 67
Figure 24. Freezing Efficiency as a function of Forcing and Stability 69
Figure 25. Freezing Efficiency for C1 = 1. and C2 = .4 71
Figure 26. Freezing Efficiency for C1 = .5 and C2 = .8 72
Figure 27. Freezing Efficiency for C1 = .2 and C2 = 2. 73

I. INTRODUCTION

The production of sea ice is significant on most scales of interactions between the Arctic oceanic and atmospheric boundary layers. The Arctic ice pack and marginal ice zone (MIZ) have been studied to determine on various scales the interactions of the ice on the local environment and the importance to the global climate. These studies range from ocean wave-ice interactions (Martin and Kauffman, 1981, Christensen, 1983, Squire, 1984, Wadhams et al., 1988), internal wave activity (Muench et al., 1983, Morison, 1985, Levine and Paulson, 1987, Sandven and Johannessen, 1987, Foster and Eckert, 1987, McPhee and Kantha, 1989, Eckert and Foster, 1990), inertial oscillations (McPhee, 1978, Lagerloef and Muench, 1987), ice edge banding (Martin et al., 1983, Wadhams, 1983, Smedstad and Roed, 1985, Chu, 1987), leads (Andreas, 1981, Kozo, 1983, Chu, 1986, Gow et al., 1990), polynyas (Topham et al., 1983, Smith et al., 1983, Hartog et al., 1983, Chu, 1986), ice floe collisions (Shen et al., 1987, Martin and Becker, 1987, 1988, Lu et al., 1989), sea ice motion (Thorndike and Colony, 1982, Colony and Thorndike, 1984, 1985, Thorndike, 1987, Thompson et al., 1988, Serreze et al., 1989), and basin wide climate studies (Washington et al., 1980, Hibler and Walsh, 1982, Niebauer, 1983, Semtner, 1987, Nakamura and Oort, 1988, Ingram et al., 1989, Hakkinen and Mellor, 1990, Aagaard and Carmack, 1990).

On smaller scales, it has been found that for newly formed sea ice, frazil and grease ice, the drag coefficient can be decreased to one half of that of the open ocean (Macklin, 1983, Guest and Davidson, 1991). On the other hand, a build up in thickness and increase in surface roughness from lateral stresses can increase the drag coefficient from 2 to 3 times that of the open ocean (Macklin, 1983, Pease et al., 1983, Walter et al., 1984, Overland, 1985, Guest and Davidson, 1987, Guest and Davidson, 1991). The effect on wind-stress imparted momentum to the ocean and ice can dominate the flow of the sea ice and the underlying surface water.

In higher latitudes the ocean moderates the atmospheric temperature, with air temperature being close to sea surface temperature. While the ocean is ice free there can be a large heat flux into the atmosphere. As sea ice forms and decreases the amount of open water exposed to the atmosphere, the heat flux to the atmosphere will decrease significantly. There is a similar affect on the moisture flux from the sea surface to the atmosphere as the areal coverage of sea ice extent increases. This results in seasonal

changes in clouds and fog over the ice, with a maximum in cloud cover in summer and a minimum in winter (Sater et al., 1971).

The formation of sea ice also influences the radiation budget of the atmosphere. The differences in albedo between open water, thin ice, thick ice, and snow covered ice, will change significantly the penetration of incoming solar radiation into the ocean as well as reradiation back to the atmosphere (Grenfell and Perovich, 1984, Maykut, 1986, Ross and Walsh, 1987, Ingram et al., 1989). Longwave energy, coupled with the moisture of the atmospheric boundary layer, is greatly influenced when open water becomes covered with sea ice and snow.

In the past decade there has been increased investigation into the formation, extent, and compaction of sea ice. Ice physics studies have shed new light on the mechanisms of ice formation (Hanley, 1978, Omstedt and Svensson, 1984), growth (Bauer and Martin, 1983, Wakatsuchi and Ono, 1983), and compaction (Lepparanta and Hibler, 1985) on many scales. Modelers have progressed from one dimensional models to three dimensional dynamic and thermodynamic models of varying scales of the ice pack and the MIZ (Pollard et al., 1983, Mcphee, 1983, Roed, 1984, Ikeda, 1986, Mellor et al., 1986, McPhee, 1987, McPhee et al., 1987, Semtner, 1987, Houssais, 1988, Kantha and Mellor, 1989, Mellor and Kantha, 1989, Ikeda, 1989, Lu et al., 1990). These model studies have improved the understanding of the formation of deep water from freezing (Carmack and Aagaard, 1973, Swift and Aagaard, 1981, Hakkinen, 1987, Swift and Koltermann, 1988), salt chimneys (Killworth, 1979), eddy formation and interaction (Manley and Hunkins, 1985, Hakkinen, 1986, Johannessen et al, 1987, Smith and Bird, 1988, Padman et al., 1990), and other small to large scale features found in the arctic. Unfortunately, few studies have been done on the effects of the dynamical properties of the mixed layer and their various interactions which contribute to ice formation, or prevent ice formation. Chu and Garwood (1988) have indicated that there may be some coupled ice-ocean domains where the effect of entrainment and surface buoyancy flux may not be fully understood.

This study will focus on various thermodynamic and dynamic properties of the mixed layer, wind stress and buoyancy effects to better understand the air-sea coupling leading to the formation of sea ice. The identification of regimes where freezing can occur will be of special interest.

Chapter II introduces the theory of mixed layer dynamics and thermodynamics involved in the freezing of salt water. Chapter III presents a simple one-dimensional model with associated thermodynamic equations. Chapter IV shows the interaction of

the various dynamic and thermodynamic processes, and solutions are developed for the problem of finding regimes of freezing.

II. THEORY

A. MIXED LAYER DYNAMICS

1. The Oceanic Mixed Layer

The oceanic mixed layer is a quasi-homogeneous layer in the ocean, from the ocean surface to a depth called the mixed layer depth, in which the various properties of the water, thermal energy, and salinity are well mixed by the turbulence.

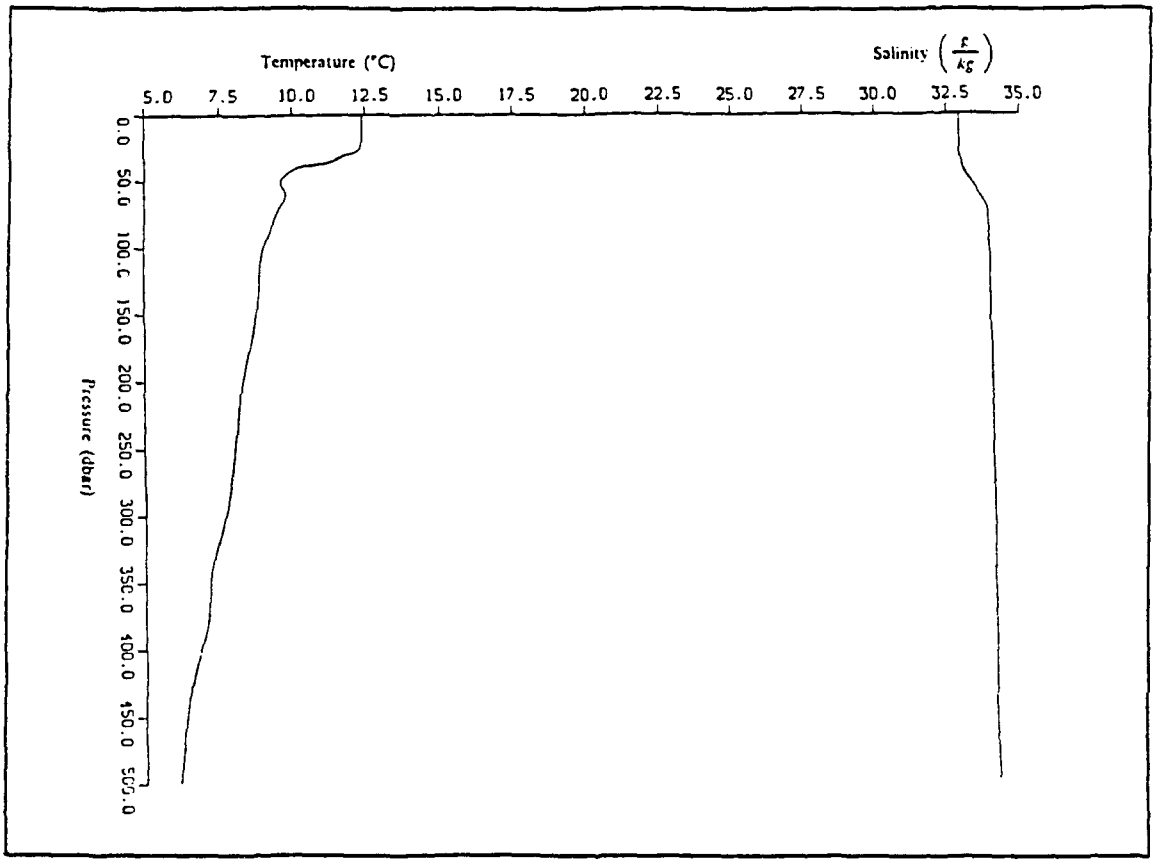

Figure 1. Sample Midlatitude Temperature, Salinity, Depth Profiles: The temperature profile shows a uniform Mixed Layer temperature and decreasing temperature with depth. The salinity profile shows a uniform mixed layer salinity and a gradual increase with depth. (Jessen et al., 1989)

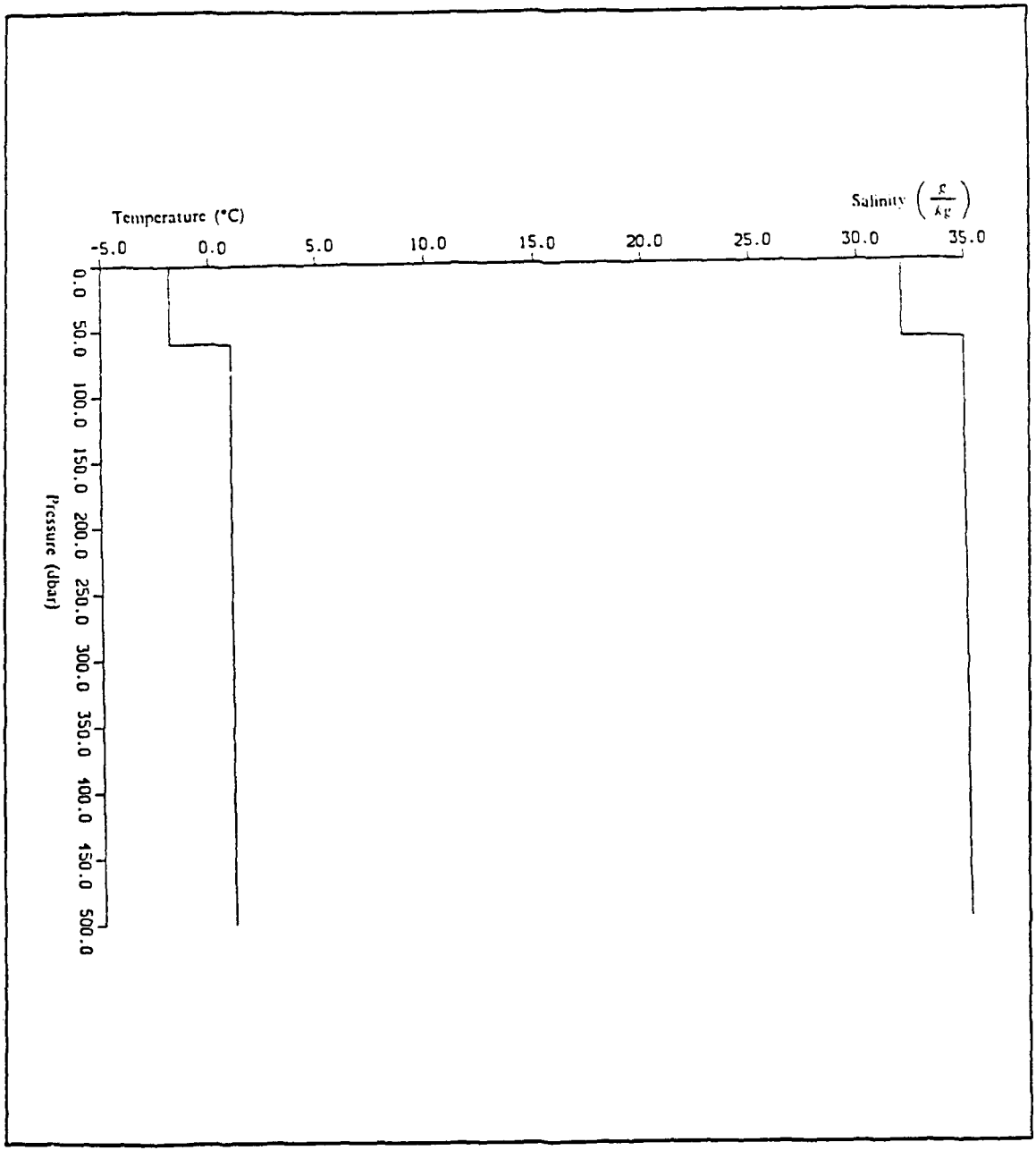

Figure 2. **Typical Arctic Temperature And Salinity Depth Profile:** The temperature profile shows a cold shallow mixed layer over a warmer deeper layer. The salinity profile shows a less saline mixed layer over a more saline deeper layer.

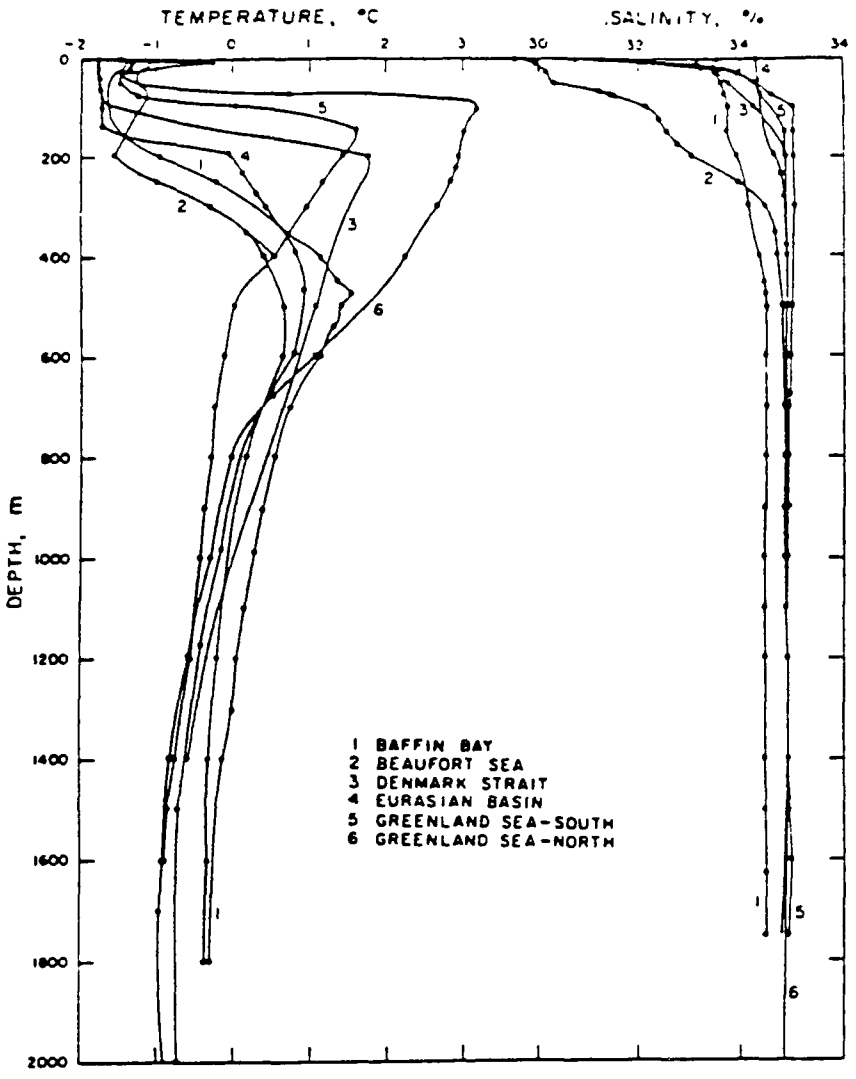

Figure 17. VERTICAL DISTRIBUTIONS OF TEMPERATURE AND SALINITY AT SIX LOCALITIES

Figure 3. Vertical Distribution of Temperature and Salinity at Six Locations: Salinity and Temperature profiles at six locations in the Arctic Ocean and adjacent seas. All temperature profiles show a cooler mixed layer overlying a warmer layer, and all salinity profiles show less saline mixed layer water overlying more saline water. (Courtesy Sater et al., 1971)

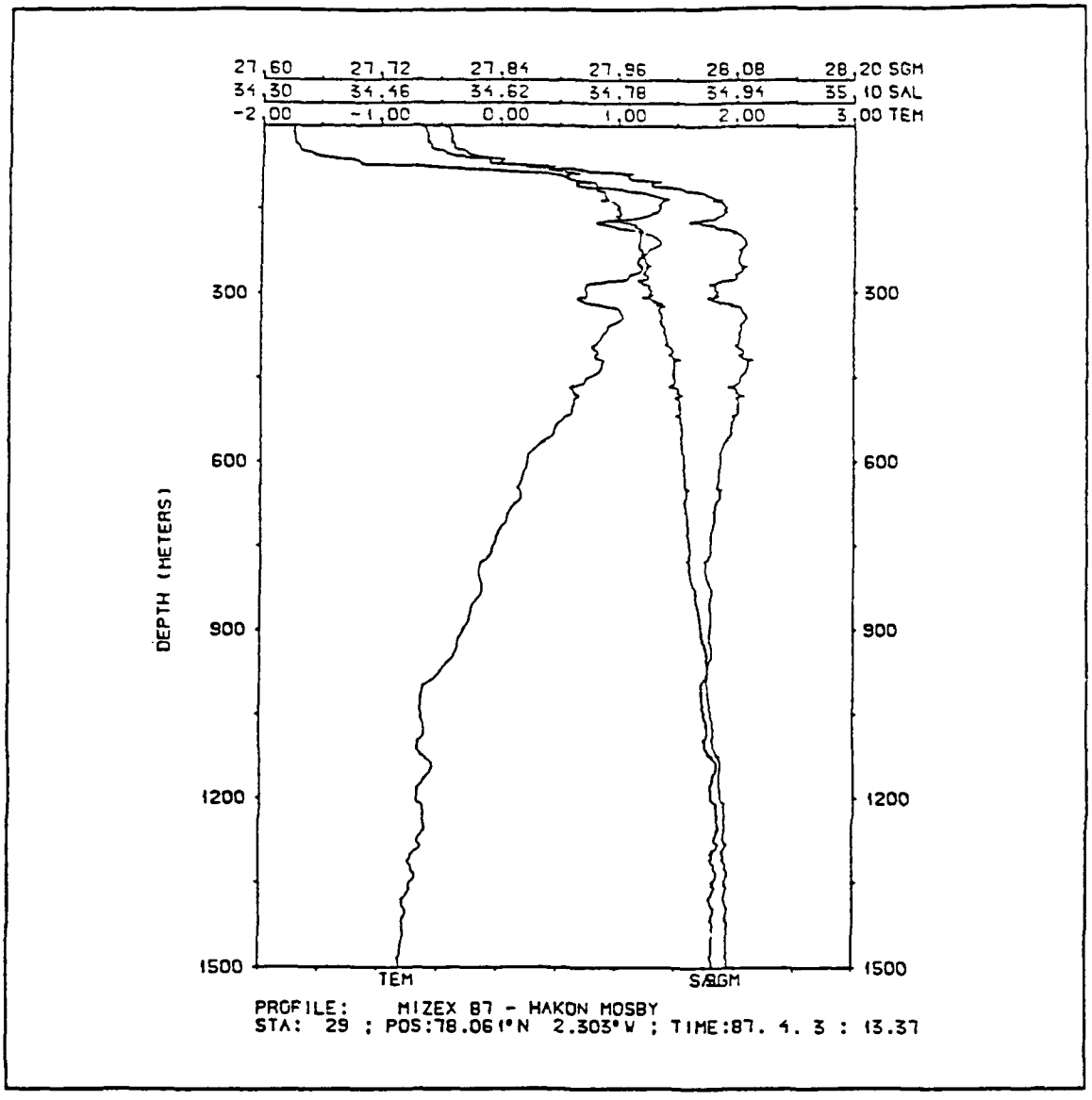

Figure 4. **MIZEX 87 Temperature, Salinity, Density Profile:** Temperature, Salinity and Density profiles from R/V HAKON MOSBY taken at 78.1 °N 2.5°W on 3 April 1987. The temperature profile shows a uniform mixed layer temperature of -1.8 °C to 80 meters and a rapid increase to 1.0° C at 120 meters and then decrease with depth. The Salinity profile shows a relatively uniform salinity of 34.5 in the mixed layer increasing to 34.95 at 150 meters and maintaining a relatively constant value below 150 meters. The Density profile shows a large density increase just below the mixed layer. (Sandven, et al., 1987)

Over much of the ocean the mixed layer temperature profile is similar to Figure 1, taken off the California coast (Jessen et al., 1989), where the mixed layer is warmer than the underlying water. In the mid-latitudes where the amount of evaporation is exceeded by precipitation, the mixed layer salinity is lower than that of the underlying water column, as is evident in Figure 1. Here the water density difference between the mixed layer and the lower layer is a function of both temperature and salinity. However, in the Arctic, the mixed layer is typically colder than the underlying water as shown in Figure 2. For the arctic, the salinity of the mixed layer is typically less than that of the underlying water as shown in Figure 2. (Figure 2 shows hypothetical conditions that are simplified for use in a one-dimensional mixed layer model.)

For temperatures close to the freezing point, changes in water density are mostly a function of salinity. This allows a cooler less saline mixed layer to be much more buoyant than a warmer more saline layer. Therefore salinity dominates the density gradient, allowing colder water to overlie warmer water (cooler water is normally denser than warmer water). Depending on the season and the proximity to fresh water from river run off, the mixed layer may be near freezing and up to 4 $^{\circ}C$ cooler than the underlying water. The salinity also may be up to 5 $\frac{g}{kg}$ less in the mixed layer than in the layer below. Figure 3 shows a variety of temperature and salinity profiles from six different locations in the Arctic Ocean and outlying seas. The general conditions of cooler less saline waters overlying warmer more saline waters appears in all six of the regions depicted in Figure 3.

The energy needed to mix the surface layer properties comes from two sources. The normally dominant source is the stress imparted by the wind to the water or ice surface. As the wind speed increases the energy imparted to the mixing process increases. The second source of energy is due to density, or buoyant instabilities in the water column. Buoyant instabilities are caused by three sources: heating from below, cooling from above, and downward salinity flux at the surface or at the ice-water interface. The salinity fluxes occur when there are net changes in the mixed layer due to freezing, melting, evaporation, or precipitation at the surface.

2. Freezing Processes

In the Arctic and Antarctic waters, a typical temperature, salinity, and density profile would show cooler, less saline and less dense water overlying warmer, more saline and more dense water. Figure 4 shows temperature, salinity and density profiles obtained from the R/V HAKON MOSBY during the MIZEX 87 experiment (Sandven et al., 1987), demonstrating these properties. These profiles will be used later as a guideline for model initial conditions in chapter 4. During the winter freezing period, very cold air, -10 ° C to -25 °C, usually overlies the ice and the open ocean near the ice edge. This causes a heat flux from the ocean surface to the air. In the case where ice is already present, the heat flux is from the ocean through the ice to the air. This upward heat flux cools the mixed layer to the freezing point [where the freezing point is mainly a function of salinity]. Also, heat may flux from the warmer underlying waters into the mixed layer, which may slow down the cooling of the mixed layer, or, depending on the amount of heat flux from below, it may even warm the mixed layer.

Bauer and Martin (1983) describe two conditions when freezing occurs in open leads or open ocean, for both windy or calm conditions. Under calm conditions a thin horizontal sheet of ice forms and grows downward. Under these conditions the major thermodynamic process is long-wave radiative cooling of the surface leading to cooling and freezing.

Under windy conditions small disc-shaped crystals, called frazil ice, are formed and driven down wind where they can become concentrated and freeze together in the form of grease ice. In leads, Bauer and Martin (1983) have shown that this process of ice formation will grow initially downward to a minimal depth and then grow horizontally to the upwind edge and eventually close off the lead. Under windy conditions the major thermodynamic processes for freezing are from the latent heat fluxes and sensible heat fluxes.

Lewis and Perkins (1983) describe conditions where freezing occurs under already existing ice. This happens when the ice surface near the ice-ocean interface is colder than the freezing point, and ice crystals form and grow downward. They describe a process where in some cases the mixed layer undergoes an upward heat flux until a condition called supercooling occurs. For this case the water at the interface is actually colder than freezing by about .01 °C, and only then will freezing begin. (Lewis and Perkins, 1983; Omstedt and Svenson, 1984).

3. Heat Fluxes in the Mixed Layer

The heat fluxed across the water surface or ice surface generates and sustains the freezing process, and so surface heat flux is the primary parameter considered in the formation of ice. The various mechanisms that produce this heat flux have different effects on the mixed layer. The largest component of the heat flux process at an ice-ocean interface is the sensible heat flux. The primary heat lux processes at the air-ocean or air-ice interfaces include:

- Shortwave Radiation
- Longwave Radiation
- Latent Heat Flux
- Sensible Heat Flux
- Conductive Heat Flux

The latent and sensible heat fluxes are dependent on air-sea differences and on wind stresses at the air-ocean or air-ice interfaces. The radiative heat fluxes depend more on cloud cover, i.e. clear skies, fog, low clouds, high clouds, etc.

a. Shortwave radiation

Shortwave radiation, or solar radiation, is a downward radiation into the ice or the ocean mixed layer. Maykut (1986) has parameterized the net shortwave energy flux, F_r, as

$$F_r = F_o(1 - kc^3)(1 - \alpha) \tag{2.1}$$

where

- F_o = incoming solar radiation (function of sun angle)
- k = seasonal cloudiness parameter ranging from .15 in March to .5 in August
- c = cloudiness in tenths
- α = albedo of the surface (function of wavelengths)

Because both the ice and ocean are translucent, the shortwave energy can penetrate the surface. Maykut (1986) has shown a relation for the heat flux F_z at depth z, of:

$$F_z = i_o F_r e^{-\bar{\kappa}(z-.1)} \tag{2.2}$$

where

- z = depth (positive downward)
- i_o = percentage absorbed in a thin surface layer (function of surface type (i.e. ice or water. For ice and z > .1 m, i_o is about .3), and frequency (more is absorbed in the red and infrared than blue and ultraviolet))
- F_r = net shortwave heat flux at the surface
- $\bar{\kappa}$ = bulk extinction coefficient of the medium

Clouds, sun angle and surface type will determine how much energy is incident at the water or ice surface, and turbidity and ice type determine how much energy passes through to the mixed layer and below.

b. Longwave Radiation

Longwave radiation is the net radiation between that given off by the water or ice surface to the atmosphere, and that absorbed by the ice or water surface when radiated by the atmosphere. Maykut and Church (1973) parameterized the downward longwave radiation, F_{l_d} , by:

$$F_{l_d} = .7855(1 + .2232c^{2.75})\sigma T_a^4 \tag{2.3}$$

where

- c = cloudiness in tenths
- σ = Stefan-Boltzman constant
- T_a = air temperature ($°k$)

and upward longwave radiation, F_{l_u}, by:

$$F_{l_u} = \varepsilon_s T_s^4 \tag{2.4}$$

where:

- ε_s = emissivity of the surface (.97 for ice, water, melt ponds, leads, and .99 for snow)
- T_s = water/ice surface temperature ($°k$)

The net longwave radiation, F_l, can be derived from equations (2.3) and (2.4) as:

$$F_l = .7855(1 + .2232c^{2.75})\sigma T_a^4 - .97\sigma T_s^4 \tag{2.5}$$

With this formula, Maykut and Church found no relation between the water vapor and the longwave radiation, possibly due to the low values of vapor pressure found in the Arctic. This shows the role the clouds play, and also the major role of the air temperature on longwave radiation.

c. Latent Heat Flux

Latent heat flux is caused by the evaporation of water at the water surface or ice surface. Maykut (1986) has parameterized the latent heat flux, F_e, as

$$F_e = \rho L C_e u(q_a - q_o) \tag{2.6}$$

where

- ρ = air density
- L = latent heat of vaporization, or sublimation
- C_e = bulk transfer coefficient for latent heat (a function of surface roughness)
- u = wind speed
- q_a = specific humidity of the air at a reference level (usually 10 meters)
- q_o = specific humidity of the air at the surface

This shows the major factors affecting the latent heat flux, the humidity difference between the air and the water surface, and the wind speed. Thus, latent heat flux will have its greatest effect during dry windy events, and its least effect during moist windy events or calm events.

d. Sensible Heat Flux

Sensible heat flux is the result of turbulent heat conduction between the atmosphere and the water or ice surface. Maykut (1986) has expressed the sensible heat flux, F_s, as

$$F_s = \rho c_p C_s u(T_a - T_o) \tag{2.7}$$

where

- ρ = density of the air
- c_p = specific heat of the air
- C_s = bulk transfer coefficient for sensible heat (a function of surface roughness)
- u = wind speed
- T_a = air temperature at a reference level (usually 10 meters)
- T_o = temperature at the surface

This shows the major factors affecting the sensible heat, the temperature difference between the air and the ice/water surface, and the wind speed.

e. Conductive Heat Flux

For freezing to continue after initial ice formation there must be a heat flux through the ice. This is a conductive heat flux, F_c , and has been parameterized by Maykut (1986) as

$$F_c = k_i(\frac{\partial T}{\partial z})_o \tag{2.8}$$

where

- $(\frac{\partial T}{\partial z})_o$ = the temperature gradient at the surface
- k_i = thermal conductivity of the ice (a function of temperature and salinity of the ice)

For sea ice, k_i may be expressed as

$$k_I = (k_o + \frac{\beta S_i}{T_i}) \tag{2.9}$$

where

- k_o = thermal conductivity in pure ice (a function of temperature)
- β = .13 W/m
- S_i = salinity of the ice in ppt
- T_i = temperature of the ice in $^\circ C$

The effect of snow on the ice is to insulate the ice from the air due to the low conductivity of snow, which is about one order of magnitude lower than in pure ice (Maykut, 1986).

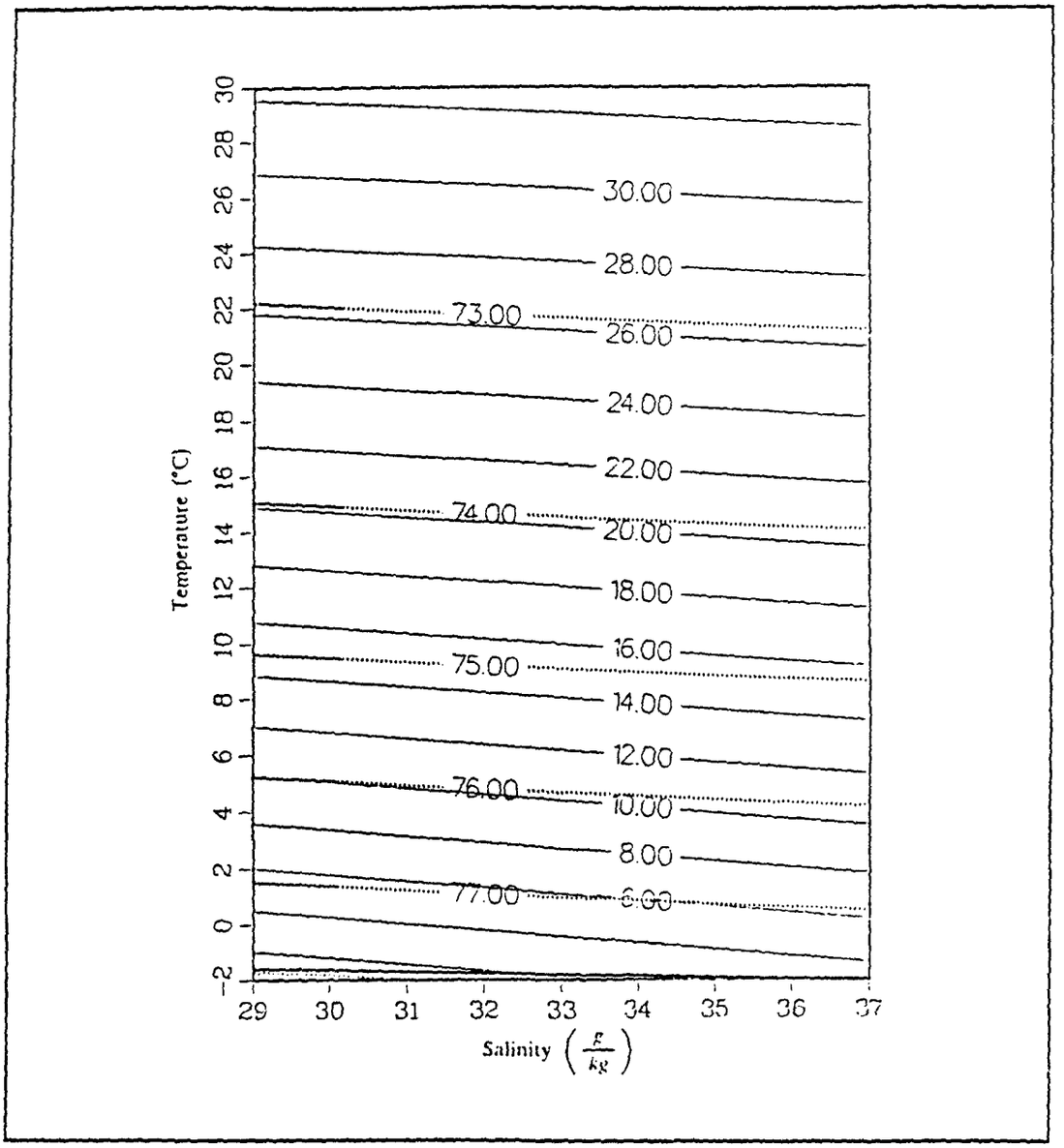

Figure 5. Values of α g and β g at Various Temperatures and Salinities: The relationship between the coefficient of thermal expansion, $\alpha g \times 10^4$, at different temperatures and salinities (solid lines), and the coefficient of haline contraction, $\beta g \times 10^4$, at different temperatures and salinities (dashed lines).

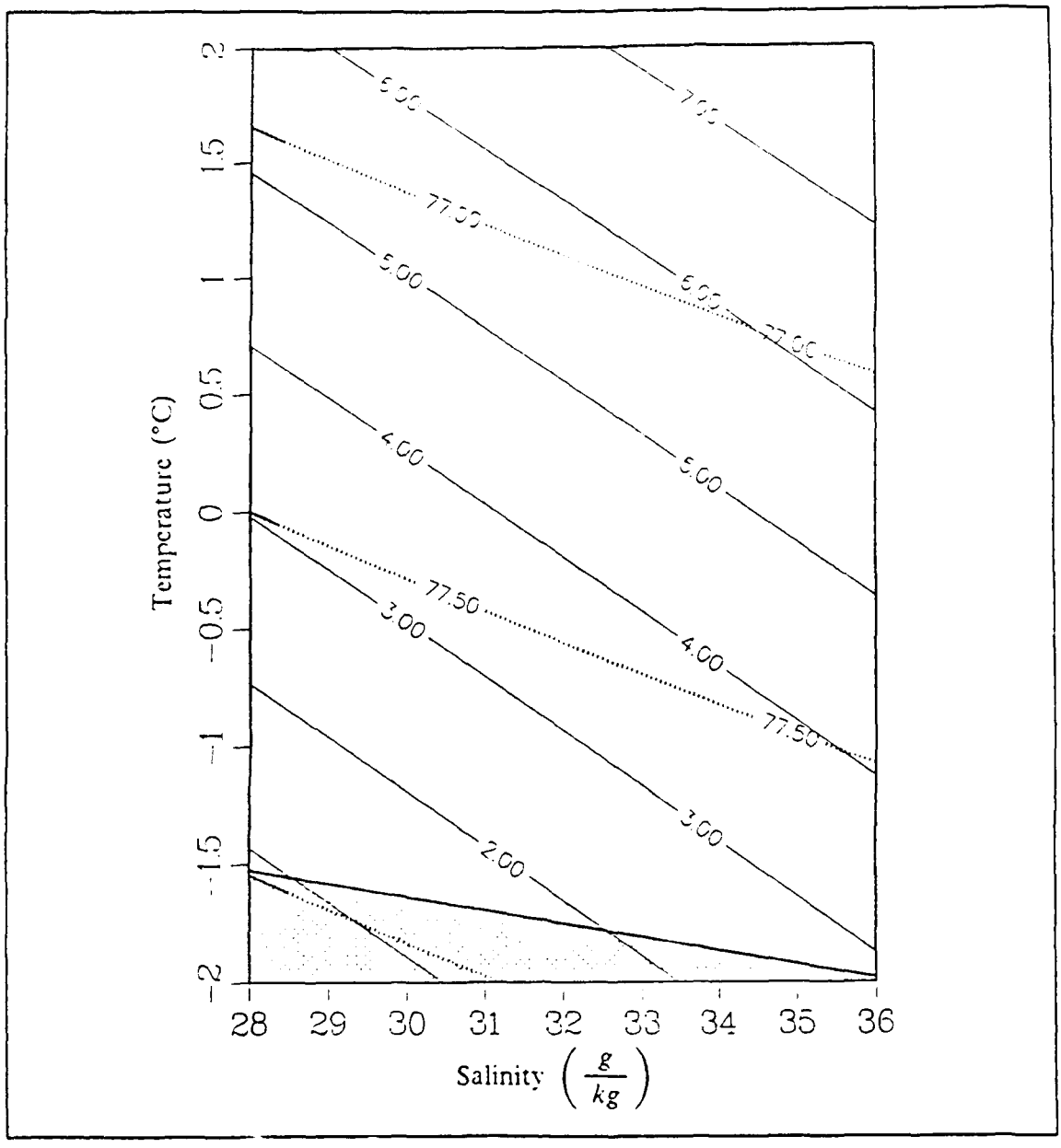

Figure 6. Values of α g And β g Near Freezing Temperatures: The relationship between the coefficient of thermal expansion, αg x 10^4 (solid lines), at different temperatures and salinities, and the coefficient of haline contraction, βg x 10^4 (dashed lines), at different temperatures and salinities, near freezing temperatures. At these temperatures, αg tends to 0, while βg is slightly larger than it is for warmer temperatures.

4. Salinity Fluxes in the Mixed Layer

Salinity fluxes in the mixed layer are dependent on processes at the two interfaces. A virtual salt flux into the mixed layer will occur when there is evaporation or freezing caused by decreasing the water volume while keeping the salt mass relatively constant. A second process occurs when more saline water from below is mixed into the mixed layer by entrainment.

A virtual salt flux out of the mixed layer occurs when there is precipitation or melting of ice, resulting in an increase in water volume while keeping the salt mass relatively constant. Another mechanism occurs when there is entrainment of less saline water from below resulting in a net decrease in salinity. Under the usual conditions in the arctic, the water under the mixed layer is more saline so this condition is not as common.

The salinity of the water affects the freezing temperature of the water. The greater the salinity the lower the freezing temperature of the saline water. Hakkinen's (1987) formula for the freezing temperature of salt water as a function of salinity was:

$$T_f = -.003 - .0527S - 4. \times 10^{-5} S^2 \tag{2.10}$$

where

- T_f is the freezing temperature (° C)
- S is the salinity (parts per thousand)

This shows a nearly linear relationship between the freezing temperature and the salinity due to the S^2 term being small.

5. Salinity and Temperature Effects on Buoyancy

A linearized parameterization for density at the water surface can be used to demonstrate the relative affects of salinity and temperature fluxes on density:

$$\rho = \rho_o(1 - \frac{\partial}{\partial T}(T - T_o) + \frac{\partial}{\partial S}(S - S_o)) \tag{2.11}$$

where:

- ρ = water density $(\frac{kg}{m^3})$

- $\frac{\partial}{\partial T} \equiv \alpha$ = coefficient of thermal expansion of water $(\frac{1}{^\circ C})$
- $\frac{\partial}{\partial S} \equiv \beta$ = coefficient of salinity contraction of water $(\frac{1}{\text{ppt}})$
- T = water temperature $(^\circ C)$
- T_o = reference temperature $(^\circ C)$
- S = water salinity (ppt)
- S_o = reference salinity (ppt)

The parameters α and β are function of temperature, salinity, and pressure, but for small changes in T and S, α and β can be considered constant.

Equation (2.11) can be used to form a difference equation for small changes to ρ, giving:

$$\Delta\rho \approx -\alpha\rho_o\Delta T + \beta\rho_o\Delta S \tag{2.12}$$

A difference buoyancy equation results by multiplying equation (2.12) by $\frac{g}{\rho_o}$:

$$\Delta b = \frac{\Delta\rho}{\rho_o} g = -\alpha g\Delta T + \beta g\Delta S \tag{2.13}$$

where:

- Δb = difference in buoyancy $(\frac{m}{s^2})$
- $\Delta\rho$ = difference in density $(\frac{kg}{m^3})$
- g = acceleration of gravity $(\frac{m}{s^2})$
- ρ_o = reference density (ppt)
- α = coefficient of thermal expansion (constant for small changes) $(\frac{1}{^\circ C})$
- ΔT = difference in temperature $(^\circ C)$
- β = coefficient of salinity contraction $(\frac{1}{\text{ppt}})$
- ΔS = difference in salinity (ppt)

Figure 5 shows the relative values of αg and βg for various temperatures and salinities. In the extratropical oceans the values of αg and βg are on the order of 25 x 10^4 and 73 x 10^4 respectively. When a slight warming of the surface occurs, Δb is negative, producing a stabilizing decrease in surface density. In the polar regions, the temperatures are near the freezing point of sea water. Figure 6 shows an expansion of

Figure 5 near $0°C$. In this region the values of αg and βg are on the order of 2×10^{4} and 78×10^{4} respectively. A slight temperature change causes a negligible change in density, but a slight salinity increase, from salt rejection during the freezing of salt water, can substantially increase the density, producing a destabilizing increase in density, or decrease in buoyancy at the surface.

6. Entrainment

The mixed layer depth will increase if water mass comes from either the surface, ie. rain, snow, or melting ice, or from below. When the mass comes from below by mixing, it is called entrainment. Garwood (1977) and others have defined the entrainment velocity to be

$$W_e = \frac{\partial h}{\partial t} \tag{2.14}$$

where

- W_e = the entrainment velocity
- h = the mixed layer depth
- t = time

B. THE TURBULENT KINETIC ENERGY BUDGET

1. Total Turbulent Kinetic Energy Equation

Garwood (1987) uses the total turbulent kinetic energy (TKE) equation to quantify the rates associated with the production, transport, storage, and dissipation of turbulent kinetic energy. This equation is derived from the Navier-Stokes equation for fluids following Garwood's method. The total TKE equation is

$$\frac{\partial}{\partial t}\left(\frac{\overline{u'^2}}{2}+\frac{\overline{v'^2}}{2}+\frac{\overline{w'^2}}{2}\right)=\left[-\overline{u'w'}\frac{\partial\bar{u}}{\partial z}-\overline{v'w'}\frac{\partial\bar{v}}{\partial z}\right]-\frac{\overline{w'\rho'}}{\rho_o}g$$

$$-\frac{\partial}{\partial z}\left[\overline{w'\left(\frac{u'^2}{2}+\frac{v'^2}{2}+\frac{w'^2}{2}+\frac{p'}{\rho_o}\right)}\right]$$

$$-\upsilon\left[\overline{\left(\frac{\partial u'}{\partial x}\right)^2}+\overline{\left(\frac{\partial u'}{\partial y}\right)^2}+\overline{\left(\frac{\partial u'}{\partial z}\right)^2}\right] \qquad (2.15)$$

$$-\upsilon\left[\overline{\left(\frac{\partial v'}{\partial x}\right)^2}+\overline{\left(\frac{\partial v'}{\partial y}\right)^2}+\overline{\left(\frac{\partial v'}{\partial z}\right)^2}\right]$$

$$-\upsilon\left[\overline{\left(\frac{\partial w'}{\partial x}\right)^2}+\overline{\left(\frac{\partial w'}{\partial y}\right)^2}+\overline{\left(\frac{\partial w'}{\partial z}\right)^2}\right]$$

where $\frac{\overline{u'^2}}{2}+\frac{\overline{v'^2}}{2}+\frac{\overline{w'^2}}{2}\equiv$ the total Turbulent Kinetic Energy.

2. Total TKE Change

The term on the left side of equation (2.15),

$$\frac{\partial}{\partial t}\left(\frac{\overline{u'^2}}{2}+\frac{\overline{v'^2}}{2}+\frac{\overline{w'^2}}{2}\right)$$

describes the change of the total TKE with time. The forcing functions on the right side of the equation will determine how the total TKE changes with time. This term can be either positive or negative, for an increase in TKE or decrease in TKE respectively.

3. Stress Terms

The first term on the right,

$$\left[-\overline{u'w'}\frac{\partial\bar{u}}{\partial z}-\overline{v'w'}\frac{\partial\bar{v}}{\partial z}\right]$$

is the change in TKE due to a vertical shear in the horizontal mean flow. This term is always positive, or it will always contribute to an increase in turbulent kinetic energy.

When a wind stress in the $+x$ direction acts on the water surface, it usually will set up a positive gradient, $\frac{\hat{c}\bar{u}}{\hat{c}z} > 0$, and a negative Reynolds stress, $\overline{u'w'} < 0$, with the result that an increase in wind stress will increase the TKE.

4. Buoyancy Term

The second term on the right,

$$- \frac{\overline{w'\rho'}}{\rho_o} g$$

describes the change in TKE due to a vertical density flux, or equivalently a buoyancy flux. This term will decrease TKE (term is negative) if the density increases with depth, a stable condition. An unstable condition where density decreases with depth would be associated with an increase in TKE with time. Thermodynamic forcing or salinity forcing could cause an unstable situation; such conditions could be heating from below, cooling from above, evaporation at the water surface, or salt rejection from the freezing of salt water at the surface. All these situations can occur in freezing regimes. When this term is negative it acts to dampen TKE. When it is positive it acts to produce TKE by buoyant production.

5. Turbulent Transport Terms

The third term on the right,

$$- \frac{\hat{c}}{\hat{c}z} \left[\overline{w' \left(\frac{u'^2}{2} + \frac{v'^2}{2} + \frac{w'^2}{2} + \frac{p'}{\rho_o} \right)} \right]$$

consists of two types of terms. The first three on the left

$$- \frac{\hat{c}}{\hat{c}z} \left[\overline{w' \left(\frac{u'^2}{2} + \frac{v'^2}{2} + \frac{w'^2}{2} \right)} \right]$$

redistribute turbulence in the vertical while the forth term

$$- \frac{\partial}{\hat{c}z} \left(\overline{w' \frac{p'}{\rho_o}} \right)$$

is a pressure transport of TKE. This term will be positive or negative depending upon whether the transport causes TKE to converge or diverge from a given level in the vertical.

6. Dissipation Terms

The last series of terms on the right

$$-\upsilon\left[\overline{\left(\frac{\partial u'}{\partial x}\right)^2}+\overline{\left(\frac{\partial u'}{\partial y}\right)^2}+\overline{\left(\frac{\partial u'}{\partial z}\right)^2}\right]-\upsilon\left[\overline{\left(\frac{\partial v'}{\partial x}\right)^2}+\overline{\left(\frac{\partial v'}{\partial y}\right)^2}+\overline{\left(\frac{\partial v'}{\partial z}\right)^2}\right]$$

$$-\upsilon\left[\overline{\left(\frac{\partial w'}{\partial x}\right)^2}+\overline{\left(\frac{\partial w'}{\partial y}\right)^2}+\overline{\left(\frac{\partial w'}{\partial z}\right)^2}\right]$$

are the dissipation terms. They will always be negative and will tend to decrease the TKE with time. They are also called the viscous damping terms, meaning the turbulence is dampened out due to the viscosity of the fluid. This is the principle loss term for the TKE budget.

7. TKE Summary

The Total TKE equation explains the TKE budget: the way turbulent kinetic energy is changed with time. The major sources of TKE are the horizontal velocity shear in the vertical and buoyancy instabilities, while the primary sinks of TKE are increasing the buoyancy of the fluid in the form of an increase of potential energy and the viscous dissipation off TKE.

III. THE MIXED LAYER MODEL

The processes involved in the freezing of salt water are not completely understood, and there are various ways of modeling the thermodynamics of the freezing process. Although the details of the physics are not completely understood, the most important processes have been studied extensively. In developing a model that is be used to study the interaction of the various processes, the salient processes are parameterized using various degrees of sophistication. To get a better understanding of the interaction of the relevant variables, it is best to start with a simple model to understand fully the process interactions before developing a more complex model. Although some systems of model equations can be solved analytically and valuable information can be gleaned, such models usually have been simplified and may lack realism.

For this research, simplifying assumptions are made in the general equations to study more completely the various parameters of mixed layer dynamics and their effect on the onset of freezing. To evaluate the most important processes, a variation of the Kraus-Turner one-dimensional mixed layer model (Kraus and Turner, 1967) was chosen and simplifying assumptions were made to investigate the relative importance of the forcing terms, initial conditions, and their dynamic interactions.

A. THE ONE-DIMENSIONAL MODEL

The model used for this study is derived from the total turbulent kinetic energy equation, equation (2.15), with simplifying assumptions and simplifying parameterizations.

1. Model Assumptions

The model assumptions following Niiler and Kraus (Niiler and Kraus, 1977) are:

1. The mean temperature, salinity, and horizontal velocity are uniform within the mixed layer.
2. On the depth and time scales of the model, temperature and salinity discontinuities can exist across the lower boundary of the mixed layer. Thus we neglect the effect of diffusion and conduction across this lower boundary.

3. Temperature changes associated with the frictional dissipation of kinetic energy can be neglected.
4. There is horizontal homogeneity of wind stress, turbulent kinetic energy, salinity, temperature, and viscous dissipation. Thus horizontal advection is neglected.
5. Only the case of a deepening mixed layer associated with a freezing regime will be considered. Shallowing mixed layers will not be considered.
6. The temperature of the water surface is approximately the temperature of the mixed layer. Thus ice formation will only occur when the mixed layer is at the freezing point, neglecting the effect of supercooling at the water surface.
7. The effects of internal waves are ignored.

2. Vertically Integrated TKE Equation

Using the above assumptions the TKE equation is integrated vertically over the depth of the mixed layer. First, a further assumption is made that the TKE budget is in an approximate steady state, with a balance between production and dissipation. TKE is produced by both buoyancy flux and stress production.

The first term of equation (2.1), the total TKE change term will be zero, not allowing the total TKE to change. Thus,

$$\frac{\partial}{\partial t}\left(\frac{\overline{u'^2}}{2}+\frac{\overline{v'^2}}{2}+\frac{\overline{w'^2}}{2}\right)=0$$

a. Stress Terms

The first term on the right of equation (2.1), the shear production term, is integrated vertically, giving

$$\int_{-h}^{0}\left[-\overline{u'w'}\frac{\partial\bar{u}}{\partial z}-\overline{v'w'}\frac{\partial\bar{v}}{\partial z}\right]dz\simeq-\overline{u'w'}\bar{u}-\overline{v'w'}\bar{v}\simeq u_*^2\,\delta\bar{u}$$

where u_*, is the friction velocity. The friction velocity, u_* is defined as

$$\left|\overline{w'(u'e_x+v'e_y)}\right|=\frac{\tau_o}{\rho}\equiv u_*^2=\frac{\rho_a}{\rho}C_a u_a^2$$

where

- ρ is the water density

- ρ_a is the air density
- τ_o is the wind stress magnitude at the surface
- u_a is the velocity of the wind at a reference height (normally 10 meters)
- C_a is the drag coefficient at the reference level

If $\delta\bar{u}$ is proportional to u_*, then

$$\int_{-h}^{0}\left[- \overline{u'w'}\frac{\partial\bar{u}}{\partial z} - \overline{v'w'}\frac{\partial\bar{v}}{\partial z}\right] dz \equiv a\,u_*^3 \qquad (3.1)$$

where $a \sim 6$.

b. The Buoyancy Flux

The second term on the right in equation (2.15) can be rewritten using the definition of buoyancy,

$$b = \frac{\rho_o - \rho}{\rho_o} g = \frac{\rho_o - (\bar{\rho} - \rho')}{\rho_o} g$$

But,

$$\bar{b} = \frac{\rho_o - \bar{\rho}}{\rho_o} g$$

and thus

$$b' = - \frac{\rho' g}{\rho_o}$$

This gives

$$- \frac{\overline{w'\rho'}}{\rho_o} g \equiv \overline{b'w'}$$

The vertically integrated buoyancy flux thus can be expressed as

$$\int_{-h}^{0} \overline{b'w'} dz = h[\overline{b'w'}(0) + \overline{b'w'}(-h)]$$

where

- h is the mixed layer depth
- $\overline{b'w'}(0)$ is the buoyancy flux at the surface
- $\overline{b'w'}(-h)$ is the buoyancy flux at the lower interface

Using the linearized equation of state

$$\rho = \rho_o[1 - \alpha(T - T_o) + \beta(S - S_o)]$$

where

- ρ is the density
- ρ_o is the reference density at T_o and S_o
- α is the coefficient of thermal expansion
- β is the coefficient of haline contraction
- g is gravity
- T is the water temperature
- T_o is a reference temperature
- S is the water salinity
- S_o is a reference salinity

the mean density is

$$\overline{\rho} = \rho_o[1 - \alpha(\overline{T} - T_o) + \beta(\overline{S} - S_o)]$$

leaving the fluctuating component

$$\rho' = \rho_o[- \alpha T' + \beta S']$$

This gives

$$\overline{b'w'} = - \frac{\overline{\rho'w'}}{\rho_o} g = \alpha g \overline{T'w'} - \beta g \overline{S'w'} \tag{3.2}$$

The vertically integrated buoyancy flux can now be written as

$$\begin{aligned} \int_{-h}^{0} \overline{b'w'} dz &= h(\alpha g \overline{T'w'}(0) - \beta g \overline{S'w'}(0)) \\ &+ h(\alpha g \overline{T'w'}(-h) - \beta g \overline{S'w'}(-h)) \end{aligned} \tag{3.3}$$

c. Transport Terms

The transport terms can also be related to the friction velocity cubed, so that

$$\int_{-h}^{0} -\frac{\partial}{\partial z}\left[\overline{w'\left(\frac{u'^2}{2}+\frac{v'^2}{2}+\frac{w'^2}{2}+\frac{p'}{\rho_o}\right)}\right]dz \simeq bu_*^3 \qquad (3.4)$$

d. Dissipation Terms

The dissipation term has nine components:

$$\varepsilon = \upsilon\left[\overline{\left(\frac{\partial u'}{\partial x}\right)^2}+\overline{\left(\frac{\partial u'}{\partial y}\right)^2}+\overline{\left(\frac{\partial u'}{\partial z}\right)^2}\right]$$

$$+\upsilon\left[\overline{\left(\frac{\partial v'}{\partial x}\right)^2}+\overline{\left(\frac{\partial v'}{\partial y}\right)^2}+\overline{\left(\frac{\partial v'}{\partial z}\right)^2}\right]$$

$$+\upsilon\left[\overline{\left(\frac{\partial w'}{\partial x}\right)^2}+\overline{\left(\frac{\partial w'}{\partial y}\right)^2}+\overline{\left(\frac{\partial w'}{\partial z}\right)^2}\right]$$

Kraus and Turner (1967) incorrectly neglected dissipation, but here it is assumed to be of the form:

$$\int_{-h}^{0} \varepsilon dz \simeq cu_*^3 \qquad (3.5)$$

e. Reduced TKE Equation

Substituting equations (3.2), (3.3), (3.4), and (3.5), into the TKE equation gives

$$0 = au_*^3 + bu_*^3 + cu_*^3 + h(\alpha g\overline{T'w'}(0) - \beta g\overline{S'w'}(0))$$

$$+ h(\alpha g\overline{T'w'}(-h) - \beta g\overline{S'w'}(-h))$$

For $h \neq 0$,

$$0 = \frac{1}{h}(au_*^3 + bu_*^3 + cu_*^3) + \alpha g\overline{T'w'}(0) - \beta g\overline{S'w'}(0)$$

$$+ \alpha g\overline{T'w'}(-h) - \beta g\overline{S'w'}(-h)$$

The three constants of proportionality (a, b and c) are combined into one constant, C_1, so

$$\frac{1}{h}(au_*^3 + bu_*^3 + cu_*^3) = \frac{C_1 u_*^3}{h}$$

This gives the final form of the TKE equation,

$$0 = \frac{C_1 u_*^3}{h} + \alpha g\overline{T'w'}(0) - \beta g\overline{S'w'}(0)$$

$$+ \alpha g\overline{T'w'}(-h) - \beta g\overline{S'w'}(-h) \tag{3.6}$$

Using equation (3.2), an equivalent form of the TKE budget is

$$0 = \frac{C_1 u_*^3}{h} + \overline{b'w'}(0) + \overline{b'w'}(-h) \tag{3.6A}$$

The physical meaning of the terms of equation (3.6) are:

1. Turbulent kinetic energy is created in the mixed layer by the wind stress at the surface, and it is distributed over the full depth of the mixed layer
2. The excess TKE from the wind stress is moderated by the buoyancy flux associated with the heat flux and the salinity flux at the surface.
3. The remaining TKE is dampened by the negative buoyancy flux at the bottom of the mixed layer by entraining denser deep water from below.

3. Buoyancy Fluxes

The buoyancy fluxes at the surface and the bottom of the mixed layer will be dependent on the heat fluxes and the salinity fluxes at the top and bottom of the mixed layer. For this study of the onset of freezing, the heat flux at the surface will be transformed mostly into a salinity flux via the thermodynamic equations (3.7, 3.15, 3.16, 3.17, and 3.18). Depending on the initial conditions below the mixed layer, there may be a stability problem, resulting in the overturning of the whole water column. These cases will not be investigated here.

a. Surface Heat Flux

The $\overline{T'w'}(0)$ term represents the surface heat flux into the mixed layer,

$$\rho C_p \overline{T'w'}(0) = -Q_n \tag{3.7}$$

where

- Q_n is the net downward heat flux at the surface
- ρ is the density of the water
- C_p is the specific heat of water
- $\overline{T'w'}(0)$ is the temperature flux associated with the heat flux

In a freezing situation, which is the emphasis in this study, there exists a state when any further heat flux out of the mixed layer will not result in further cooling but will result in the formation of ice.

b. Surface Salinity Flux

The $\overline{S'w'}(0)$ term represents the surface salinity flux out of the mixed layer,

$$\overline{S'w'}(0) = -S(E-P) - (S-S_i)(F-M) \tag{3.8}$$

where

- S is the salinity of the mixed layer in g/kg
- S_i is the salinity of the ice formed or melted in g/kg
- E is the evaporation rate in m/sec
- P is the precipitation rate in m/sec
- F is the freezing rate in m/sec
- M is the melting rate in m/sec

c. Surface Buoyancy Flux

The surface buoyancy flux can be written as a function of the heat flux and the components of the salinity flux, using equations (3.2), (3.7), and (3.8):

$$\overline{b'w'}(0) = -\alpha g \frac{Q_n}{\rho C_p} + \beta g(E-P)S + \beta g(F-M)(S-S_i) \tag{3.9}$$

d. Heat Flux at the Lower Boundary

The temperature flux at the bottom of the layer is $\overline{T'w'}(-h)$ and represents the thermal energy brought from the deeper water into the mixed layer by entrainment. Here the effect of molecular conductivity of thermal energy across the interface is neglected. This allows the temperature flux to be written as

$$\overline{T'w'}(-h) = -\Delta T\ W_e \tag{3.10}$$

where

$$\Delta T = T - T_o$$

and where

- h is the mixed layer depth in meters
- T is the mixed layer temperature in °C
- ΔT is the temperature jump at the base of the mixed layer between the mixed layer in °C
- T_o is the deep water temperature in °C
- W_e is the entrainment velocity in m/sec

e. Salinity flux at the Lower Boundary

The salinity flux at the base of the mixed layer $\overline{S'w'}(-h)$, is caused by the entrainment of lower water with a different salinity. This can flux can be written as

$$\overline{S'w'}(-h) = -\Delta S\ W_e \tag{3.11}$$

where

$$\Delta S = S - S_o$$

and where

- h is the mixed layer depth in meters
- ΔS is the jump salinity between the mixed layer salinity and the deep water salinity in ppt
- S is the mixed layer salinity in ppt
- S_o is the deep water salinity in ppt
- W_e is the entrainment velocity in m/sec

f. Buoyancy Flux at the Lower Boundary

The buoyancy flux at the base of the mixed layer can be written from the flux equations at the base of the mixed layer, equations (3.10) and (3.11), and equation (3.2)

$$\overline{b'w'}(-h) = -\Delta b\, W_e \tag{3.12}$$

where

$$\Delta b = \alpha g \Delta T - \beta g \Delta S \tag{3.13}$$

4. Entrainment Velocity

The Entrainment Velocity, W_e, can be obtained from equation (3.6A), where a constant, C_2, will be included to tune this simplified model to fit observations.

$$0 = \frac{C_1 u_*^3}{h} + C_2\overline{b'w'}(0) + \overline{b'w'}(-h)$$

Using (3.13), this equation becomes

$$0 = \frac{C_1 u_*^3}{h} + C_2\overline{b'w'}(0) - \Delta b\, W_e$$

or

$$\Delta b\, W_e = \frac{C_1 u_*^3}{h} + C_2\overline{b'w'}(0)$$

Solving for the entrainment velocity, W_e,

$$W_e = \frac{1}{\Delta b}\left(\frac{C_1 u_*^3}{h} + C_2\overline{b'w'}(0)\right)$$

or

$$W_e = \frac{1}{\alpha g \Delta T' - \beta g \Delta S'} \frac{C_1 u_*^3}{h}$$

$$+ \frac{1}{\alpha g \Delta T' - \beta g \Delta S'} C_2 \left[- \alpha g \frac{Q_n}{\rho c_p} + \beta g (E - P) S + \beta g (F - M)(S - S_i) \right] \tag{3.14}$$

Furthermore, it is required that $W_e \geq 0$, or only deepening.

The model tuning constants C_1 and C_2 are used to allow the model to fit observations. Chu and Garwood (1988) indicate that the value between 2 and 1 should be used for C_1, and a value near .2 should be used for C_1 . For this study a normal value of 2. for C_1 and .2 for C_2 will be used.

When the value of Δb nears zero the model becomes computationally unstable. This condition is beyond the scope of this study. Thus the entrainment velocity here will have a realistic upper limit, consistent with observations.

B. THE THERMODYNAMIC MODEL

The thermodynamic equations will relate the energy needed to lower the water temperature to the freezing point and the energy removal needed to freeze the water. Since the mixed layer regimes for the onset of freezing are the primary focus of this study. only the conditions involving a net upward surface heat flux are of interest.

1. The Surface Heat Flux

The net heat fluxed out of the mixed layer is:

$$Q_n = Q_r + Q_l + Q_e + Q_s$$

where

- Q_n = net heat flux
- Q_r = heat flux from shortwave radiation
- Q_l = heat flux from longwave radiation
- Q_e = latent heat flux
- Q_s = sensible heat flux

From chapter II, equations (2.1), (2.5), (2.6), (2.7), give

$$Q_n = F_o(1 - kc^3)(1 - \alpha) + .7855(1 + .2232c^{2.75})\sigma T_a^4 - .97\sigma T_s^4 + \rho_a L C_e U(q_a - q_o) + \rho_a c_{p_a} C_s U(T_a - T_s)$$

where:

- Q_n = net heat flux
- F_o = incoming solar radiation
- k = seasonal cloudiness parameter
- c = cloudiness in tenths
- α = albedo of the surface
- σ = Stefan-Boltzman constant
- T_a = air temperature at the reference level
- ρ_a = air density
- L = latent heat of vaporization
- C_e = latent heat bulk transfer coefficient
- U = wind speed
- q_a = specific humidity of the air at the reference level
- q_o = specific humidity of the air at the reference level
- ρ_a = density of the air
- c_{p_a} = specific heat of air
- C_s = sensible heat bulk transfer coefficient
- T_s = temperature at the surface

To simplify the equations, only the polar night will be investigated thus eliminating any solar radiation, i.e. $Q_r = 0$. Other assumptions are that the specific humidity at the surface will be at saturation and the temperature at the surface will be the mixed layer temperature, $T_s = T$. The values of C_e and C_s are assumed constant. This gives an equation that is dependent on the air temperature, specific humidity of the air, sea surface temperature, wind speed and cloudiness:

$$Q_n = .7855(1 + .2232c^{2.75})\sigma T_a^4 + \rho_a L C_e U(q_a - q_o) + \rho_a c_{p_a} C_s U(T_a - T) - .97\sigma T^4 \quad (3.15)$$

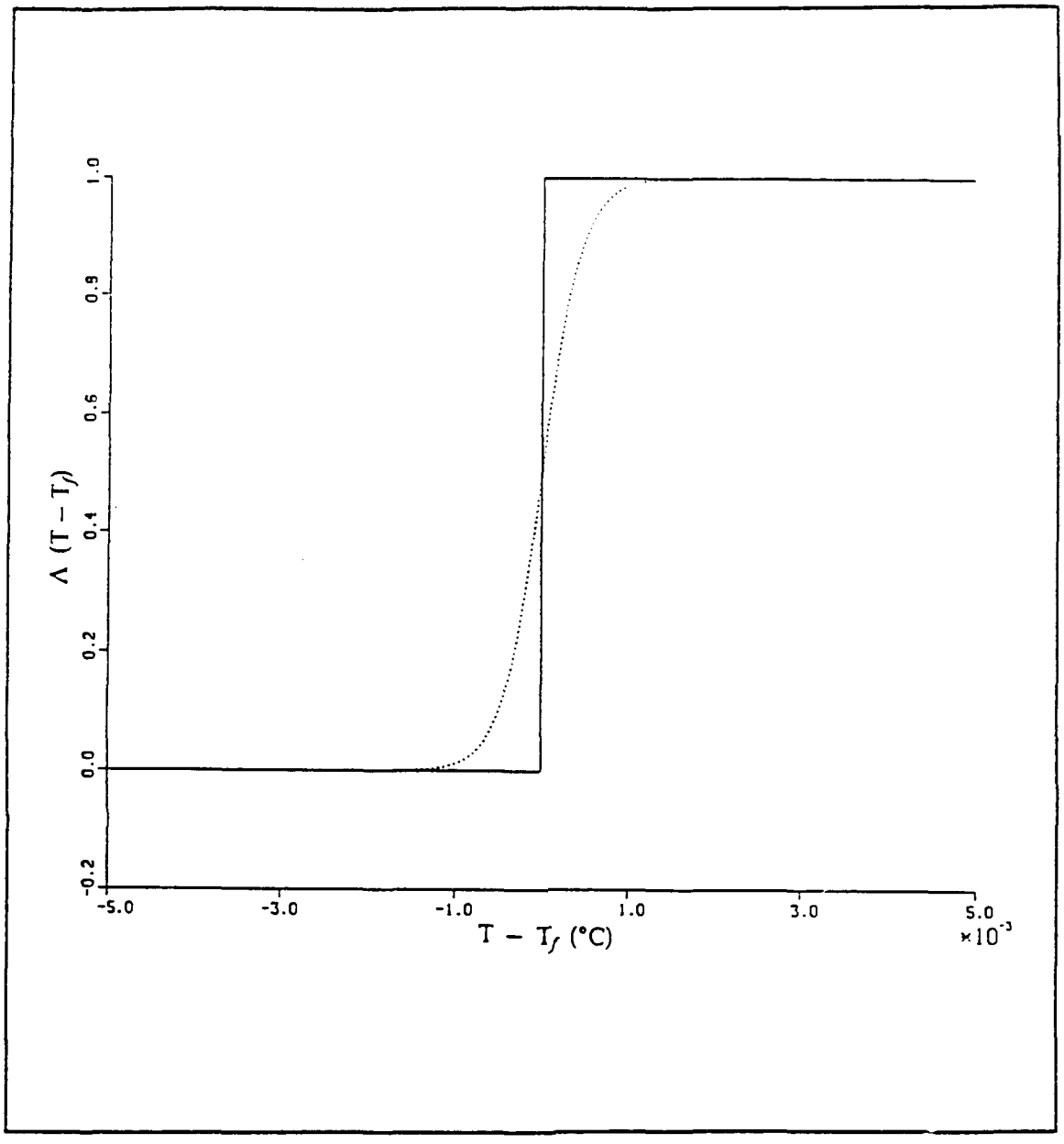

Figure 7. Heavyside Step Function And Modified Heavyside Step Function: The Heavyside Step Function (solid line) which is 0 for values of $T - T_f \leq 0$ and is 1 for values of $T - T_f > 0$. This function has sharp corners and is second-order non-continuous at 0. The dotted line is a modified Heavyside Step Function which has smooth corners and is second-order continuous. This function was used in place of the Heavyside Step Function to reduce computational noise.

2. The Freezing Temperature

The freezing temperature formula of Hakkinen (1987) is used:

$$T_f = -.003 - .0527S - 4.0\text{x}10^{-5}S^2 \tag{3.16}$$

where

- T_f is the freezing temperature of salt water
- S is the salinity of the water (°%)

To ensure no loss of energy when the mixed layer is near the freezing temperature, a distinction was made between a decrease in water temperature and the production of ice using the Heavyside Step function, Λ:

$$\Lambda(T, T_f) = \begin{cases} 0 \text{ for } T \leq T_f \\ 1 \text{ for } T > T_f \end{cases}$$

Figure 7 shows the Heavyside Step Function.

To reduce computational noise caused by this second order non-continuous function, Λ is approximated with:

$$\Lambda(T, T_f) = \frac{1 + \text{TANH}((T - T_f)2200)}{2} \tag{3.17}$$

Figure 7 shows the modified Heavyside Step Function. Here the corners are slightly rounded, and the function is second order continuous. This function eliminated computational noise.

3. The Freezing Rate

The freezing rate was determined by the amount of energy remaining after first lowering the mixed layer temperature to freezing:

$$F = \frac{c_p}{L_f}\left(-\frac{Q_n}{\rho c_p} + \Delta T W_e\right)(1 - \Lambda(T, T_f)) \tag{3.18}$$

where:

- F is the freezing rate
- c_p is the specific heat of water
- L_f is the latent heat of fusion of ice
- Q_n is the net heat flux
- ρ is the water density
- ΔT is the difference between the mixed layer and lower layer temperature
- W_e is the entrainment velocity
- Λ is the Heavyside-step function approximation

C. THE NUMERICAL MODEL

In the numerical model, ordinary differential equations are used of the form:

$$\frac{\partial(\ )}{\partial t} = \frac{1}{h}[-\overline{(\ )'w'}(0) - \{-\overline{(\ )'w'}(-h)\}] \tag{3.19}$$

1. The Time Dependent Equations

From equation (3.19) the time dependent thermal equation is

$$\frac{\partial T}{\partial t} = \frac{1}{h}[-\overline{T'w'}(0) - \{-\overline{T'w'}(-h)\}]\Lambda(T, T_f)$$

Using equations (3.7) and (3.10) this can be written as

$$\frac{\partial T}{\partial t} = \frac{1}{h}\left[\frac{Q_n}{\rho c_p} - \Delta T\, W_e\right]\Lambda(T, T_f) \tag{3.20}$$

Similarly the time dependent Salinity equation is

$$\frac{\partial S}{\partial t} = \frac{1}{h}[-\overline{S'w'}(0) - \{-\overline{S'w'}(-h)\}]$$

Using equations (3.8) and (3.11) this can be written as

$$\frac{\partial S}{\partial t} = \frac{1}{h}[\overline{S}(E-P) + (\overline{S} - \overline{S}_l)(F-M) - \Delta S\, W_e] \tag{3.21}$$

The time dependent equation for the buoyancy is

$$\frac{\partial b}{\partial t} = \frac{1}{h}[-\overline{b'w'}(0) - \{-\overline{b'w'}(-h)\}]$$

From equations (3.9) and 3.12) this can be written as

$$\frac{\partial b}{\partial t} = \frac{1}{h}\left[\alpha g \frac{Q_n}{\rho c_p} - \beta g(E-P)S - \beta g(F-M)(S-S_i) - \Delta b\, W_e\right] \quad (3.22)$$

The time dependent mixed layer depth equation is

$$\frac{\partial h}{\partial t} = W_e - w(-h) - (E - P + F - M) \quad (3.23)$$

where

- W_e is the entrainment velocity
- $w(-h)$ is a time dependent function for vertical velocity (i.e. internal wave, tides)
- E is the evaporation rate
- P is the precipitation rate
- F is the freezing rate
- M is the melting rate

The time dependent equation for ice growth is

$$\frac{\partial h_i}{\partial t} = F\frac{\rho}{\rho_i} \quad (3.24)$$

where

- h_i is the thickness of the ice
- F is the freezing rate
- ρ is the density of the water
- ρ_i is the density of the ice

2. Model Formulas

All the formulas used to define the model variables, and the model constants, are summarized below and in Tables 1 through 4.

$$W_e = \frac{1}{\alpha g \Delta T - \beta g \Delta S'} \frac{C_1 u_*^3}{h}$$

$$+ \frac{1}{\alpha g \Delta T - \beta g \Delta S'} C_2 \left[- \alpha g \frac{Q_n}{\rho c_p} + \beta g (E - P) S + \beta g (F - M)(S - S_i) \right] \tag{3.14}$$

for $W_e \geq 0$, otherwise $W_e = 0$

$$F = \frac{c_p}{L_f} \left(- \frac{Q_n}{\rho c_p} + \Delta T W_e \right) (1 - \Lambda(T, T_f)) \tag{3.18}$$

$$\overline{b'w'}(0) = - \alpha g \frac{Q_n}{\rho c_p} + \beta g (E - P) S + \beta g (F - M)(S - S_i) \tag{3.9}$$

$$\overline{b'w'}(-h) = - \Delta b \, W_e \tag{3.12}$$

$$\Delta b = \alpha g \Delta T - \beta g \Delta S \tag{3.13}$$

$$\Delta T = T - T_o$$

$$\Delta S = S - S_o$$

$$u_* = U \sqrt{\frac{\rho_a}{\rho} C_a}$$

$$T_f = -.003 - .0527 S - 4.0 \times 10^{-5} S^2 \tag{3.16}$$

$$\Lambda(T, T_f) = \frac{1 + \mathrm{TANH}((T - T_f) 2200)}{2} \tag{3.17}$$

$$Q_n = .7855(1 + .2232 c^{2.75}) \sigma T_a^4 + \rho_a L C_e U (q_a - q_o) + \rho_a c_{p_a} C_s U (T_a - T) - .97 \sigma T^4 \tag{3.15}$$

Table 1. MODEL VARIABLES

Variable	Units	Description
α	$\frac{1}{^\circ C}$	Coefficient of Thermal Expansion
β	$\frac{kg}{g}$	Coefficient of Salinity Contraction
b	$\frac{m}{s^2}$	Buoyancy of the Mixed Layer
Δb	$\frac{m}{s^2}$	Buoyancy Difference between the Mixed Layer and the Deep Layer
$\overline{b'w'}(0)$	$\frac{m^2}{s^3}$	Buoyancy Flux at the Surface of the Mixed Layer
$\overline{b'w'}(-h)$	$\frac{m^2}{s^3}$	Buoyancy Flux at the Bottom of the Mixed Layer
c	Tenths	Cloudiness
E	$\frac{m}{s}$	Evaporation Rate
F	$\frac{m}{s}$	Freezing Rate
h	m	Depth of the Mixed Layer
h_i	m	Thickness of the Ice
Λ		Heavyside Step Function (Modified)
M	$\frac{m}{s}$	Melting Rate of the Ice
P	$\frac{m}{s}$	Precipitation Rate into the Mixed Layer
q_a		Specific Humidity of the Air at the reference level

Table 2. MODEL VARIABLES CONTINUED

Variable	Units	Description
q_s		Specific Humidity of the Air at the Surface
Q_n	$\frac{W}{m^2}$	Net Heat Flux downward at the Surface of the Mixed Layer (Downward is Positive)
ρ	$\frac{kg}{m^3}$	Density of the Mixed Layer Water
ρ_a	$\frac{kg}{m^3}$	Density of the Air at the reference level
ρ_i	$\frac{kg}{m^3}$	Density of the Ice
S	$\frac{g}{kg}$	Salinity of the Mixed Layer
S_i	$\frac{g}{kg}$	Salinity of the Ice
S_o	$\frac{g}{kg}$	A Salinity of the Deep Water
ΔS	$\frac{g}{kg}$	Salinity Difference between the Mixed Layer and the Deep Water
t	s	Time
T	°C	Temperature of the Mixed Layer
T_a	°C	Temperature of the Air at the reference level
T_f	°C	Temperature of Freezing
T_o	°C	Temperature of the Deep Water
T_s	°C	Temperature of the Air at the Surface of the Water (assumed to be equal to T)

Table 3. MODEL VARIABLES CONTINUED

Variable	Units	Description
ΔT	°C	Temperature Difference between the Mixed Layer and the Deep Water
u_*	$\frac{m}{s}$	Friction Velocity of the Mixed Layer
U , u	$\frac{m}{s}$	Velocity of the Air at the reference level
w	$\frac{m}{s}$	A Vertical Velocity Function at the Interface of the Mixed Layer and the Deep Water due to some Forcing (i.e. tides, internal waves, etc.)
W_e	$\frac{m}{s}$	Entrainment Velocity

Table 4. MODEL CONSTANTS

Constant	Units	Value	Description
c_p	$\frac{J}{kg°C}$	$4.18x10^3$	Specific Heat of Water
c_{p_a}	$\frac{J}{kg°C}$	1004	Specific Heat of Air
C_a	none	$1.3x10^{-3}$	Drag Coefficient for the Air at a Reference Level
C_e	none	$1.28x10^{-3}$	Latent Heat Bulk Transfer Coefficient
C_s	none	$1.4x10^{-3}$	Sensible Heat Bulk Transfer Coefficient
C_1	none	2.0	Tuning Constant for Friction Velocity Term
C_2	none	0.2	Tuning Constant for Surface Buoyancy Flux Term
g	$\frac{m}{s^2}$	9.83	Acceleration due to Gravity
L	$\frac{J}{kg}$	$2.5x10^6$	Latent Heat of Vaporization
L_f	$\frac{J}{kg}$	$302.0x10^3$	Latent Heat of Fusion of Ice
σ	$\frac{kg}{s^3(°K)^4}$	$5.67x10^{-8}$	Stefan-Boltzman Constant

IV. MODEL RESULTS

A. MODEL INITIAL CONDITIONS AND BOUNDARY CONDITIONS

For this study the model was run for various initial conditions and boundary conditions. For boundary conditions, the wind speed and various parameters affecting Q_n, i.e. air temperature, specific humidity of the air, and cloudiness, were considered. For initial conditions, or pre-conditioning situations, consideration was given to the initial mixed layer salinity, which determines the mixed layer freezing temperature, the deep water's temperature, the deep water's salinity, and the initial mixed layer depth.

Table 5. NORMAL VALUES AND SENSITIVITY RUN VALUES

Variable	Normal Values	Other Values Used For Sensitivity Analysis
Wind Speed, U	$5\ \frac{m}{s}$	0, .5, 1, 1.5, 2, 2.5, 3, 3.5, 4, 4.5, 5, 5.5, 6, 6.5, 7, 7.5, 8, 8.5, 9, 9.5, 10, 10.5, 11, 11.5, 12
Salinity Jump, ΔS	$.5\ \frac{g}{kg}$	.3, .4, .5, .6, .7, .8, .9, 1.0, 1.2, 1.5, 2.0, 2.5, 3.0, 4.0, 5.0, 6.0, 6.5, 7.0, 7.5, 8.0, 8.5, 9.0, 9.5, 10.0, 11.0, 12.0, 13.0, 14.0, 15.0, 16.0, 17.0, 18.0, 19.0, 20.0, 25.0
Temperature Jump, ΔT	2.8688 °C	-1, -.5, 0, .5, 1, 1.5, 2, 2.2, 2.4, 2.6, 2.7, 2.8, 2.868, 2.9, 3.0, 3.5, 4.0, 5.0, 10.0
Mixed Layer Depth, h	60 m	5, 10, 30, 40, 50, 60, 70, 80, 90, 100, 120, 150, 160, 175, 200, 250, 300, 500, 1000
Surface Heat flux, Q_n	$-350\ \frac{W}{m^2}$	100, 0, -100, -200, -300, -350, -400, -450, -500, -600, -700, -800

Model simulations were made with the mixed layer temperature close to its freezing temperature, allowing the mixed layer to begin freezing. The specific ranges of boundary conditions ranged from the most severe arctic storm conditions, wind > 60 knots, to calm winds, while varying the factors affecting Q_n between physically realistic maximum

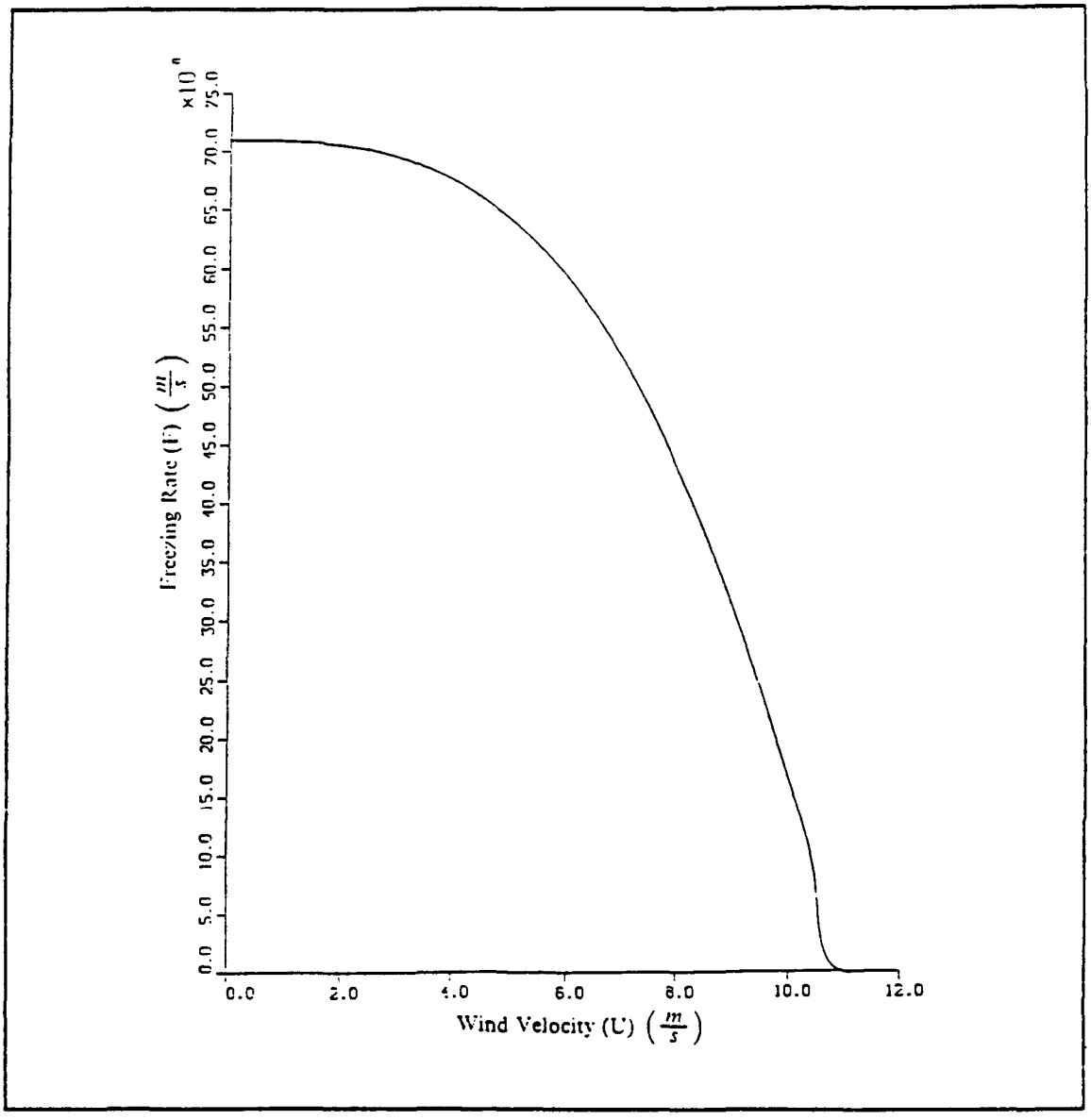

Figure 8. Freezing Rate as a Function of Wind Speed, U, Only: Results of model runs for variations in wind speed, without changing any other initial condition or boundary condition. For a constant net heat flux upward, there is a maximum freezing rate under no-wind conditions where the effects of wind induced turbulent mixing is negligible. Under higher wind conditions, wind speeds over 11 $\frac{m}{s}$, the heat flux into the mixed layer from the entraining of warmer water below overcomes the heat flux upward out of the mixed layer and net mixed layer warming occurs.

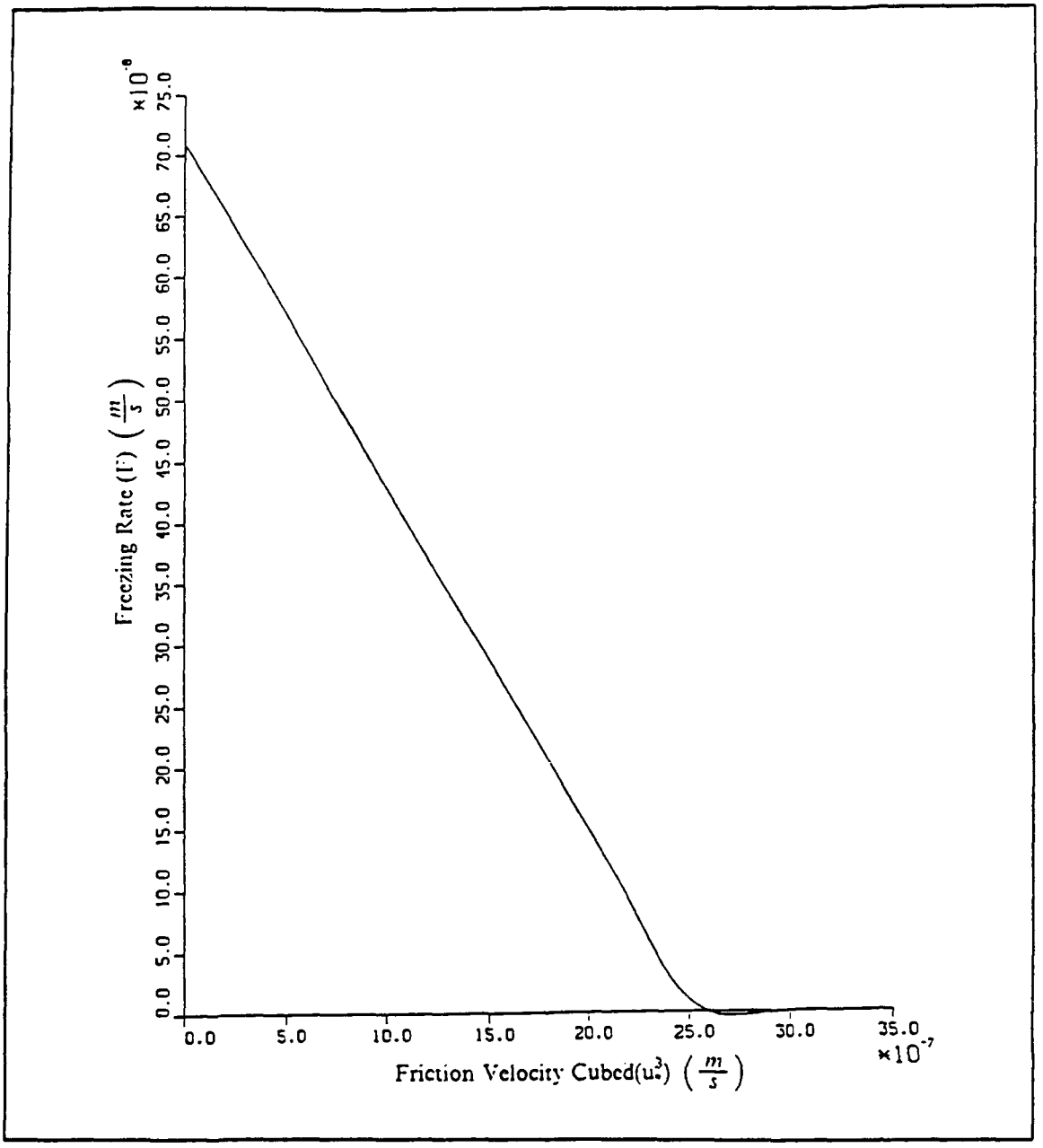

Figure 9. Freezing as a Function of u *: Results of model runs where the wind speed was varied, without varying other initial conditions or boundary conditions. The results show the linear relationship between the freezing rate and W_o, which at small freezing rates, is a linear function of u_*^3.

and minimum values. The initial salinity and water temperature values were varied between realistic limits. Unrealistic conditions were also considered to determine if the model would produce unstable conditions.

A major consideration for this thesis is the regimes where freezing occurs and does not occur, and the boundary between them. For this reason the freezing rate is considered as the model output that will be used to compare the results of the model runs.

Table 5 shows the values that were considered as standard initial conditions and boundary values, plus those values that were used on the model runs.

1. Model Sensitivity To Wind

The model was run under varying ranges of wind conditions without varying any other factors. This takes into consideration regimes where the wind speed, U, increases or decreases with an appropriate change in sensible and latent heat fluxes to keep the net heat flux, Q_n, constant. As an example, for a constant condition of $Q_n = -350 \frac{W}{m^2}$, and $U = 5 \frac{m}{s}$, an appropriate air temperature would be -21 °C. $T_a = -21°C$. For a wind speed of $U = 30 \frac{m}{s}$ an appropriate air temperature would be -.03 °C. $T_a = -.03°C$

The only physically unrealistic situation was for calm winds, where the maximum attainable realistic Q_n is on the order of -200 $\frac{W}{m^2}$.

Figure 8 shows the results of the model runs. Because only the wind speed was varied, this mostly represents the effect of varying the entrainment of warmer water from below. From equation (3.14), if Q_n is constant and F is small, the entrainment velocity acts as a cubic function of u_*. From equation (3.18), again if Q_n is constant, the freezing rate should be a function of $\Delta T W_e$, which is negative under these conditions, and the resulting curve should reflect a negative turning cubic function. Under conditions of Q_n being held constant at -350 $\frac{W}{m^3}$, the heat flux at the bottom of the mixed layer, from entraining warmer water, overcomes the heat flux out of the surface when the wind speed nears 11 $\frac{m}{s}$. For higher wind speeds a net mixed layer warming occurs. Figure 9 shows the relationship of the freezing rate as a function of u_*^3, vice U. This shows the near linear relationship of the W_e, a function of u_*^3, and the freezing rate.

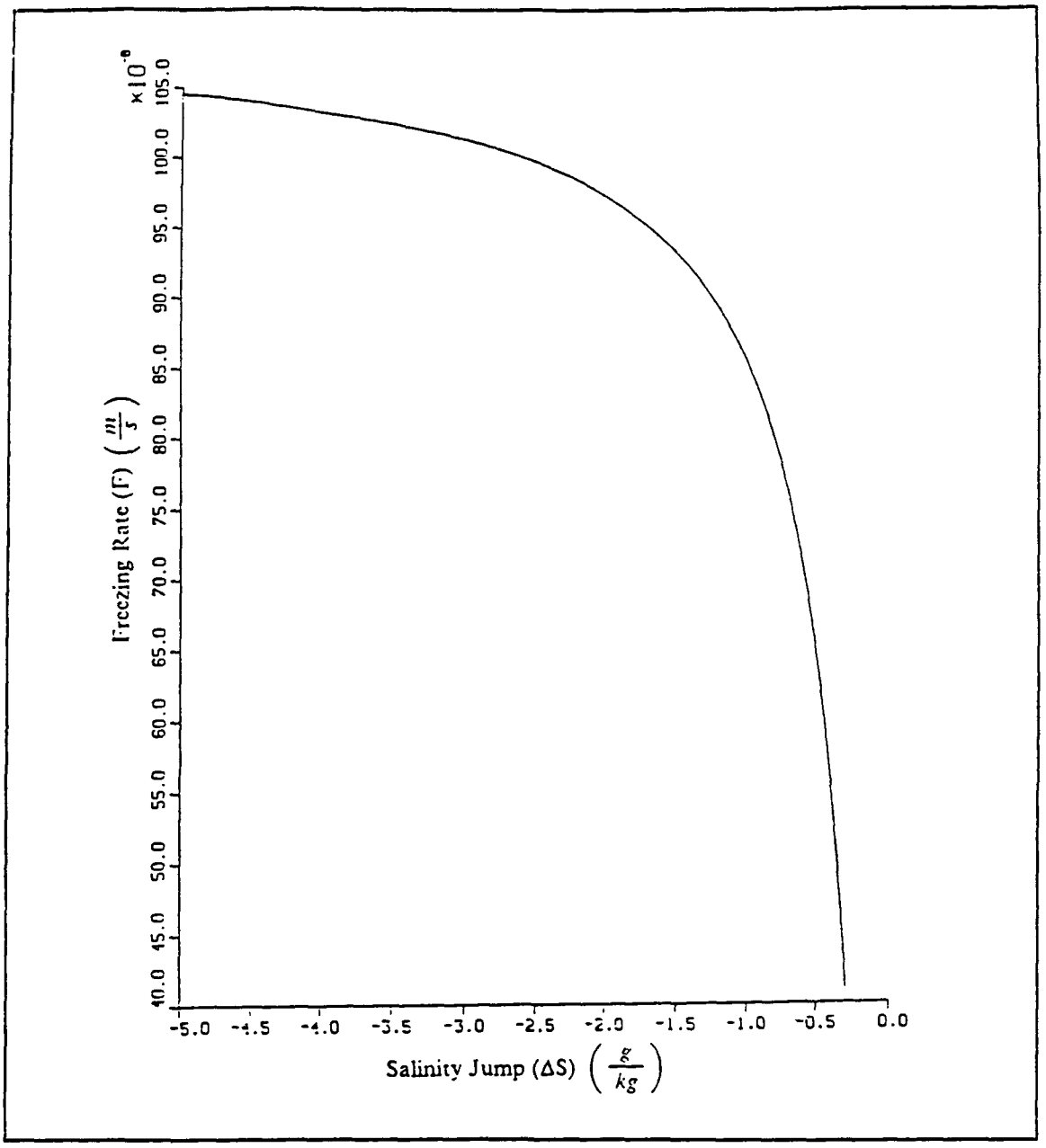

Figure 10. Freezing Rate as a Function of the Salinity Jump: Results of model runs where the salinity jump, ΔS, was varied, without varying other initial conditions or boundary conditions. The results show a rapid decrease in freezing rate as the salinity jump nears -.3, and a slow near linear increase for $\Delta S < -2.5$.

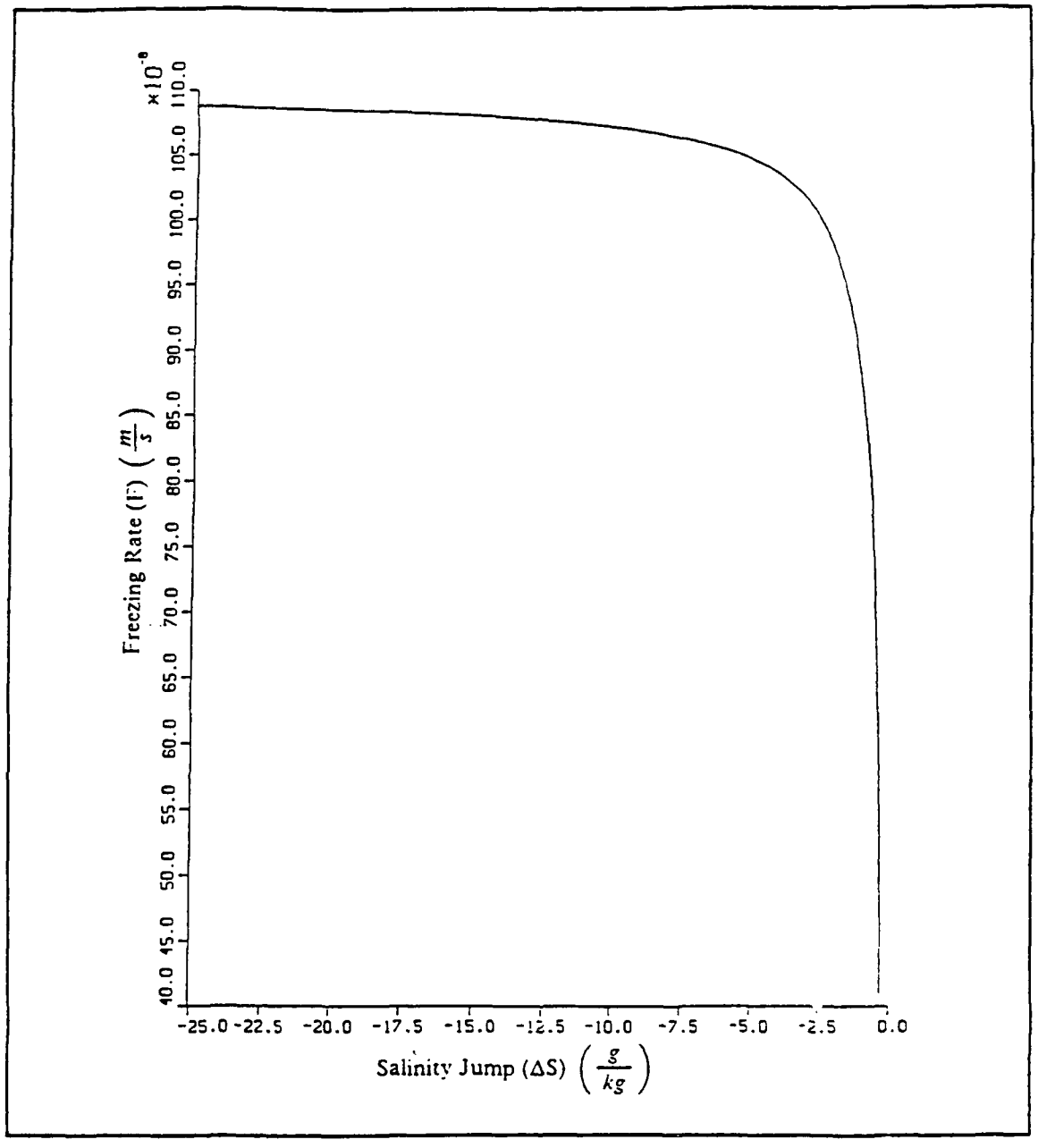

Figure 11. Freezing Rate as a Function of Salinity Jump: An extension of Figure 10 for values of Salinity Jump, ΔS, to -25.0 °C. The extended values past -5.0 show the leveling off trend for greater magnitudes of ΔS and its approach toward the maximum freezing available of $F = 112.8x10^{-6}$.

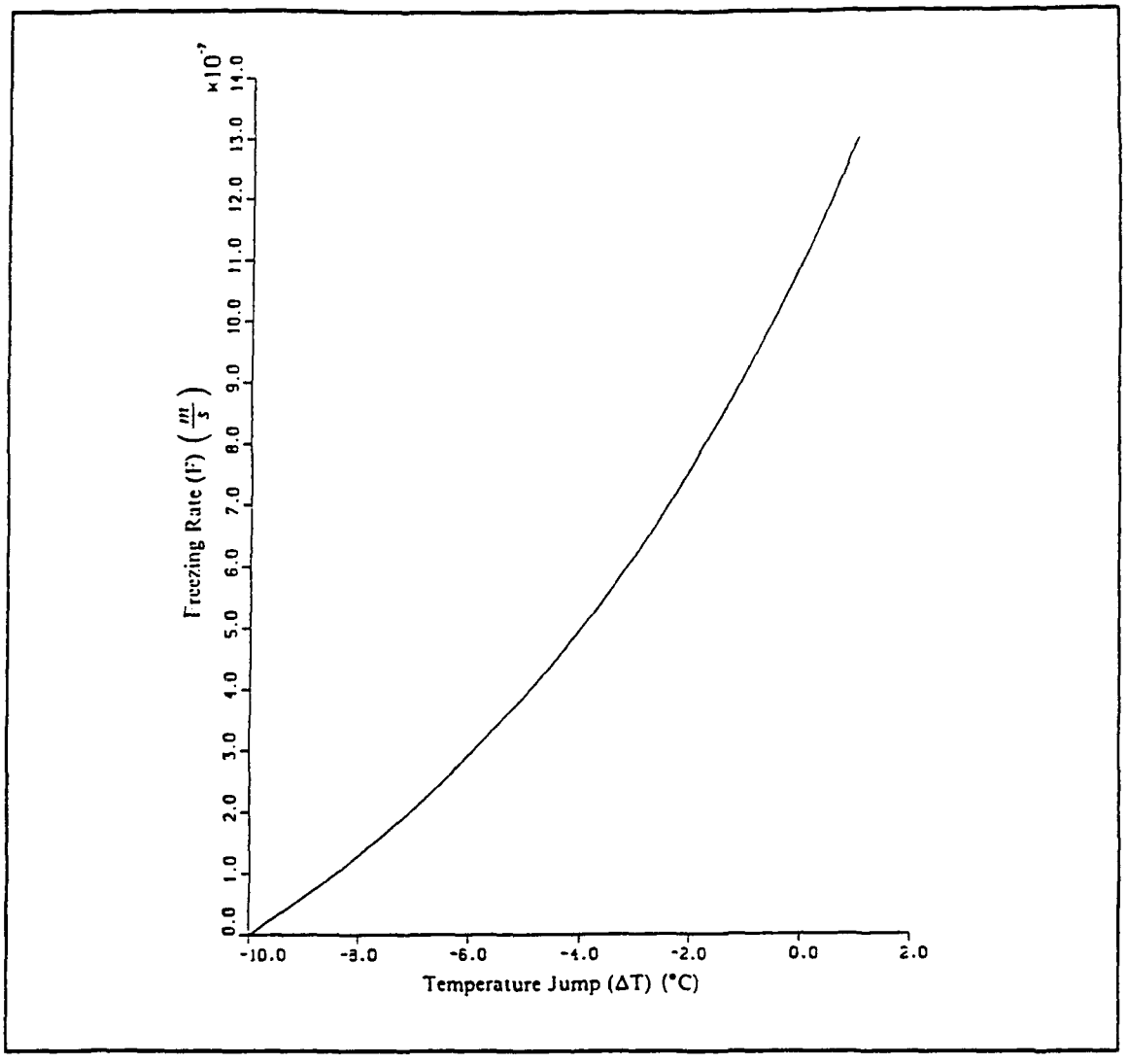

Figure 12. Freezing Rate as a Function of Temperature Jump: Results of model runs where the temperature jump, ΔT is varied, without varying the other initial conditions or boundary conditions. The results show a near linear decrease in freezing rate, F, as the temperature jump increases in magnitude. For values of $\Delta T > -1.8$, the freezing rate is greater than would be expected form just the surface thermal flux alone. As the magnitude of ΔT nears -10.0, the thermal flux from entrainment is greater than the surface thermal flux and net warming of the mixed layer occurs and freezing stops.

2. Model Sensitivity To Salinity Jump

Figure 10 shows the results of only varying the salinity of the deep layer, resulting in a change in the salinity jump, ΔS, between the layers. The general trend of the results are an increasing freezing rate with an increasing salinity jump, or increasingly negative ΔT.

For conditions where the salinity of the two layers is too close, $\Delta T > -.3$, there was an over turning of the water column and no freezing occurred. This occurs when the mixed layer density is increased by increasing the salinity to a point where its density is the same or greater than the deep layer.

When the salinity jump is increased, the freezing rate begins to level off. This occurs due to the decreasing heat flux at the base of the mixed layer. From equation (3.10), the thermal flux at the base of the mixed layer is a function of the entrainment velocity, W_e, and the temperature jump, ΔT. The temperature jump is not changing but the entrainment velocity is. From equation (3.14), the entrainment velocity, W_e, is a function of the inverse of the buoyancy difference, Δb. As the salinity difference increases the buoyancy difference increases and the entrainment velocity decreases. From equation (3.18), when the entrainment velocity decreases, the freezing rate increases.

Figure 11 shows the results of increasing the density jump to much higher levels. This shows the leveling off of the freezing rate at higher density jump values. The limit for this is the maximum freezing available, near $112.8x10^{-8}$ $\frac{m}{s}$, the situation where there is relatively no entrainment of warmer water and the full surface heat flux is converted into the production of ice. The large density difference between layers acts to virtually insulate the two layers from each other. This relative salinity difference can occur when fresh water runoff overlies more saline deeper water which has not been well mixed by wind stress.

3. Model Sensitivity To Temperature Jump

Figure 12 shows the results of varying only the temperature jump by varying only the deep water temperature. The general trend is for an increase in freezing rate with a lowering of the deep layer temperature, or ΔT gets more positive. The curvature of this curve is much more linear than the curves in Figures 10 and 11 because the effect

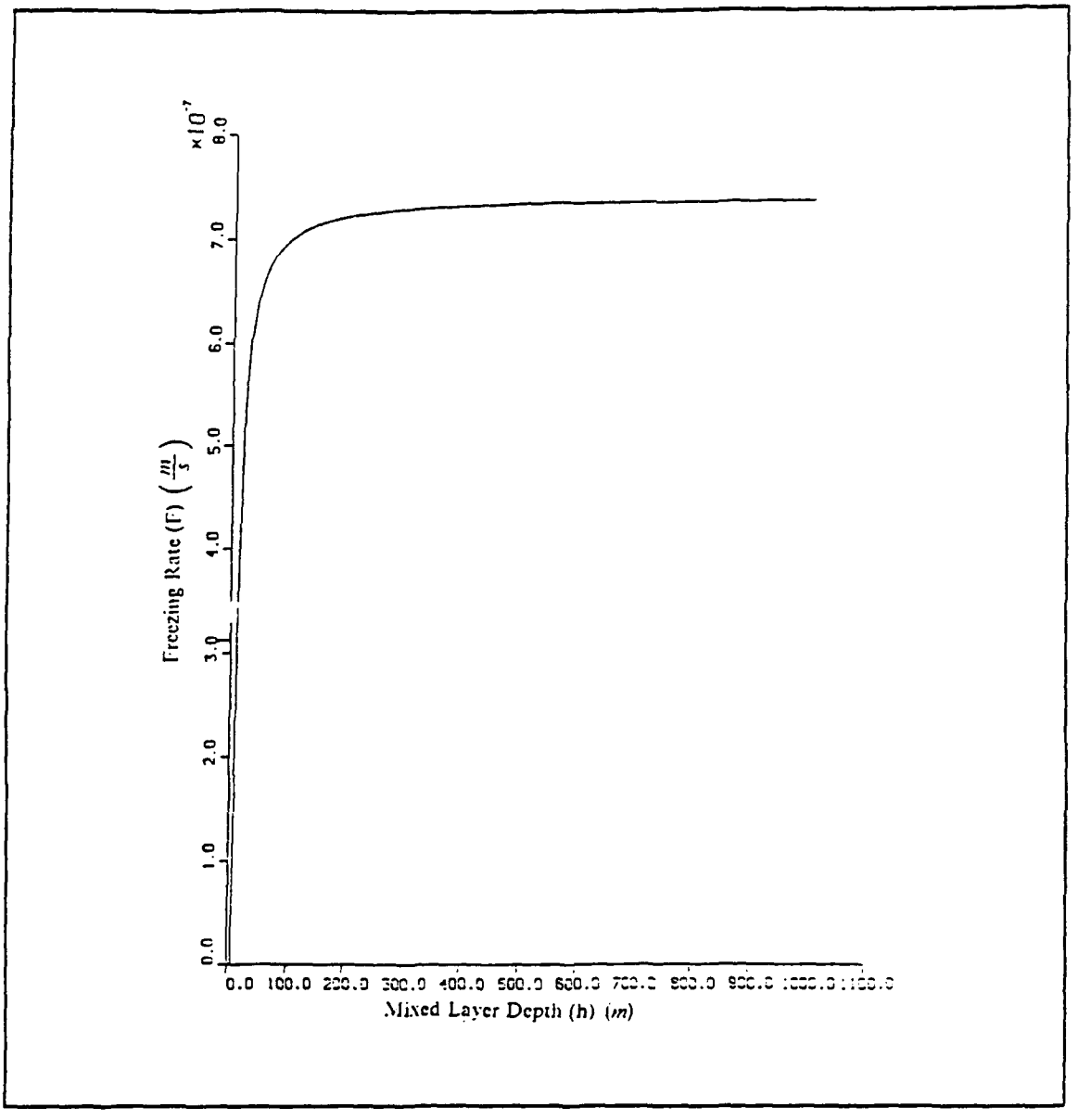

Figure 13. Freezing Rate as a Function of Mixed Layer Depth: Results of model runs where the mixed layer depth, h, is varied, without varying the other initial conditions or boundary conditions. The results show a rapid increase in freezing rate, F, as depth increases past 10 m to 150 m. This is from the decreasing effect of entrainment of warmer deep water from wind generated TKE as the depth increases.

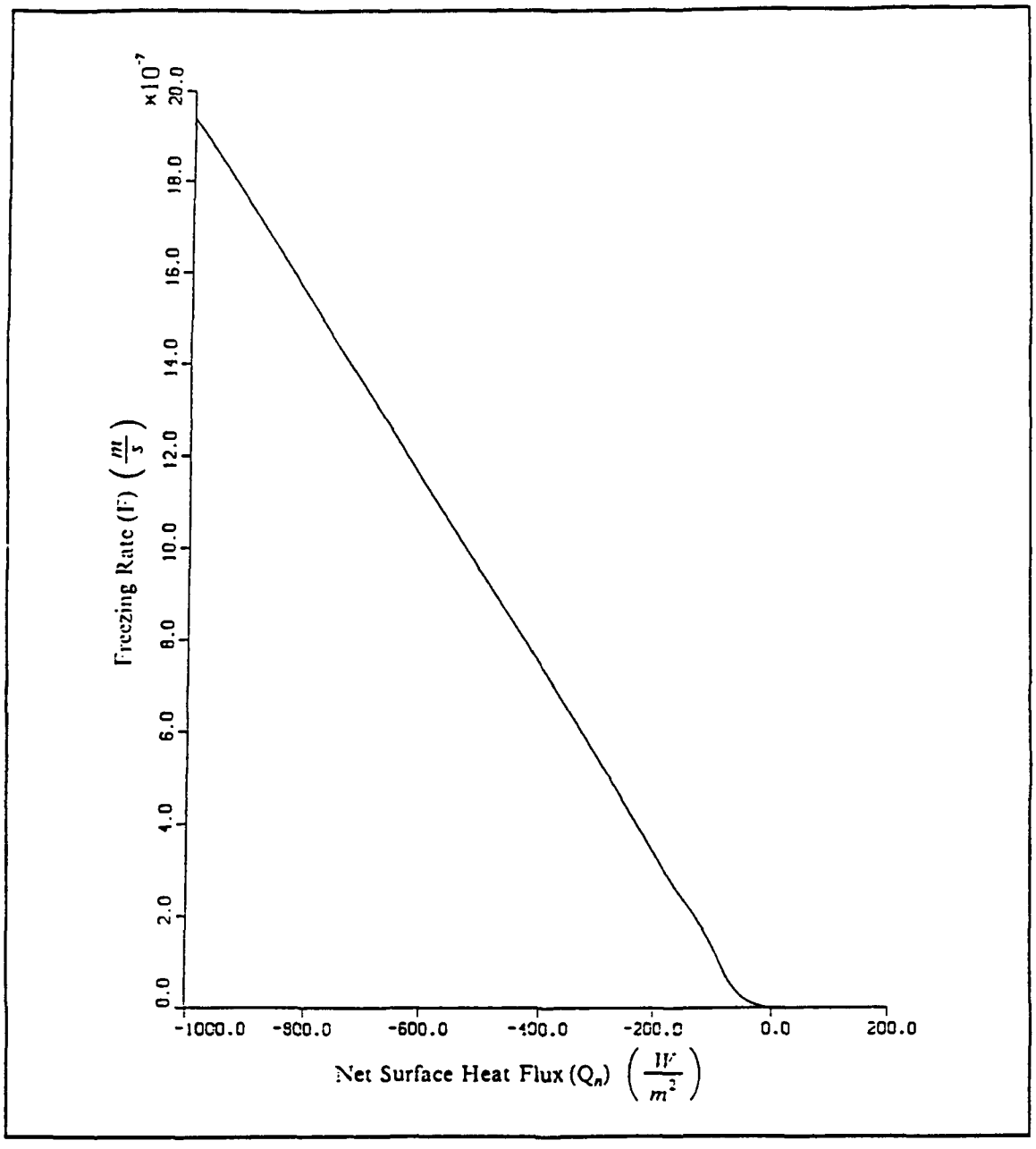

Figure 14. Freezing Rate as a Function of Surface Heat Flux: Results of model runs where the surface heat flux, Q_n is varied, without varying the other initial conditions or boundary conditions. The results show the near linear increase in freezing rate with an increase in upward heat flux out of the mixed layer.

of the temperature differences on Δb is so much less than the effect of a salinity difference from the small value of α. relative to β of $\frac{79.0}{2.56}$.

In the region of $\Delta T > 0$, the freezing rate is greater than the maximum attainable from just the surface heat flux. This could occur when a more saline deep layer is near its freezing temperature, which is colder than the mixed layer freezing temperature, and any entrainment of deep water actually increases the freezing rate. This can be seen from equation (3.18), when $\Delta T > 0$, the two thermal fluxes work together to increase the freezing rate.

At the other extreme, there is a ΔT so great that entrainment of the warmer water overpowers the surface heat flux and a warming of the mixed layer occurs. From equation (3.18) and under these model conditions of $\Delta T < -10.0$, the effect of $\Delta T\, W_e$, which is negative, is greater in magnitude than the surface thermal flux, $\frac{-Q_n}{\rho c_p}$, which is positive.

4. Model Sensitivity To Mixed Layer Depth

Figure 13 shows the results on the freezing rate of only varying the mixed layer depth. The general trend is for a rapidly increasing freezing rate when increasing the mixed layer depth from 3 *m* to 50 *m*, a gradual increase of freezing rate for mixed layer depths from 50 *m* to 175 *m*, and then a near asymptotic increase in the freezing rate for mixed layer depths greater than 175 *m*.

The rapidly increasing freezing rate for small values of mixed layer depth reflect the relative importance of the TKE generated by wind stress distributed over the mixed layer. From equation (3.14), when h is small, the $\frac{1}{\Delta b}\frac{C_1 u_*^3}{h}$ term is very large and varies inversely with mixed layer depth, h. This results in a large value for the entrainment velocity, W_e, which rapidly overpowers the thermal flux at the surface.

As the mixed layer depth increases the relative value of the $\frac{1}{\Delta b}\frac{C_1 u_*^3}{h}$ term is increasingly smaller and becomes less important in the freezing of the mixed layer and the freezing rate approaches that of the maximum possible freezing rate. This is reflected in the figure by the assymtotic approach to a constant value as h increases.

5. Model Sensitivity To Surface Heat Flux

Figure 14 shows the nearly linear relationship of the surface heat flux, Q_n and the freezing rate. The general trend is a linear increase in freezing rate as the surface

heat flux increases. When the surface heat flux is close to 0 or positive there is insufficient cooling to counter the entrainment flux that causes a net warming of the mixed layer.

From equation (3.14), the entrainment velocity is a nearly linear function of Q_n since h and u_*^3 are held constant. From equation (3.18), the freezing rate should approximate a linear function since W_e will be a nearly linear function of Q_n, and ΔT is held constant.

B. NON-DIMENSIONAL PARAMETERIZATION

1. Formation of Non-Dimensional Parameters

To understand the relationship between many varying variables it is useful to organize the variables into non-dimensional parameters that can give significant information when analyzed. Non-dimensional parameters can be formed from the various forcing variables and boundary variables that will simplify the understanding of the mixed layer interaction problem.

2. Freezing Efficiency Parameter

The first parameter is a freezing efficiency parameter. This is the ratio of the freezing rate to the heat loss from the surface, or the maximum heat loss normally available for freezing. The parameter will be called E^*, for Efficiency. To formulate the E^* parameter, the freezing rate, F, in $\frac{m}{s}$, will be divided by the maximum freezing available, $\frac{Q_n}{L_f\rho}$, which is also in $\frac{m}{s}$. Therefore E^* is defined as

$$E^* = \frac{F}{\frac{Q_n}{L_f\rho}}$$

To make the E^* positive under normal conditions, the negative of Q_n will be used.

$$E^* = \frac{F\rho L_f}{-Q_n} \tag{4.1}$$

This parameter has a value of unity when all the energy given up as heat flux from the surface is used in the production of ice. Whenever this parameter is less than 1.0, some of the heat flux from the surface has been countered by a heat flux into the mixed layer by entrainment of warmer water from below. The only way the absolute value of this parameter should be greater than 1.0, would be when a less saline mixed layer overlies a more saline deeper layer that is near freezing temperature, and entrainment cools the mixed layer. This causes a negative heat flux across the lower boundary of the mixed layer, and it would give a value of $E > 1.0$.

3. Forcing Ratio Parameter

A ratio of the wind forcing, which provides TKE for mixing and entrainment, to the buoyancy flux at the surface, also providing TKE for mixing and entrainment, would provide information about the relative magnitudes of the two TKE-generating factors. This parameter will be called F, for forcing, and can be defined as:

$$F^* = \frac{\frac{u_*^3}{h}}{\overline{b'w'}(0)}$$

or

$$F^* = \frac{u_*^3}{h\overline{b'w'}(0)} \tag{4.2}$$

When $F < 1.0$ the buoyancy flux from freezing dominates the wind stress at the surface. This can occur when the mixed layer is deep, the wind is low, or rapid freezing occurs from a large heat flux to the atmosphere.

When $F > 1.0$ then the wind forcing dominates the buoyancy flux at the surface. This occurs when the wind speed is high, the mixed layer is shallow, or there is little freezing due to entrainment of much warmer water or due to very little heat flux from the mixed layer to the atmosphere.

4. Stability Ratio Parameter

A ratio of the two parameters which affect the stability of the mixed layer over the deeper layer give information about the overall stability of the two systems. Under normal freezing conditions in the Arctic, a cooler layer over a warmer layer decreases stability or buoyancy of the mixed layer. A less saline layer over a more saline layer increases stability or buoyancy of the mixed layer. The ratio is a measure of the effectiveness of the salinity jump in maintaining stability over the temperature jump's effectiveness in decreasing stability. The stability ratio will be called S^*, and can be formed by dividing the buoyancy due to the temperature jump over the buoyancy due to the salinity jump:

$$S^* = \frac{\alpha g \Delta T}{\beta g \Delta S} = \frac{\alpha \Delta T}{\beta \Delta S} \tag{4.3}$$

When $S^* = 1.0$, the two layer are neutrally buoyant, meaning there is no density difference between the two layers even though there may be a salinity and temperature difference between the layers. In this case, the model is computationally unstable and would predict the complete overturning of the water column.

When $S^* > 1.0$, the temperature jump is dominant and entrainment may lead to a warming of the mixed layer and may stop freezing altogether.

A density ratio has been used by Schmitt (1918, 1987, 1988) and others to described domains where thermohaline staircases could be found. Schmitt (1988) defines his ratio the density ratio, R_ρ , but used T_z = vertical temperature gradient, instead of the temperature jump, ΔT, and S_z = vertical salt gradient, instead of the salinity jump, ΔS. From his research many examples of thermohaline staircases have been found and documented. He has found that staircases are most likely when $1.0 > R_\rho > 1.6$.

When $S^* \ll 1.0$, the salinity jump dominates and entrainment would contribute very little to a heat flux from the deep layer to the mixed layer. The entrainment salinity flux into the mixed layer would have but a slight impact by lowering the freezing temperature. This condition would lead to the most efficient freezing situations.

Table 6. NON-DIMENSIONAL PARAMETERS

Non-Dimensional Variable	Formula	Significance
E^*	$\frac{\rho L_f F}{-Q_n} = \left[\frac{F}{-\frac{Q_n}{\rho L_f}} \right]$	Efficiency of freezing. Actual freezing rate over the thermal energy lost from the mixed layer that is available for freezing. A value near one indicates very little energy was entrained from the deep layer.
F^*	$\frac{u_*^3}{h\overline{b'w'(0)}} = \left[\frac{\frac{u_*^3}{h}}{\overline{b'w'(0)}} \right]$	Turbulence Forcing Ratio. Turbulence forcing from wind stress over turbulence forcing from surface buoyancy flux.
S^*	$\frac{\alpha \Delta T}{\beta \Delta S} = \frac{\alpha g \Delta T}{\beta g \Delta S}$	Stability ratio. Ratio of buoyancy change due to a change in temperature over the buoyancy change due to a change in salinity. The smaller the value of the parameter the greater the stability between layers.

When $S^* < 0$, the temperature and salinity density differences both contribute to decreasing the buoyancy. The only physically possible case would be to have warmer and less saline water over cooler and more saline water. If the mixed layer were near freezing, any entrainment could increase the freezing. This is the situation mentioned above for the case when $E^* < 0.0$ also. This could occur when fresh water run off encounters calm very saline salt water close to the coast and spreads out as a thin layer over the salt water. The physical process of conduction has been ignored in this model, which would be the major heat transfer process in this situation, and this situation would not be handled well by this model. Table 6 summarizes the non-dimensional parameters considered in this study.

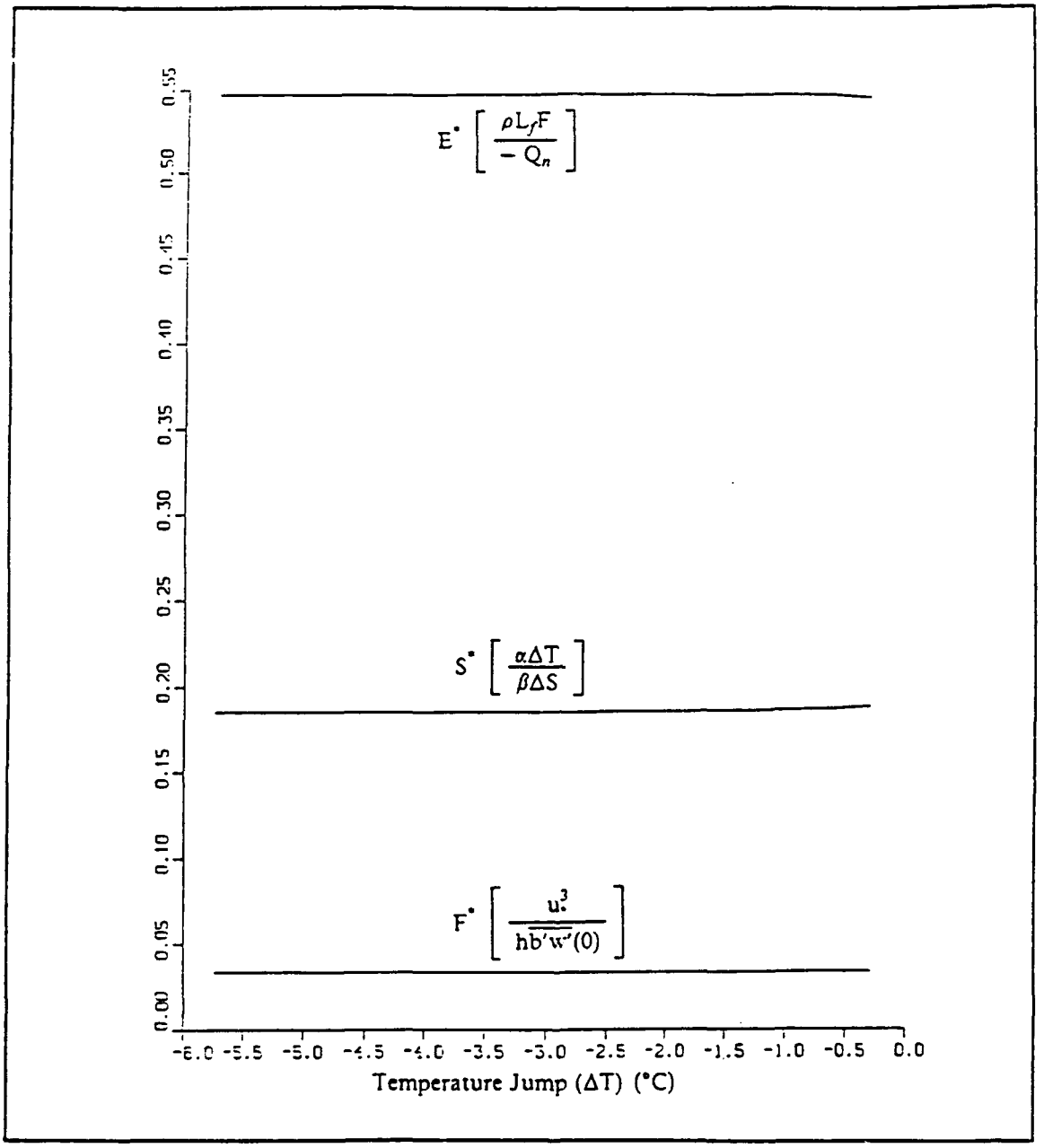

Figure 15. Model Sensitivity to S* Variable Changes vs T: Model results when F^* and S^* are held constant, but the variables within S^* are varied. Here, the freezing efficiency, E^*, is constant as are the other parameters, while ΔT has been changed.

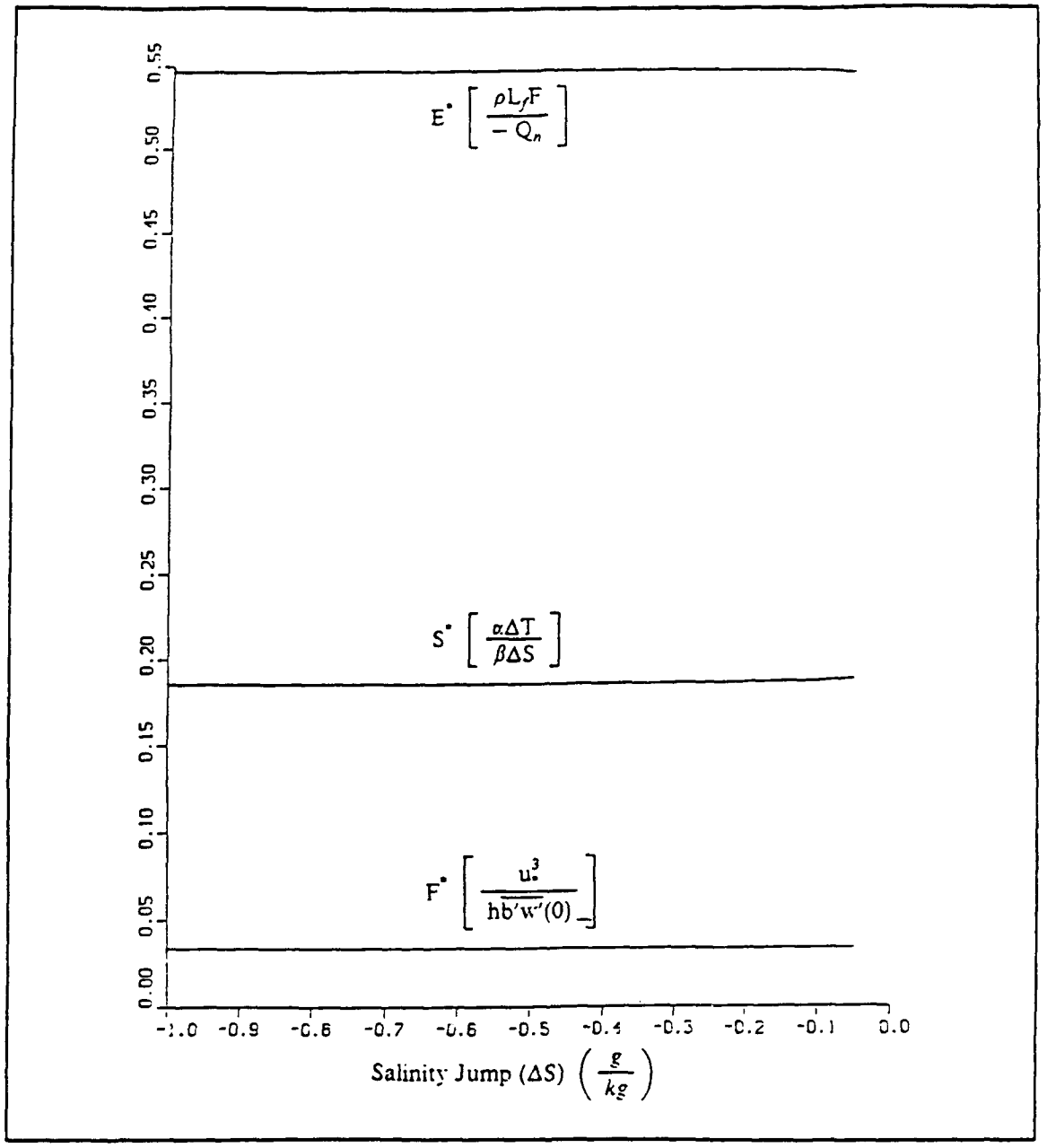

Figure 16. Model Sensitivity to S* Variable Changes vs S: Model results when F^* and S^* are held constant, but the variables within S^* are varied. Here, the freezing efficiency, E^*, is constant as are the other parameters, while ΔS has been changed.

Table 7. VALUES FOR S* SENSITIVITY MODEL RUNS

Variables	Value Pairs Used
ΔT	-.287, -.574, -1.15, -1.72, -2.01, -2.30, -2.58, -2.87, -3.44, -4.02, -4.59, -5.16, -5.74
ΔS	-0.05, -0.10, -0.20, -0.30, -0.35, -0.40, -0.45, -0.50, -0.60, -0.70, -0.80, -0.90, -1.00

C. MODEL SENSITIVITY TO NON-DIMENSIONAL PARAMETERS

To determine if most of the model variability could be accounted for by the three non-dimensional parameters, model runs were performed where the resultant non-dimensional parameters were not changed, but the individual variables in the parameters were varied.

1. Model Sensitivity to S* Variable Changes

For this study the two model variables comprising S^*, ΔT and ΔS, were varied so as to keep the resultant value of S^* constant. Table 7 lists the values used for ΔT and ΔS for these model runs. The values for all the other variables and initial conditions are as in listed in Table 5 under normal values.

Figure 15 and 16 show the results of these runs where the model variables are kept constant except for varying only the two variables which make up S^*. Figure 15 shows the results relative to the various values of ΔT. There is a near constant value for F^*, S^*, and E^* as the values of ΔT varied. Figure 16 show the results relative to the various values of ΔS. Again there are near constant values for F^*, S^*, and E^* as ΔS is varied. For example, in a real situation the expected maximum freezing rate would be the same for the conditions of $T = -1.8687$, $S = 34.5$, $T_o = -1.582$, $S_o = 34.55$, as well as for the other extreme where the conditions are $T = -1.8687$, $S = 34.5$, $T_o = 3.869$, $S_o = 35.5$.

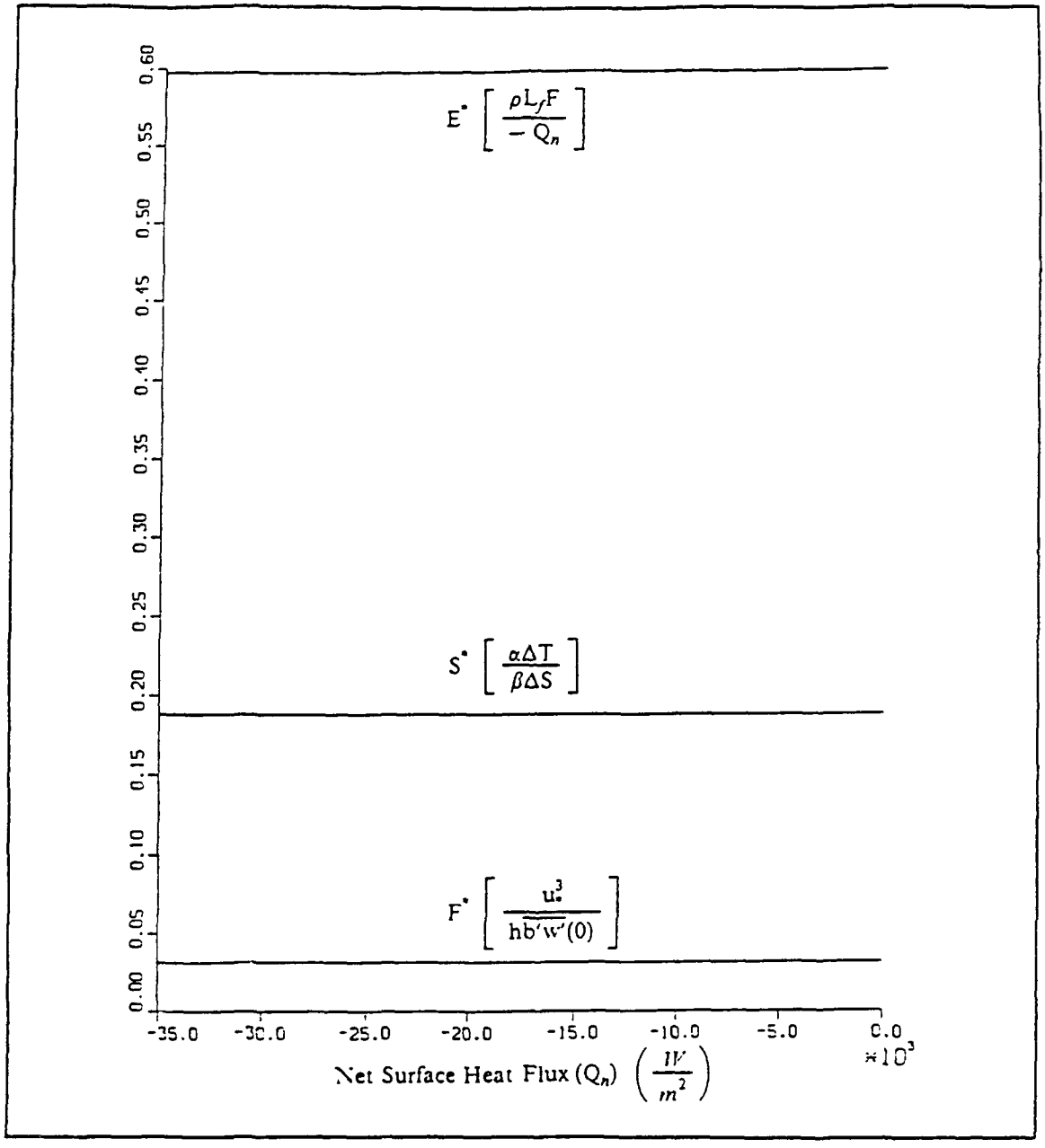

Figure 17. Model Sensitivity to F* Variable Changes vs Q: Model results when F^* and S^* are held constant, but two of the variables within F^*, Q_n and h, are varied. Here, the freezing efficiency, E^*, is constant as are the other parameters, while Q_n has been changed.

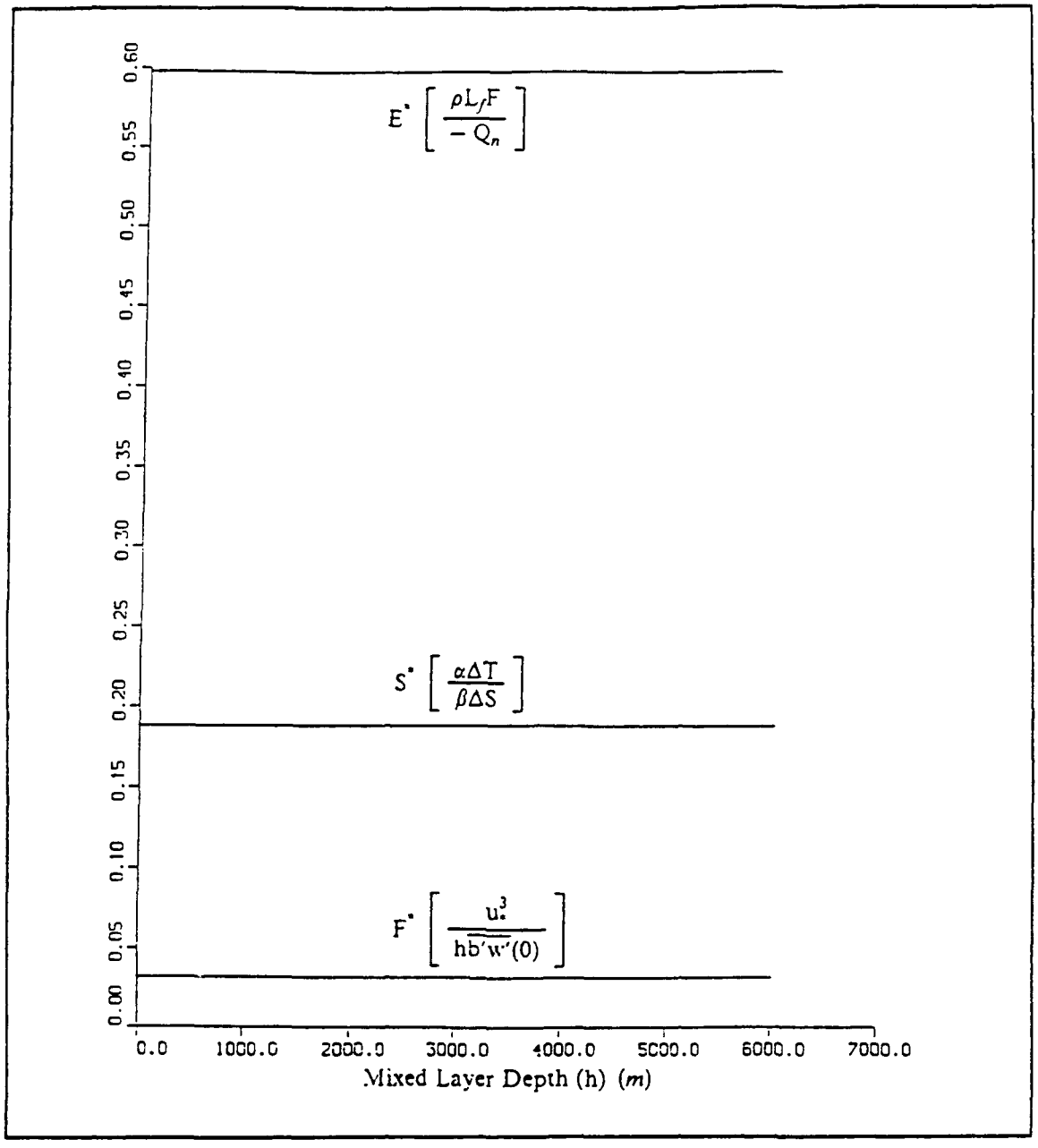

Figure 18. Model Sensitivity to F* Variable Changes vs h: Model results when F and S^* are held constant, but two of the variables within F, Q_n and h, are varied. Here, the freezing efficiency, E^*, is constant as are the other parameters, while h has been changed.

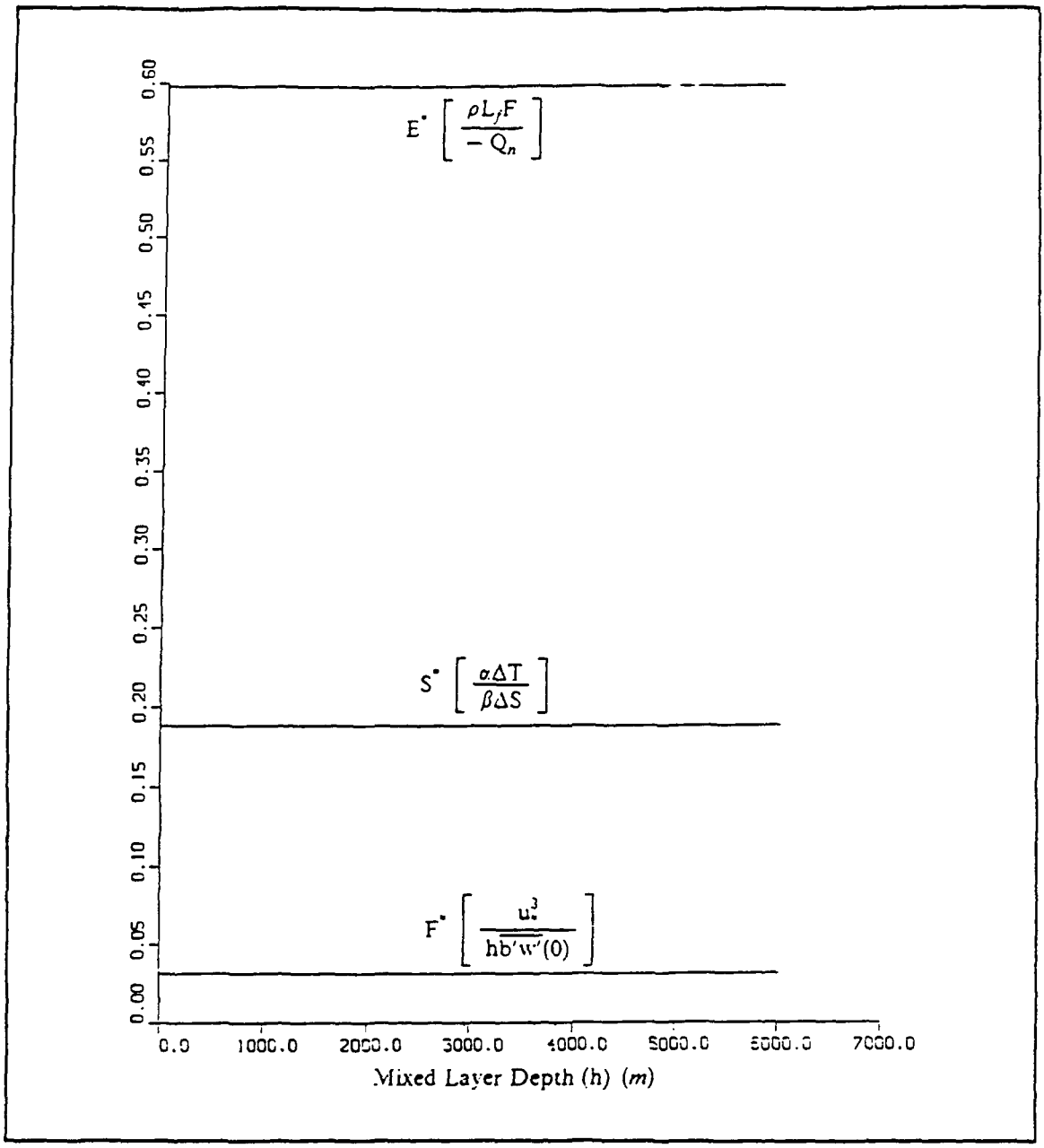

Figure 19. Model Sensitivity to F* Variable Changes vs h: Model results when F^* and S^* are held constant, but two of the variables within F^*, h and u_*^3, are varied. Here, the freezing efficiency, E^*, is constant as are the other parameters, while h has been changed.

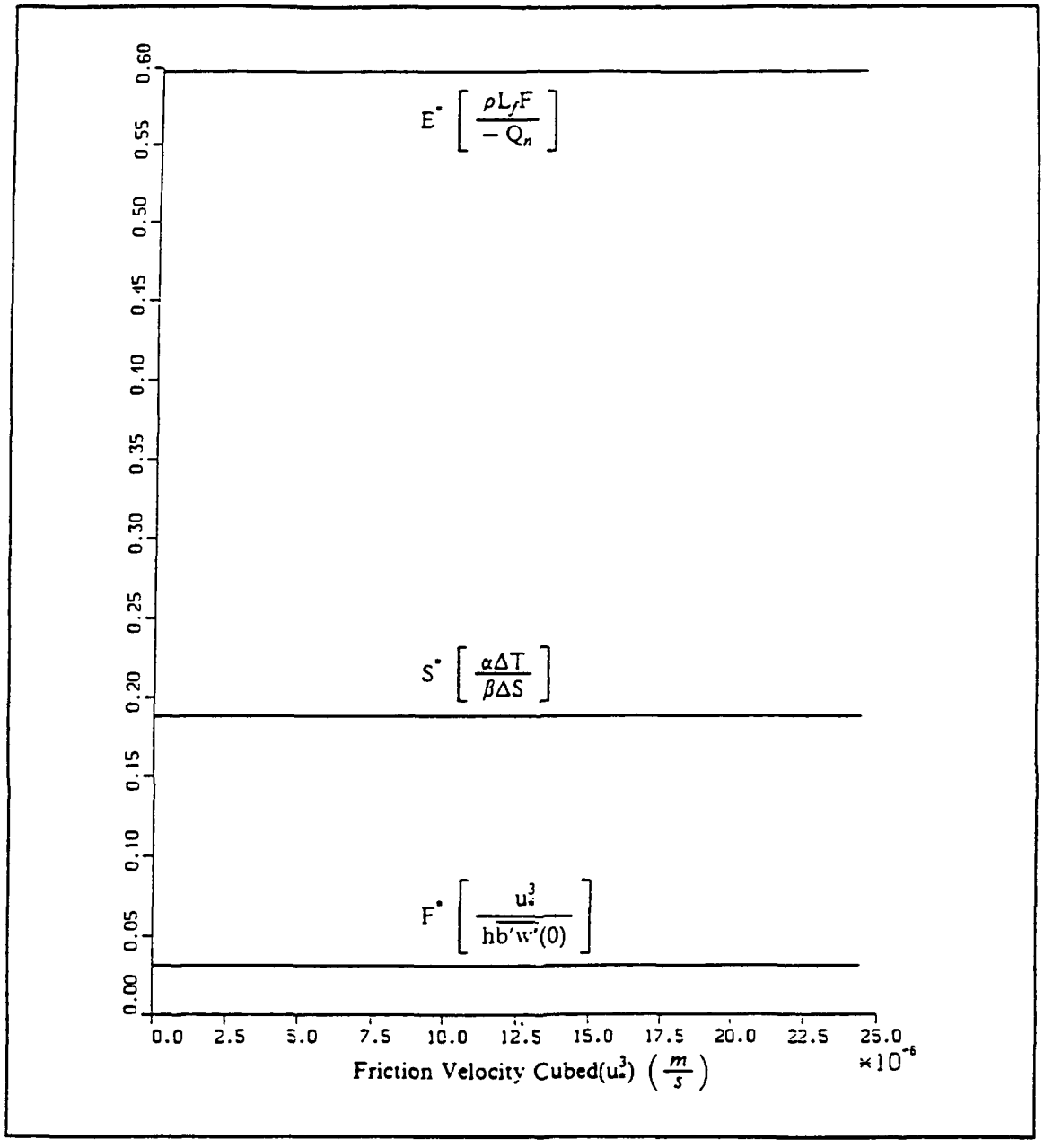

Figure 20. Model Sensitivity to F* Variable Changes vs u*: Model results when F^* and S^* are held constant, but two of the variables within F^*, h and u_*^3, are varied. Here, the freezing efficiency, E^*, is constant as are the other parameters, while u_*^3 has been changed.

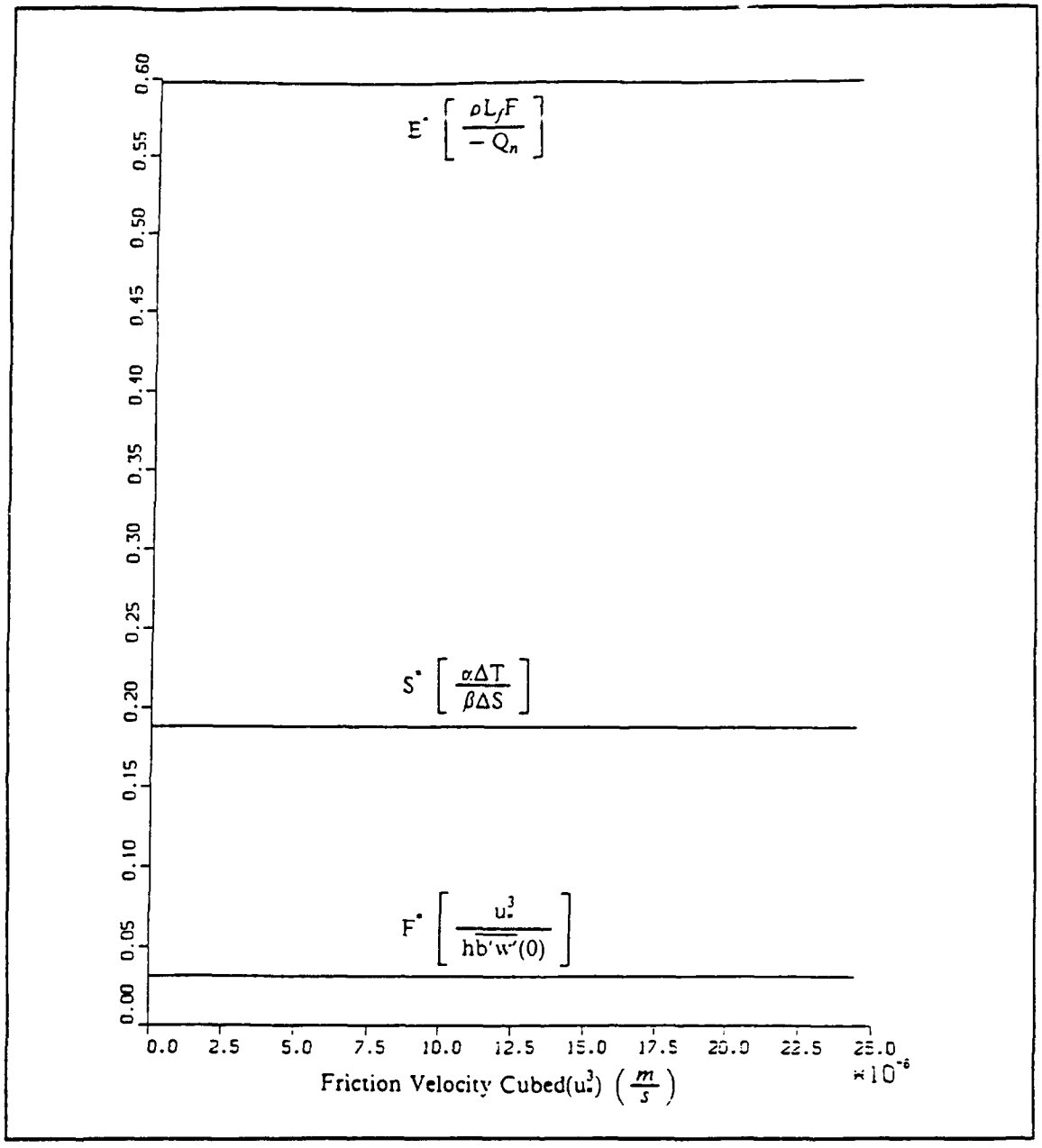

Figure 21. Model Sensitivity to F* Variable Changes vs u*: Model results when F^* and S^* are held constant, but two of the variables within F^*, u_*^3 and Q_n, are varied. Here, the freezing efficiency, E^*, is constant as are the other parameters, while u_*^3 has been changed.

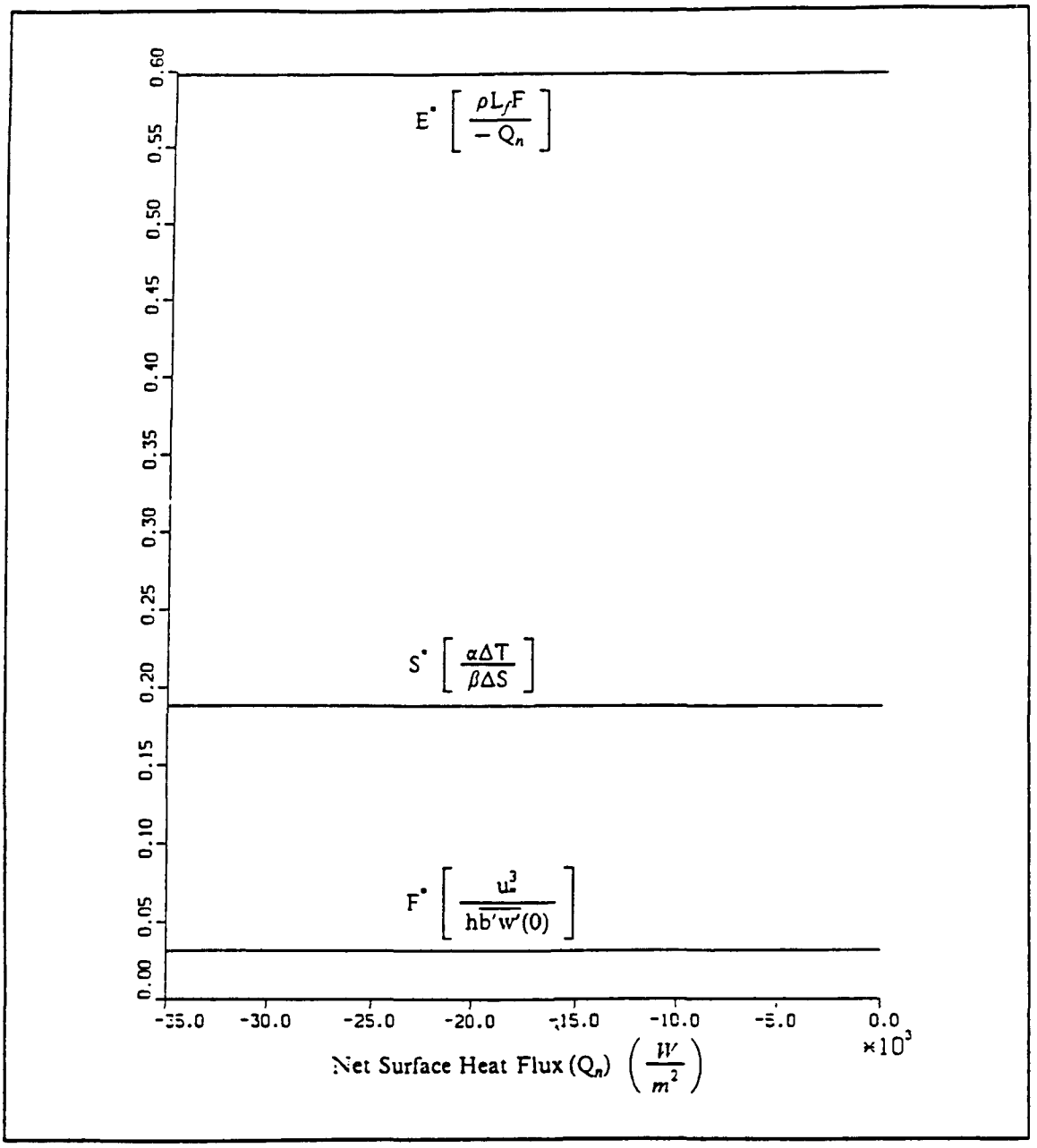

Figure 22. Model Sensitivity to F* Variable Changes vs Q: Model results when F^* and S^* are held constant, but two of the variables within F^*, u_*^3 and Q_n, are varied. Here, the freezing efficiency, E^*, is constant as are the other parameters, while Q_n has been changed.

Table 8. VALUES FOR F* SENSITIVITY MODEL RUNS

Variables Changed	Variable	Normal Value	Multiplier Value Pairs Used
Q_n , h	Q_n	$-350 \frac{W}{m^2}$	0.01, 0.02, 0.05, 0.10, 0.20, 0.50, 1.00, 2.00, 5.00, 10.0, 20.0, 50.0, 100.
	h	$60 \frac{m}{s}$	100., 50.0, 20.0, 10.0, 5.00, 2.00, 1.00, 0.50, 0.20, 0.10, 0.05, 0.02, 0.01
h , u^3	h	$60 \frac{m}{s}$	0.01, 0.02, 0.05, 0.10, 0.20, 0.50, 1.00, 2.00, 5.00, 10.0, 20.0, 50.0, 100.
	u^3	$2.44x10^{-6} \frac{m^3}{s^3}$	0.01, 0.02, 0.05, 0.10, 0.20, 0.50, 1.00, 2.00, 5.00, 10.0, 20.0, 50.0, 100.
u^3 , Q_n	u^3	$2.44x10^{-6} \frac{m^3}{s^3}$	0.01, 0.02, 0.05, 0.10, 0.20, 0.50, 1.00, 2.00, 5.00, 10.0, 20.0, 50.0, 100.
	Q_n	$-350 \frac{W}{m^2}$	0.01, 0.02, 0.05, 0.10, 0.20, 0.50, 1.00, 2.00, 5.00, 10.0, 20.0, 50.0, 100.

2. Model Sensitivity to F* Variable Changes

For this study the three model variables comprising F , u^3, h and Q_n , were varied so as to keep the resultant values of F constant.

Table 8 lists the multiplier pairs that were used on two of the three variables while the third was kept constant. For each of the model runs, the normal values of two of the variables are multiplied by constants while the normal value of the third variable is used. For example, the value used for Q_n is .01 times its normal value, the value used for h is 100 times its normal value, and the value used for u^3 is its normal value. The resultant value of hQ_n remains constant as Q_n and h are varied.

Figure 17 and 18 show the results when only Q_n and h are varied, with u^3 held constant. Figure 17 shows the results as a function of Q_n. Figure 18 shows the results as a function of h. Both figures show no change in F as the variables Q_n and h are varied.

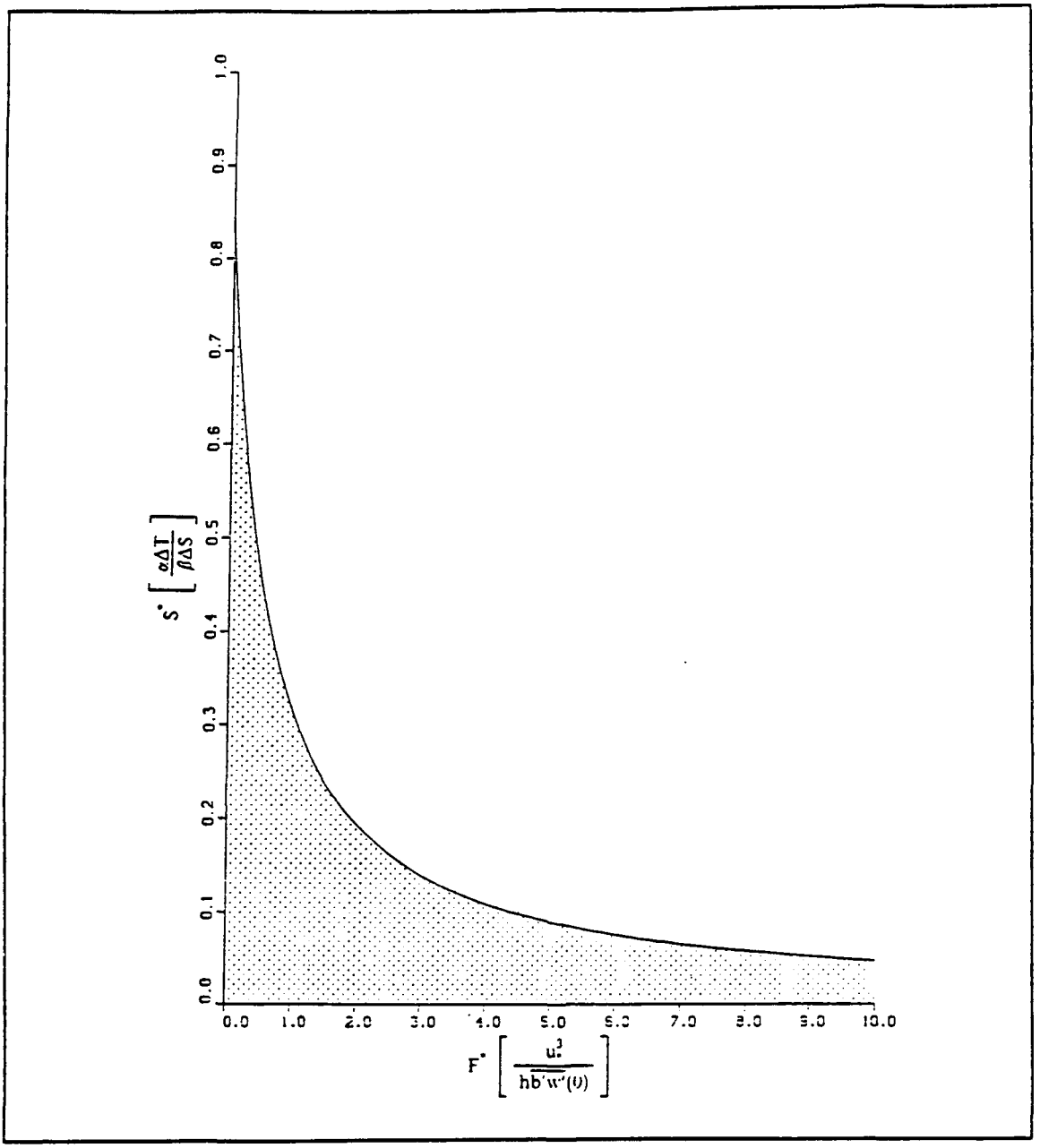

Figure 23. **The Limit of Freezing:** The solution dividing freezing and non-freezing regimes in terms of S^* and F^* The freezing regime is the hatched area close to the origin. In this area the mixed layer in capable of freezing with time. Outside it is not possible for the mixed layer to freeze until some other forcing or stability parameters are changed.

Figure 19 and 20 show the results when only h and u_*^3 are varied and Q_n is held constant. Figure 19 shows the results as a function of the values of h. Figure 20 shows the results as a function of the values of u_*^3. Both figures show no change in F^* as the variables h and u_*^3 are varied.

Figure 21 and 22 show the results when only u_*^3 and Q_n are varied while h is held constant. Again the results show no variation of F^* through the range of values used.

These results demonstrate the value of using the three non-dimensional parameters to study the result of model runs. Only variations in these parameters will be considered and not how those variations were obtained. This gives families of solutions vice thousands of individual time-dependent solutions, simplifying the understanding of how the individual variables affect any prediction.

D. THE LIMIT OF FREEZING

The regime where freezing cannot occur can be investigated using the non-dimensional parameters. Appendix A contains the derivation of a relationship separating the freezing/non-freezing regimes:

$$S^* = \frac{1}{1 + C_1 F^* + C_2} \tag{4.4}$$

This is a relationship of only four parameters: the forcing parameter, the stability parameter, and the two model constants. The reliability of the model is dependent on realistic model constants, C_1 and C_2. These two model constants represent the relative importance of the two factors used in computing the entrainment velocity, W_e, equation (3.14).

Figure 23 shows the delineation between the freezing domain, the hatched area in the figure, and the domain of no freezing, the white area in the figure, as functions of F^* and S^*. From the figure there is a definite maximum value of S^* where freezing can occur. Any higher value of S^*, a regime where the Δb is approaching 0, will result in warming of the mixed layer. Equation (4.4) also indicates that for any positive value of F^* there is a S^* where freezing can occur. For high values of F^* this equates to situations where there are very large salinity jumps. Since the coefficient of salinity contraction is so much larger than the coefficient of thermal expansion, this regime is

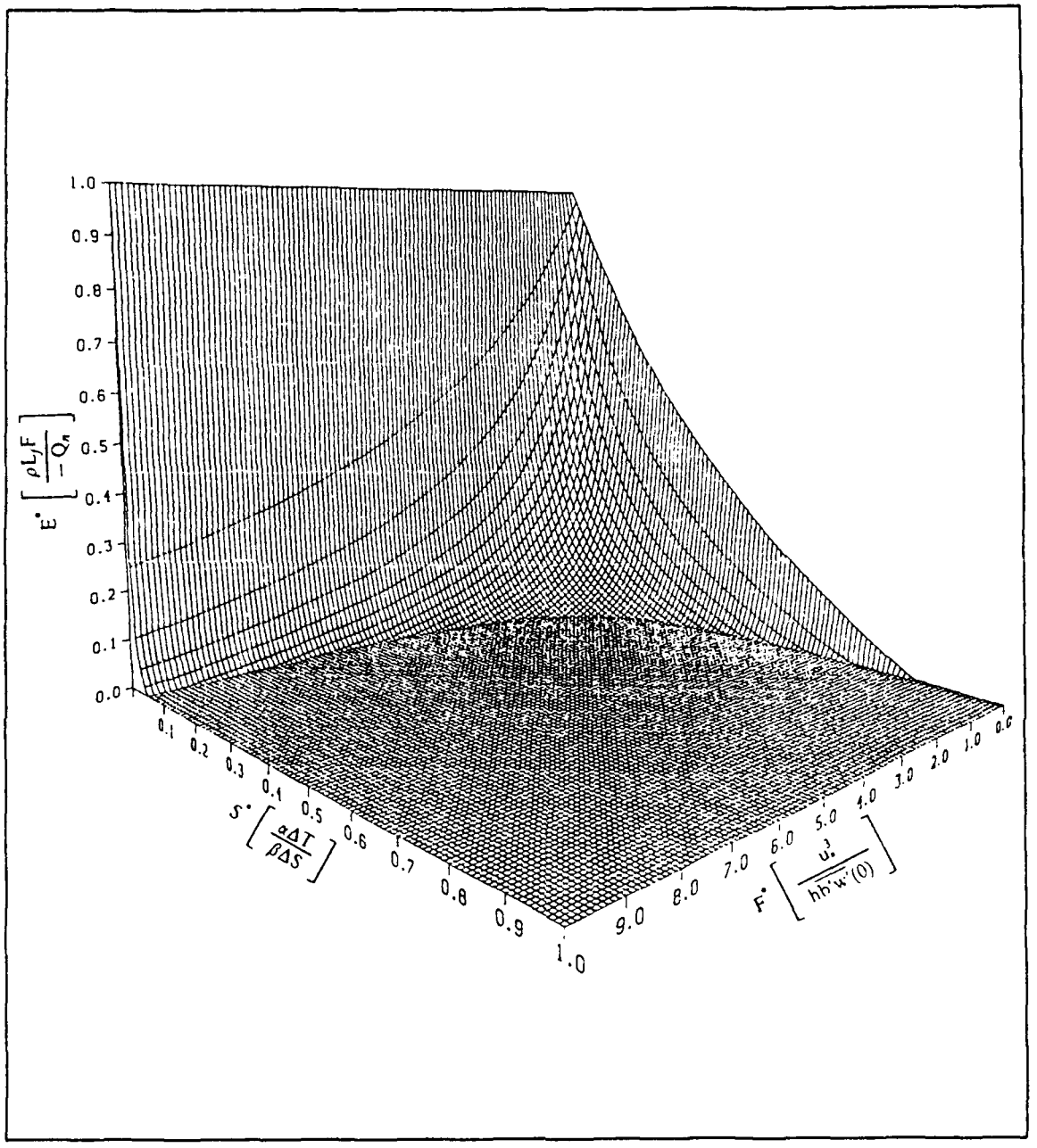

Figure 24. Freezing Efficiency as a function of Forcing and Stability: The graphical depiction of equation (4.7) where the maximum freezing, related to the Freezing Efficiency, E^*, is depicted as a surface above the F^*xS^* plane. For various conditions of forcing terms which show up in the F^* and E^* terms, and stability terms, accounted for in the S^* term, a maximum freezing rate can be determined from the E^* term.

not rare, and it occurs frequently is areas where there has been fresh water mixed into the mixed layer, i.e. the northern coasts of northern hemisphere continents where there is river run off and seasonal ice pack melting.

E. FREEZING EFFICIENCY RELATIONSHIP TO FORCING AND STABILITY

A relation can be obtained between the non-dimensional parameter E^*, the forcing parameter, F^*, the stability parameter, S^*, the model constants, C_1 and C_2, and the estimated amount of salt, or brine, extracted by freezing. Appendix B derives a relationship between the freezing rate, F, and other model variables and constants and is:

$$F = \left[\frac{ - \frac{Q_n}{\rho L_f} \left[\frac{S^* - 1}{S_*} + C_2 \right] + C_1 \frac{c_p}{L_f \alpha g} \frac{u_*^3}{h} }{ \left[\frac{S^* - 1}{S_*} \right] - C_2 \frac{\beta}{\alpha} (S - S_i) \frac{c_p}{L_f} } \right] \tag{4.5}$$

Appendix C derived an expression for $\frac{u_*^3}{h}$ in terms of other model variables and is:

$$\frac{u_*^3}{h} = \frac{Q_n}{\rho L_f} F^* g \left[\frac{ \frac{S^* - 1}{S^*} \left(\alpha \frac{L_f}{c_p} + \beta (S - S_i) \right) }{ \frac{c_p}{L_f} \frac{\beta}{\alpha} (S - S_i)(C_1 F^* + C_2) - \frac{S^* - 1}{S^*} } \right] \tag{4.6}$$

Using equations (4.5) and (4.6), Appendix D derived an expression for E^*

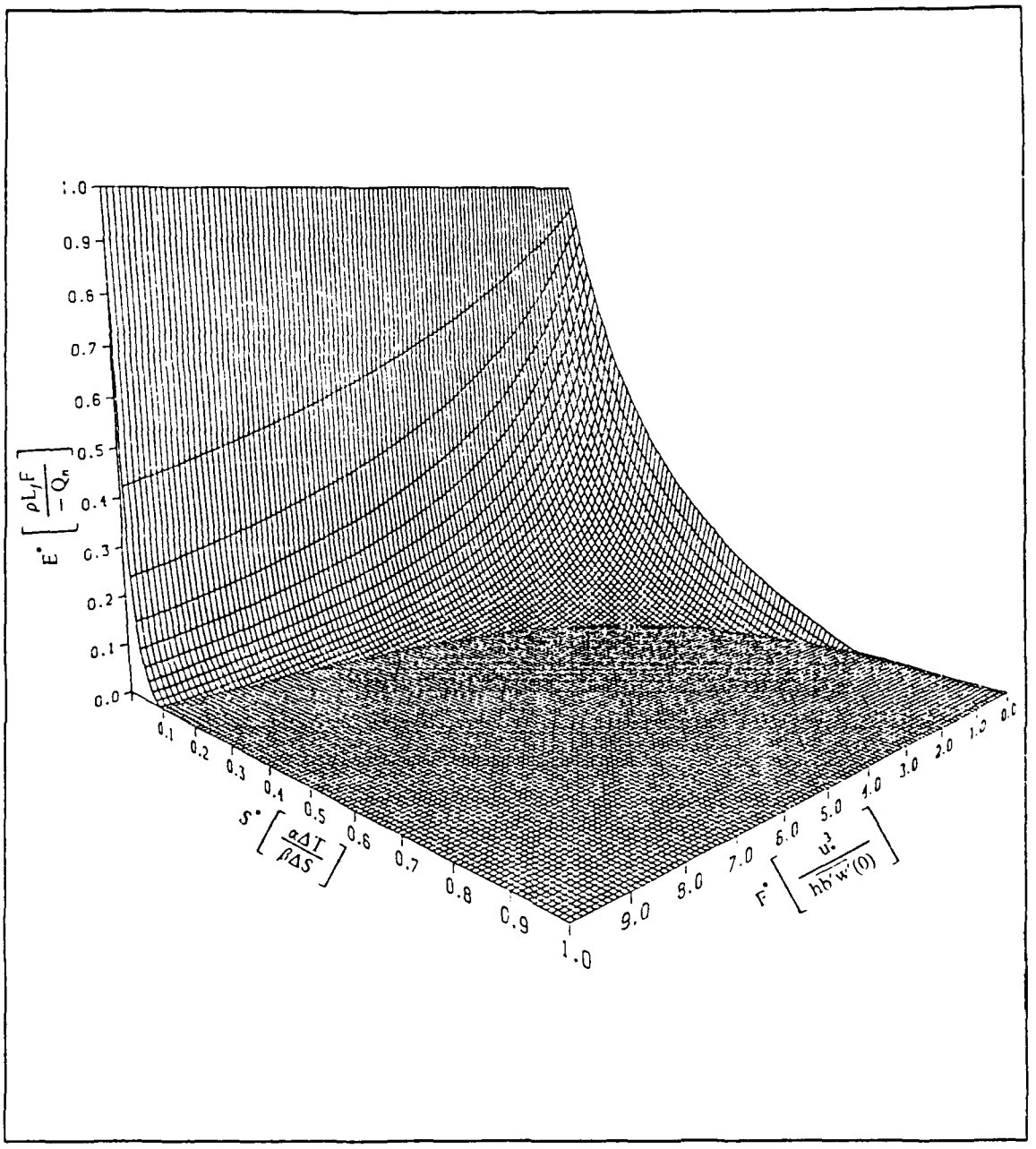

Figure 25. Freezing Efficiency for C1 = 1. and C2 = .4: The graphical solution for Freezing Efficiency with the model constants changed to $C_1 = 1.0$ and $C_2 = 0.4$.

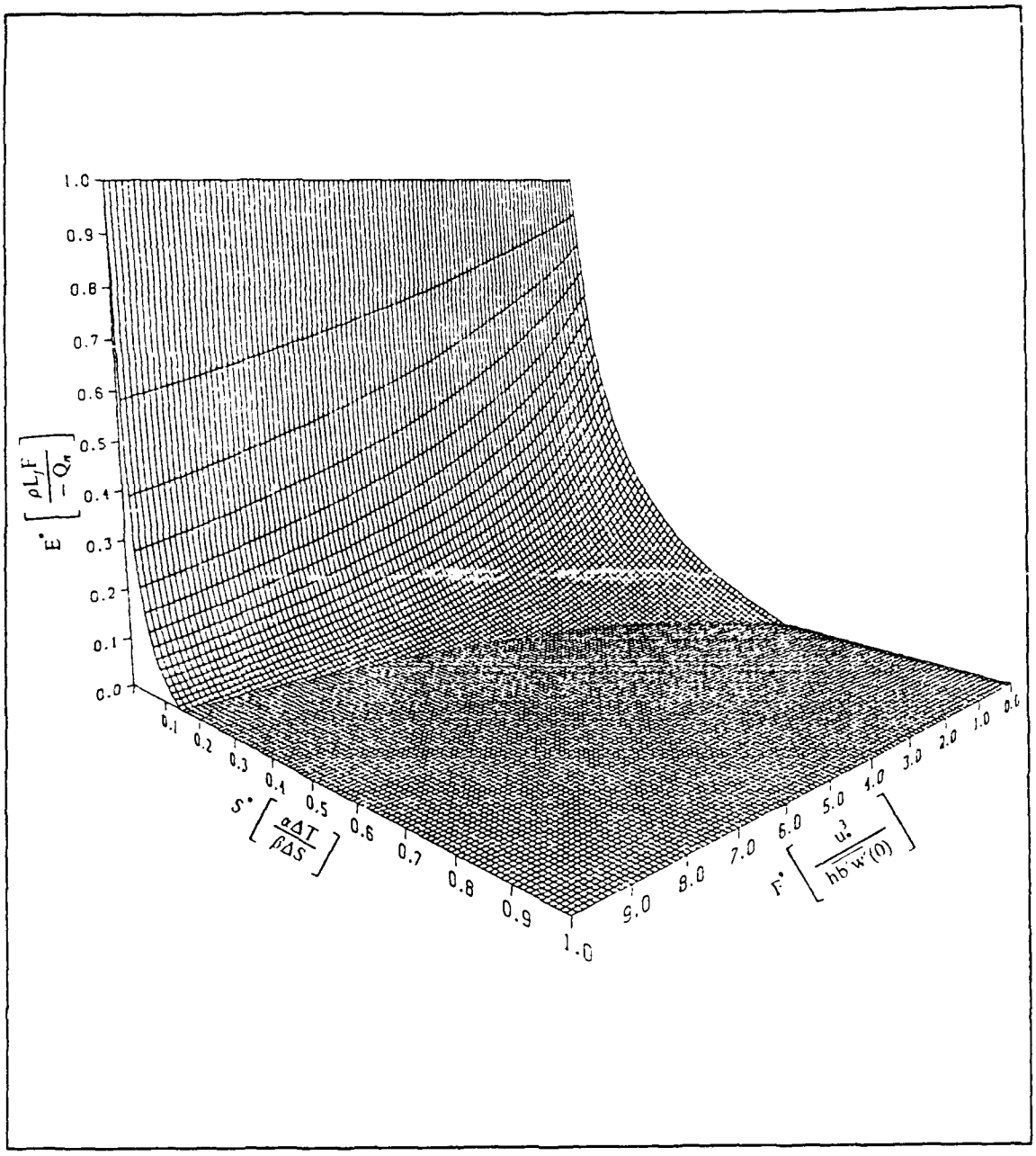

Figure 26. Freezing Efficiency for C1 = .5 and C2 = .8: The graphical solution for Freezing Efficiency with the model constants changed to $C_1 = 0.5$ and $C_2 = 0.8$.

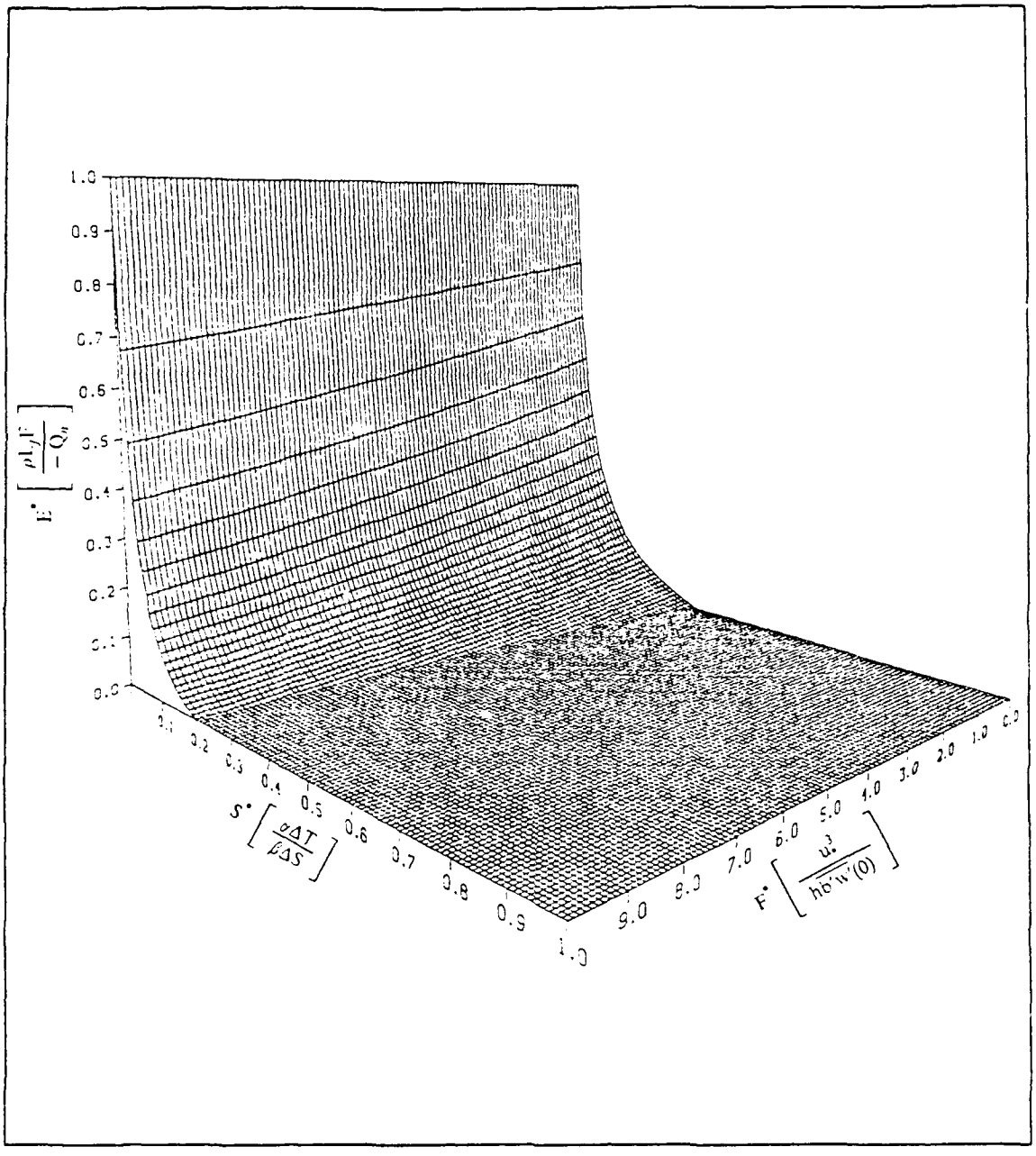

Figure 27. Freezing Efficiency for C1 = .2 and C2 = 2.: The graphical solution for Freezing Efficiency with the model constants changed to $C_1 = 0.2$ and $C_2 = 2.0$.

$$E^* = \frac{S^{*2}\left(F^*(C_1C_2LB - C_1) + (1 + C_2)(C_2LB - 1)\right) + S^*(F^*C_1 + 2 + C_2 - C_2LB) - 1}{S^{*2}\left((1 - C_2LB)(F^*C_1LB + C_2LB - 1)\right) + S^*(2 - C_1LBF^* - 2C_2LB) - 1} \quad (4.7)$$

where

- $L = \frac{c_p}{\alpha L_f}$
- $B = \beta(S - S_i)$

Figure 24 is a graphical representation of equation (4.7) in S^* x F^* x E^* space. This figure represents the maximum freezing that can be expected from any condition defined in the F^* x S^* plane.

From Figure 24, when S^* is near zero, there can be freezing for any situation where there is a heat flux up out of the surface of the mixed layer. Also, for lower values of F^* a wider range of salinity/temperature combinations will be able to produce sea ice.

When the S^* is higher than .84, there is no regime where freezing can occur because there is relatively no stability/buoyancy left between the two layers and complete overturing of the water column will occur first.

Figures 25, 26, and 27 show the effect changing the model constants , C_1 and C_2, has on the model output. From equation (3.14), as C_1 decreases in significance relative to C_2 , the effect of TKE generation from wind stress decreases and the magnitude of F^* becomes less significant. This can be seen in equation (E.7) where every F^* is multiplied by a C_1 term. As the value of C_1 decreases the effect F^* has on E^* vanishes. There is only a slight change in E^* as F^* increases in Figure 27. It does appear that the volume under the surface has remained near constant, as the decrease in E^* near F^*=0 has resulted in an increase in E^* at higher values of F^*.

V. SUMMARY

A. CONCLUSIONS

This study has investigated the relationships of the variables which define and affect mixed layer dynamics and thermodynamics with regard to the onset of freezing of sea ice. The mixed layer and underlying water column is modeled as a simple one-dimensional two layer system. The salient time dependent variables are mixed layer temperature, mixed layer salinity, mixed layer depth, and mixed layer buoyancy. Functions that relate the forcing terms and boundary values are the entrainment velocity function, and the freezing rate function.

Model runs studied the sensitivity of the model to varying only one parameter. These parameters included the wind stress, the surface heat flux, the temperature or salinity jump between the mixed layer and the deep layer, and the mixed layer depth. These studies showed:

- Increasing only the upward surface heat flux, Q_n, resulted in a nearly linear increase in freezing rate.
- Increasing the wind stress term, u^3, resulted in a nearly linear decrease in freezing rate until only a net warming of the mixed layer was possible.
- Increasing the temperature jump, ΔT, resulted in a non-linear decrease in freezing rate until only a net warming of the mixed layer was possible.
- Increasing the salinity jump, ΔS, resulted in an initial rapid increase in freezing rate followed by a very gradual increase converging toward the maximum freezing rate expected for a given surface heat flux.
- Increasing the mixed layer depth, h, resulted in an initial rapid increase in freezing rate followed by a very gradual increase converging toward a point less than the maximum freezing rate that would be expected for a given surface heat flux.

Non-dimensional ratios formed from the initial and boundary conditions were derived. A non-dimensional parameter, F^*, is a ratio of the wind stress forcing of the mixed layer of depth h to the surface buoyancy flux., A parameter, S^*, is a ratio of the buoyancy due to the temperature jump to the buoyancy due to the salinty jump, and is a measure of stability. A parameter, E^*, is a ratio of the freezing rate to the maximum freezing rate possible for a given surface heat flux. The results focus on the dependence of E^* upon F^* and S^*.

Model solutions revealed no sensitivity to changes in the model variables constituting the non-dimensional parameters, if the value of the non-dimensional parameters is held constant. This indicates that the model may be completely determined by the non-dimensional parameters in certain domains.

A relationship between the forcing parameter, F^* , and the stability non-dimensinal parameter, S^*, was derived which defined the oceanic domains where freezing could occur and where freezing could not occur.

An analytic solution of the model was derived for the case of freezing conditions. This solution showed the freezing efficiency non-dimensional parameter, E^*, was a function of F^*, S^*, physical constants, and two model constants for entrainment rate. This solution was then displayed and analyzed for significant features, showing:

- The freezing efficiency is highly dependent on the value of S^* , the stability parameter.
- If the stability parameter is large, there can be no freezing.
- If the stability parameter is near zero, there will always be a situation where freezing can occur regardless of the value of the forcing parameter.

B. RECOMMENDATIONS

The model, the results of this study, and the analytic solutions can be valuable in understanding the interactions between the variables comprising mixed layer thermodynamics and dynamics, and their relationship to the freezing process. These results could be used further to study the following:

- The possible cyclic effect of cooling from above and heating from below as studied by Welander (1977).
- The negative feedback effect of the formation of ice on the freezing rate as discussed by Chu and Garwood (1988).
- The freezing rate as the drag coefficient decreases from the values of the open ocean with the initial formation of ice, and then increases with the growth of the ice, based on the results of Guest and Davidson (1991).

APPENDIX A. THE LIMIT OF FREEZING

The transition region between freezing and not freezing will be investigated. In this regime, the mixed layer temperature is at the freezing temperature but there is no freezing. In this regime, mixed layer temperature cannot change in time. This will separate the regimes where the mixed layer cools with time and where the mixed layer warms with time. For this investigation evaporation, precipitation, melting, and freezing are all assumed zero.

A. THE MODEL EQUATIONS

For the regime of no change of mixed layer temperature with time,

$$\frac{\partial T}{\partial t} = 0$$

the point where freezing rate is zero,

$$F = 0$$

and there is no melting, evaporation, or precipitation, giving

$$E = F = P = M = 0 \tag{A.1}$$

and when the mixed layer is at the freezing temperature,

$$T = T_f$$

the model equations will be investigated for a solution.

For the condition of no change of temperature with time, the temperature flux at the base of the mixed layer and the temperature flux at the top of the mixed layer must be equal.

$$\overline{T'w'}(0) = \overline{T'w'}(-h)$$

From equation (3.10), the thermal flux at the base of the mixed layer is

$$\overline{T'w'}(-h) = -\Delta T\, W_e$$

and from equation (3.7) the thermal flux at the top of the mixed layer is

$$\overline{T'w'}(0) = -\frac{Q_n}{\rho c_p}$$

This gives

$$-\frac{Q_n}{\rho c_p} = -\Delta T\, W_e \tag{A.2}$$

Rearranging equation (A.2) for W_e gives,

$$W_e = \frac{Q_n}{\rho c_p \Delta T} \tag{A.3}$$

Equation (3.14) with equation (A.1) gives

$$W_e = \frac{1}{\Delta b}\left(C_1 \frac{u_*^3}{h} - C_2 \alpha g \frac{Q_n}{\rho c_p}\right) \tag{A.4}$$

Equating equations (A.3) and (A.4) together gives

$$\frac{Q_n}{\rho c_p \Delta T} = \frac{1}{\Delta b}\left(C_1 \frac{u_*^3}{h} - C_2 \alpha g \frac{Q_n}{\rho c_p}\right) \tag{A.5}$$

Equation (A.5) can be manipulated to give

$$\Delta b = \frac{\Delta T \rho c_p}{Q_n}\left(C_1 \frac{u_*^3}{h} - C_2 \alpha g \frac{Q_n}{\rho c_p}\right)$$

or

$$\Delta b = \Delta T\left[C_1\left[\frac{u_*^3}{h \frac{Q_n}{\rho c_p}}\right] - C_2 \alpha g\right]$$

or

$$\Delta b = \alpha g \Delta T \left[C_1 \left[\frac{u_*^3}{h \frac{\alpha g Q_n}{\rho c_p}} \right] - C_2 \right] \tag{A.6}$$

From equations (3.9) and (A.1)

$$\overline{b'w'}(0) = - \alpha g \frac{Q_n}{\rho c_p} \tag{A.7}$$

Substituting equation (A.7) into equation (A.6) gives

$$\Delta b = \alpha g \Delta T \left[C_1 \left[\frac{u_*^3}{- h \overline{b'w'}(0)} \right] - C_2 \right] \tag{A.8}$$

Using the definition of F, equation (4.2), equation (A.8) becomes

$$\Delta b = \alpha g \Delta T \left(- C_1 F^* - C_2 \right) \tag{A.9}$$

Using equation (3.13) equation (A.9) becomes

$$\alpha g \Delta T - \beta g \Delta S = \alpha g \Delta T \left(- C_1 F^* - C_2 \right) \tag{A.10}$$

Rearranging equation (A.10)

$$\alpha g \Delta T (1 + C_1 F^* + C_2) = \beta g \Delta S$$

or

$$1 + C_1 F^* + C_2 = \frac{\beta g \Delta S}{\alpha g \Delta t} \tag{A.11}$$

B. THE FREEZING LIMIT SOLUTION

From the definition of S^*, equation (4.3), equation (A.11) can be rewritten

$$1 + C_1 F^* + C_2 = \frac{1}{S^*} \tag{A.12}$$

Solving equation (A.12) for S^*

$$S^* = \frac{1}{1 + C_1 F^* + C_2} \tag{A.13}$$

This gives a relationship of four parameters: the forcing parameter, the stability parameter, and the two model constants. This indicates that the reliability of the model is dependent on realistic model constants.

Equation (A.12) can be solved for F^*

$$F^* = \frac{1}{C_1}\left(\frac{1}{S^*} - (1 + C_2)\right) \tag{A.14}$$

APPENDIX B. AN EXPRESSION FOR THE FREEZING RATE

A. THE CONDITIONS

It may be possible to derive an analytic solution for the freezing rate from the equations used with the model. This solution will be useful for comparing model results with analytic results, but also useful for clarifying relationships between the model variables.

The main purpose for finding an analytic solution would be to find regimes where we would expect freezing or regimes where we would not expect freezing. This has very useful applications in ocean areas where preconditioning may or may not permit rapid freezing to occur. Naval operations may be extended if conditions are not met for freezing when freezing is a limitation to operations, or operations may need to be curtailed early due to forecast conditions which could lead to freezing conditions.

B. ESSENTIAL EQUATIONS

The basic equations which will be needed are the equation defining freezing rate, entrainment velocity, and the equations defining the non-dimensional parameters. Equations (3.18) and (3.14) will be used.

C. THE DERIVATION

From equation (3.18), F, the Freezing Rate, is defined as

$$F = \left[- \frac{Q_n}{\rho c_p} + \Delta T W_e \right] \frac{c_p}{L_f}$$

From equation (3.14), W_e, the Entrainment Velocity, is defined as

$$W_e = \frac{1}{\Delta b}\left[C_1 \frac{u_*^3}{h} - C_2\left[\alpha g \frac{Q_n}{\rho c_p} - \beta g F(S - S_i)\right]\right]$$

Substituting equation (3.14) into (3.18) for W_e gives

$$F = \left[-\frac{Q_n}{\rho c_p} + \Delta T\left[\frac{1}{\Delta b}\left[C_1 \frac{u_*^3}{h} - C_2\left[\alpha g \frac{Q_n}{\rho c_p} - \beta g F(S - S_i)\right]\right]\right]\right]\frac{C_p}{L_f} \quad \text{(B.1)}$$

or

$$F = -\frac{Q_n}{\rho L_f} + C_1 \frac{\Delta T}{\Delta b}\frac{u_*^3}{h}\frac{c_p}{L_f} - C_2 \alpha g \frac{\Delta T}{\Delta b}\frac{Q_n}{\rho L_f} + C_2 \beta g F(S - S_i)\frac{\Delta T}{\Delta b}\frac{c_p}{L_f}$$

Collecting terms gives

$$F\left[1 - C_2 \beta g (S - S_i)\frac{\Delta T}{\Delta b}\frac{c_p}{L_f}\right] = -\frac{Q_n}{\rho L_f}\left[1 + C_2 \alpha g \frac{\Delta T}{\Delta b}\right] + C_1 \frac{c_p}{L_f}\frac{\Delta T}{\Delta b}\frac{u_*^3}{h} \quad \text{(B.2)}$$

From equation (3.13) and (4.3)

$$\frac{\Delta b}{\Delta T} = \frac{\alpha g \Delta T - \beta g \Delta S}{\Delta T}$$

or

$$\frac{\Delta b}{\Delta T} = \alpha g\left[1 - \frac{1}{S^*}\right] \quad \text{(B.3)}$$

Multiplying both sides of equation (B.2) by (B.3) gives

$$F\left[\alpha g\left[\frac{S^* - 1}{S_*}\right] - C_2 \beta g (S - S_i)\frac{c_p}{L_f}\right] = -\frac{Q_n}{\rho L_f}\left[\alpha g\left[\frac{S^* - 1}{S_*}\right] + C_2 \alpha g\right] + C_1 \frac{c_p}{L_f}\frac{u_*^3}{h} \quad \text{(B.4)}$$

or

$$F\left[\left[\frac{S^{*}-1}{S_{*}}\right]-C_{2}\frac{\beta}{\alpha}(S-S_{l})\frac{c_{p}}{L_{f}}\right]=\frac{-Q_{n}}{\rho L_{f}}\left[\frac{S^{*}-1}{S_{*}}+C_{2}\right]+C_{1}\frac{c_{p}}{L_{f}\alpha g}\frac{u_{*}^{3}}{h} \quad \text{(B.5)}$$

Finally

$$F=\left[\frac{-\frac{Q_{n}}{\rho L_{f}}\left[\frac{S^{*}-1}{S_{*}}+C_{2}\right]+C_{1}\frac{c_{p}}{L_{f}\alpha g}\frac{u_{*}^{3}}{h}}{\left[\frac{S^{*}-1}{S_{*}}\right]-C_{2}\frac{\beta}{\alpha}(S-S_{l})\frac{c_{p}}{L_{f}}}\right] \quad \text{(B.6)}$$

D. POINTS OF INTEREST

From equation (B.6), as $S^{*}\Rightarrow 0$ then

$$F\Rightarrow -\frac{Q_{n}}{\rho L_{f}}$$

or from equation (4.1)

$$E^{*}\Rightarrow 1$$

For $F = 0$

$$\frac{Q_{n}}{\rho L_{f}}\left(\frac{S^{*}-1}{S_{*}}+C_{2}\right)=C_{1}\frac{c_{p}}{L_{f}\alpha g}\frac{u_{*}^{3}}{h}$$

or

$$\left(\frac{S^{*}-1}{S_{*}}+C_{2}\right)=C_{1}\frac{\frac{u_{*}^{3}}{h}}{L_{f}\frac{\alpha g}{c_{p}}\frac{Q_{n}}{\rho L_{f}}} \quad \text{(B.7)}$$

From equation (3.9), when $F = 0$, then

$$\overline{b'w'}(0) = - \alpha g \frac{Q_n}{\rho c_p} \tag{B.8}$$

Substituting (B.8) into equation (4.2) gives

$$F^* = \frac{u_*^3}{\alpha g \frac{Q_n}{\rho c_p}} \tag{B.9}$$

Substituting equation (B.9) into (B.7) gives

$$\left(\frac{S^* - 1}{S_*} + C_2 \right) = C_1 (- F^*) \tag{B.10}$$

Solving for S^* gives

$$S^* = \left(\frac{1}{1 + C_2 + C_1 F^*} \right) \tag{B.11}$$

This is the same result as equation (A.13), the distinction between regimes of freezing and not freezing.

APPENDIX C. AN EXPRESSION FOR U*

A. BEGINNING EQUATIONS

An expression for u_*^3 can be obtained from the model equations and from the expression of F. From equation (4.2)

$$F^* = \frac{u_*^3}{h\overline{b'w'}(0)}$$

From equation (3.9)

$$\overline{b'w'}(0) = -\alpha g \frac{Q_n}{\rho c_p} + \beta g F(S - S_i)$$

From equation (B.6)

$$F = \left[\frac{-\frac{Q_n}{\rho L_f}\left[\frac{S^* - 1}{S_*} + C_2\right] + C_1 \frac{c_p}{L_f \alpha g} \frac{u_*^3}{h}}{\left[\frac{S^* - 1}{S_*}\right] - C_2 \frac{\beta}{\alpha}(S - S_i)\frac{c_p}{L_f}} \right]$$

B. THE DERIVATION

Equation (4.2) can be rewritten

$$F^* \overline{b'w'}(0) = \frac{u_*^3}{h}$$

and substituting equations (3.9) and (B.6) in gives

$$F^*\left[-\alpha g\frac{Q_n}{h} + \beta g(S-S_i)\left[\frac{-\frac{Q_n}{\rho L_f}\left(\frac{S^*-1}{S^*}+C_2\right)+C_1\frac{c_p}{\alpha g L_f}\frac{u_*^3}{h}}{\frac{S^*-1}{S^*}-C_2\frac{\beta}{\alpha}\frac{c_p}{L_f}(S-S_i)} \right]\right]=\frac{u_*^3}{h}$$

Multiplying both sides by the denominator gives

$$F^*\left[-\alpha g\frac{Q_n}{\rho c_p}\left(\frac{S^*-1}{S^*}-C_2\frac{\beta}{\alpha}\frac{c_p}{L_f}(S-S_i)\right)\right]$$

$$+F^*\left[\beta g(S-S_i)\left[-\frac{Q_n}{\rho L_f}\left(\frac{S^*-1}{S^*}+C_2\right)+C_1\frac{c_p}{\alpha g L_f}\frac{u_*^3}{h}\right]\right] \qquad \text{(C.1)}$$

$$=\frac{u_*^3}{h}\left(\frac{S^*-1}{S^*}-C_2\frac{\beta}{\alpha}\frac{c_p}{L_f}(S-S_i)\right)$$

or

$$F^*\left[-\alpha g\frac{Q_n}{\rho c_p}\frac{S^*-1}{S^*}+C_2\beta g\frac{Q_n}{\rho L_f}(S-S_i)\right]$$

$$+F^*\left[\beta g(S-S_i)\frac{-Q_n}{\rho L_f}\left(\frac{S^*-1}{S^*}+C_2\right)+C_1\frac{\beta}{\alpha}\frac{c_p}{L_f}\frac{u_*^3}{h}(S-S_i)\right]$$

$$=\frac{u_*^3}{h}\frac{S^*-1}{S^*}-C_2\frac{\beta}{\alpha}\frac{c_p}{L_f}(S-S_i)\frac{u_*^3}{h}$$

Gathering terms

$$\frac{u_*^3}{h}\left[C_1\frac{\beta}{\alpha}\frac{c_p}{L_f}F^*(S-S_i) + C_2\frac{\beta}{\alpha}\frac{c_p}{L_f}(S-S_i) - \frac{S^*-1}{S^*}\right] =$$

$$\frac{Q_n}{\rho L_f}\left[\alpha g F^*\frac{L_f}{c_p}\frac{S^*-1}{S^*} - C_2F^*\beta g(S-S_i) + \beta g(S-S_i)F^*\left(\frac{S^*-1}{S^*}+C_2\right)\right]$$

or

$$\frac{u_*^3}{h}\left[\frac{\beta}{\alpha}\frac{c_p}{L_f}(C_1F^* + C_2)(S-S_i) - \frac{S^*-1}{S^*}\right]$$

$$= \frac{Q_n}{\rho L_f}F^*g\left[\frac{S^*-1}{S^*}\left(\alpha\frac{L_f}{c_p} + \beta(S-S_i)\right)\right]$$

Isolating $\frac{u_*^3}{h}$ yields

$$\frac{u_*^3}{h} = \frac{Q_n}{\rho L_f}F^*g\left[\frac{\frac{S^*-1}{S^*}\left(\alpha\frac{L_f}{c_p} + \beta(S-S_i)\right)}{\frac{c_p}{L_f}\frac{\beta}{\alpha}(S-S_i)(C_1F^* + C_2) - \frac{S^*-1}{S^*}}\right] \qquad \text{(C.2)}$$

C. POINTS OF INTEREST

From equation (C.2) some points can be drawn. First, when $S^* \Rightarrow 0$ then

$$\frac{u_*^3}{h} = -\frac{Q_n}{\rho L_f}F^*g\left[\alpha\frac{L_f}{c_p} + \beta(S-S_i)\right]$$

This means that when the mixed layer has no temperature jump between it and the mixed layer, i.e. $\Delta T = 0$, then the freezing rate is only a function of the thermal heat flux out of the mixed layer. The reduction of TKE is accomplished only thru the entrainment of more dense saline deep water.

When $S^{*} \Rightarrow 1$, $\frac{u^3}{h} \Rightarrow 0$ or $h \Rightarrow \infty$ This means that any buoyancy flux at the surface cannot be countered by a buoyancy flux at the bottom of the mixed layer and the subsequent condition would be an over turning of the water column.

APPENDIX D. FREEZING EFFICIENCY

A. THE EQUATIONS

A expression for E will be derived from equations (B.6) and (C.2). The resulting expression will be a function of the model constants, the salinity, and the non-dimensional parameters F^* and S^*. This will allow an analysis of the possible maximum freezing rate possible for any initial conditions and any boundary conditions.

B. DERIVATION

Equation (C.6) gives the expression for F as

$$F = \left[\frac{ - \frac{Q_n}{\rho L_f} \left[\frac{S^* - 1}{S_*} + C_2 \right] + C_1 \frac{c_p}{L_f \alpha g} \frac{u_*^3}{h} }{ \left[\frac{S^* - 1}{S_*} \right] - C_2 \frac{\beta}{\alpha} (S - S_i) \frac{c_p}{L_f} } \right]$$

or

$$F = \left[\frac{ - \frac{Q_n}{\rho L_f} \left(S^* - 1 + C_2 S^* \right) + C_1 \frac{c_p}{L_f \alpha g} S^* \frac{u_*^3}{h} }{ S^* - 1 - C_2 \frac{\beta}{\alpha} (S - S_i) S^* \frac{c_p}{L_f} } \right] \qquad \text{(D.1)}$$

Equation (C.2) gives the expression for $\frac{u_*^3}{h}$ as

$$\frac{u_*^3}{h} = \frac{Q_n}{\rho L_f} F^* g \left[\frac{ \frac{S^* - 1}{S^*} \left(\alpha \frac{L_f}{c_p} + \beta (S - S_i) \right) }{ \frac{c_p}{L_f} \frac{\beta}{\alpha} (S - S_i)(C_1 F^* + C_2) - \frac{S^* - 1}{S^*} } \right]$$

or

$$\frac{u_*^3}{h} = \frac{Q_n}{\rho L_f} F^* g \left[\frac{(S^* - 1)\left(\alpha \frac{L_f}{c_p} + \beta(S - S_i)\right)}{\frac{c_p}{L_f}\frac{\beta}{\alpha}(S - S_i)S^*(C_1F^* + C_2) - S^* + 1} \right] \tag{D.2}$$

To simplify the writing of the equations, let

$$L = \frac{c_p}{\alpha L_f}$$

and

$$B = \beta(S - S_i)$$

Equation (D.1) becomes

$$F = \left[\frac{-\frac{Q_n}{\rho L_f}\left(S^*(1 + C_2) - 1\right) + C_1 \frac{L}{g} S^* \frac{u_*^3}{h}}{S^* - 1 - C_2 L B S^*} \right] \tag{D.3}$$

Equation (D.2) becomes

$$\frac{u_*^3}{h} = \frac{Q_n}{\rho L_f} F^* g \left[\frac{(S^* - 1)\left(\frac{1}{L} + B\right)}{LBS^*(C_1F^* + C_2) - S^* - 1} \right] \tag{D.4}$$

Substituting equation (D.4) into (D.3) gives

$$F = \frac{-\frac{Q_n}{\rho L_f}(S^*(1 + C_2) - 1) + C_1 \frac{L}{g} S^* \frac{Q_n}{\rho L_f} F^* g \left[\frac{(S^* - 1)(\frac{1}{L} + B)}{S^*(LBC_1F^* + C_2 - 1) + 1} \right]}{S^*(1 - C_2LB) - 1}$$

or

$$\frac{\frac{F}{-Q_n}}{\rho L_f} = \frac{(S^*(1+C_2)-1) - C_1 S^* F^* \left[\frac{(S^*-1)(1+LB)}{S^*(LB(C_1F^*+C_2)-1)+1} \right]}{S^*(1-C_2 LB)-1} \quad \text{(D.5)}$$

From equation (4.1)

$$E^* = \frac{\frac{F}{-Q_n}}{\rho L_f}$$

Equation (D.5) can be written

$$E^* = \frac{(S^*(1+C_2)-1) - C_1 S^* F^* \left[\frac{(S^*-1)(1+LB)}{S^*(LB(C_1F^*+C_2)-1)+1} \right]}{S^*(1-C_2 LB)-1}$$

or

$$E^* = \frac{(S^*(1+C_2)-1)(S^*(LB(C_1F^*+C_2)-1)+1) - C_1 S^* F^* (S^*-1)(1+LB)}{(S^*(1-C_2 LB)-1)(S^*(LB(C_1F^*+C_2)-1)+1)}$$

or

$$E^* = \frac{S^{*2}(1+C_2)(LB(C_1F^*+C_2)-1) + S^*((1+C_2)-(LB(C_1F^*+C_2)-1))-1}{S^{*2}((1-C_2LB)(LB(C_1F^*+C_2)-1)) + S^*((1-C_2LB)-(LB(C_1F^*+C_2)-1))-1} \quad \text{(D.6)}$$

$$- \frac{C_1 S^* F^* (S^*(1+LB)-(1+LB))}{S^{*2}((1-C_2LB)(LB(C_1F^*+C_2)-1)) + S^*((1-C_2LB)-(LB(C_1F^*+C_2)-1))-1}$$

Finally, equation (D.6) can be written

$$E^* = \frac{S^{*2}\left(F^*(C_1C_2LB - C_1) + (1 + C_2)(C_2LB - 1)\right) + S^*(F^*C_1 + 2 + C_2 - C_2LB) - 1}{S^{*2}\left((1 - C_2LB)(F^*C_1LB + C_2LB - 1)\right) + S^*(2 - C_1LBF^* - 2C_2LB) - 1} \quad \text{(D.7)}$$

where

- $E^* = \dfrac{\rho L_f F}{-Q_n}$
- $F^* = \dfrac{u^2}{h\overline{b'w'}(0)}$
- $S^* = \dfrac{\alpha g \Delta T}{\beta g \Delta S}$
- $L = \dfrac{c_p}{\alpha L_f}$
- $B = \beta(S - S_i)$
- C_1 and C_2 are model constants

REFERENCES

Aagaard, K., and E. C. Carmack, 1989: The role of sea ice and other fresh water in the Arctic circulation. *J. Geophys. Res.*, 94, 14485-14498.

Andreas, E. L., 1980: Estimation of heat and mass fluxes over Arctic leads. *Mon Wea. Rev.*, 108, 2057-2063.

Bauer, J., and S. Martin, 1983: A model Of grease ice growth in small leads. *J. Geophys. Res.*, 89, 735-744.

Carmack, E., and K. Aagaard, 1973: On the deep water of the Greenland Sea. *Deep-Sea Res.*, 20, 687-715.

Chu, P. C., 1986: An air-ice-ocean coupled model for the formation of leads and polynyas. *Mizex Bulletin*, 7, 79-88.

Chu, P. C., 1987: An instability theory of ice-air interactions for the formation of ice edge bands. *J. Geophys. Res.*, 92, 6966-6970.

Chu, P. C., and R. W. Garwood, 1988: Comment on "A coupled dynamic-thermodynamic model of an ice-ocean system in the marginal ice zone" by Sirpa Hakkinen. *J. Geophys. Res.*, 93, 5155-5156.

Colony, R., and A. S. Thorndike, 1984: An estimate of the mean field of arctic sea ice motion. *J. Geophys. Res.*, 89, 10623-10629.

Colony, R., and A. S. Thorndike, 1985: Sea ice as a drunkard's walk. *J. Geophys. Res.*, 90, 965-974.

Eckert, E. G., and T. D. Foster, 1990: Upper ocean internal waves in the marginal ice zone of the northeast Greenland Sea. *J. Geophys. Res.*, 95, 9569-9574.

Foster, T. D., and E. G. Eckert, 1987: Fine structure, internal waves, and intrusions in the marginal ice zone of the Greenland Sea. *J. Geophys. Res.*, 92, 6903-6910.

Garwood, R. W., 1977: An oceanic mixed layer model capable of simulating cyclic states. *J. Phys. Oceanogr.*, 7, 455-468.

Garwood, R. W., 1987: OC4413 Air-Sea Interaction course notes, Sep to Dec, 1987. Naval Postgraduate School, Monterey, CA.

Gow, A. J., D. A. Meese, D. K. Perovich, and W. B. Tucker, 1990: The anatomy of a freezing lead. *J. Geophys. Res.*, 95, 18221-18232.

Grenfell, T. C., and D. K. Perovich, 1984: Spectral albedos of sea ice and incident solar irradiance in the southern Beaufort Sea. *J. Geophys. Res.*, 89, 3573-3580.

Guest, P. S., and K. L. Davidson, 1987: The effect of observed ice conditions on the drag coefficient in the summer East Greenland Sea marginal ice zone. *J. Geophys. Res.*, 92, 6943-6954.

Guest, P. S., and K. L. Davidson, 1991: The aerodynamic roughness of different types of sea ice. Accepted by *J. Geophys. Res.*.

Hakkinen, S., 1986: Coupled ice-ocean dynamics in the marginal ice zones: Upwelling/downwelling and eddy generation. *J. Geophys. Res.*, 91, 819-832.

Hakkinen, S., 1987: Upwelling at the ice edge: A mechanism for deep water Formation? *J. Geophys. Res.*, 92, 5031-5034.

Hakkinen, S., 1987: A coupled dynamic-thermodynamic model of an ice-ocean system in the marginal ice zone. *J. Geophys. Res.*, 92, 9469-9478.

Hakkinen, S., and G. L. Mellor, 1990: One hundred years of Arctic ice cover variations as simulated by a one-dimensional, ice-ocean model. *J. Geophys. Res.*, 95, 15959-15969.

Hanley, T. O., 1978: Frazil nucleation mechanisms. *J. Glaciol.*, 21, 581-587.

den Hartog, G., S. D. Smith, R. J. Anderson, D. R. Topham, R. G. Perkin, 1983: An investigation of a polynya in the Canadian Archipelago, 3, Surface heat flux. *J. Geophys. Res.*, 88, 2911-2916.

Hibler, W. D., and J. E. Walsh, 1982: On modeling seasonal and interannual fluctuations of Arctic sea ice. *J. Phys. Oceanogr.*, 12, 1514-1523.

Houssais, M.-N., 1988: Testing a coupled ice-mixed-layer model under subarctic conditions. *J. Phys. Oceanogr.*, 18, 196-210.

Ikeda, M., 1986: A mixed layer beneath melting sea ice in the marginal ice zone using a one-dimensional turbulent closure model. *J. Geophys. Res.*, 91, 5054-5060.

Ikeda, M., 1989: A coupled ice-ocean mixed layer model of the marginal ice zone responding to wind forcing. *J. Geophys. Res.*, 94, 9699-9709.

Ingram, W. J., C. A. Wilson, J. F. B. Mitchell, 1989: Modeling climate change: An assessment of sea ice and surface albedo feedbacks. *J. Geophys. Res.*, 94, 8609-8622.

Jessen, P. F., S. R. Ramp, C. A. Clark, 1989: Hydrographic data from the pilot study of the Coastal Transition Zone (CTZ) Program 15-28 June 1987. Report NPS-68-89-004, Naval Postgraduate School, Monterey, CA, 1-245.

Johannessen, J. A., O. M. Johannessen, E. Svendsen, R. Shuchman, T. Manley, W. J. Campbell, E. G. Josberger, S. Sandven, J. C. Gascard, T. Olaussen, K. Davidson, J. Van Lear, 1987: Mesoscale eddies in the Fram Strait marginal ice zone during the 1983 and 1984 marginal ice zone experiments. *J. Geophys. Res.*, 92, 6754-6772.

Kantha, L. H., and G. L. Mellor, 1989: A two-dimensional coupled ice-ocean model of the Bering Sea marginal ice zone. *J. Geophys. Res.*, 94, 10921-10935.

Killworth, P. D., 1979: On "chimney" formations in the ocean. *J. Phys. Oceanogr.*, 9, 531-554.

Kozo, T. L., 1983: Initial model results for arctic mixed layer circulation under a refreezing lead. *J. Geophys. Res.*, 88, 2926-2934.

Kraus, E. B., and J. S. Turner, 1967: A one-dimensional model of the seasonal thermocline. *Tellus*, 19, 98-105.

Lagerloef, G. E., and R. D. Muench, 1987: Near-inertial current oscillations in the vicinity of the Bering Sea marginal ice zone. *J. Geophys. Res.*, 92, 11789-11802.

Lepparanta, M., and W. D. Hibler, 1985: The role of plastic ice interaction in marginal ice zone dynamics. *J. Geophys. Res.*, 90, 11899-11909.

Levine, M. D., C. A. Paulson, J. H. Morison, 1987: Observations of internal gravity waves under th arctic pack ice. *J. Geophys. Res.*, 92, 779-782.

Lewis, E. L., and R. G. Perkin, 1983: Supercooling and energy exchange in a turbulent Ekman layer. *J. Geophys. Res.*, 89, 735-744.

Lu, Q., J. Larsen, and P. Tryde, 1989: On the role of ice interaction due to floe collisions in marginal ice zone dynamics. *J. Geophys. Res.*, 94, 14525-14537.

Lu, Q., J. Larsen, and P. Tryde, 1990: A dynamic and thermodynamic sea ice model for subpolar regions. *J. Geophys. Res.*, 95, 13433-13457.

Macklin, S. A., 1983: Wind drag coefficinet over first-year sea ice in the Bering Sea. *J. Geophys. Res.*, 88, 2845-2852.

Manley. T. O., and K. Hunkins, 1985: Mesoscale eddies of the Arctic Ocean. *J. Geophys. Res.*, 90, 4911-4930.

Martin, S., and P. Kauffman, 1981: A field and laboratory study of wave damping by grease ice. *J. Glaciol.*, 96, 283-313.

Martin, S., P. Kauffman, and C. Parkinson, 1983: The movement and decay of ice bands in the winter Bering Sea. *J. Geophys. res.*, 88, 2803-2812.

Martin, S., and P. Becker, 1987: High-frequency ice floe collisions in the Greenland Sea during the 1984 marginal ice zone experiment. *J. Geophys. Res.*, 92, 7071-7084.

Martin, S., and P. Becker, 1988: Ice floe collisions and their relation to ice deformation in the Bering Sea during February 1983. *J. Geophys. Res.*, 93, 1303-1315.

Maykut, G. A., 1986: The surface heat and mass balance. *The Geophysics of Sea Ice*, N. Untersteiner, Ed., Plenum Press, 395-463.

Maykut, G. A., and P. E. Church, 1973: Radiation climate of Barrow, Alaska, 1962-1966. *J. Appl. Met.*, 12, 620-628.

McPhee, M. G., 1978: A simulation of inertial oscillation in drifting pack ice. *Dyn. Atmos. Oceans*, 2, 107-122.

McPhee, M. G., 1983: Turbulent heat and momentum transfer in the oceanic boundary layer under melting pack ice. *J. Geophys. Res.*, 88, 2827-2835.

McPhee, M. G., 1987: A time-dependent model for turbulent transfer in a stratified oceanic boundary layer. *J. Geophys. Res.*, 92, 6977-6986.

McPhee, M. G, and L. H. Kantha, 1989: Generation of internal waves by sea ice. *J. Geophys. Res.*, 94, 3287-3302.

McPhee, M. G., G. A. Maykut, J. H. Morison, 1987: Dynamics and thermodynamics of the ice/upper ocean system in the marginal ice zone of the Greenland Sea. *J. Geophys. Res.*, 92, 7017-7031.

Mellor, G. L., M. G. McPhee, and M. Steele, 1986: Ice-seawater turbulent boundary layer interaction with melting or freezing. *J. Phys. Oceanogr.*, 16, 1829-1846.

Mellor, G. L., and L. H. Kantha, 1989: An ice-ocean coupled model. *J. Geophys. Res.*, 94, 10937-10954.

Mollo-Christensen, E., 1983: Interactions between waves and mean drift in an ice pack. *J. Geophys. Res.*, 88, 2971-2972.

Morison, J. H., C. E. Long, M. D. Levine, 1985: Internal wave dissipation under sea ice. *J. Geophys. Res.*, 90, 11959-11966.

Muench, R. D., P. H. LeBlond, L. E. Hachameister, 1983: On some possible interactions between internal waves and sea ice in the marginal ice zone. *J. Geophys. Res.*, 88, 2819-2826.

Nakamura, N., and A. H. Oort, 1988: Atmospheric heat budgets of the polar regions. *J. Geophys. Res.*, 93, 9510-9524.

Niebauer, H. J., 1983: Multiyear sea ice variability in the eastern Bering Sea: an update. *J. Geophys. Res.*, 88, 2733-2742.

Niiler, P. P., and E. B. Kraus, 1977: One-dimensional models of the upper ocean. *Modeling and Prediction of the Upper Layers of the Ocean*, E. B. Kraus, Ed., Pergamon Press, 143-172.

Omstedt, A., and U. Svensson, 1984: Modeling supercooling and ice formation in a turbulent Ekman layer. *J. Geophys. Res.*, 89, 735-744.

Overland, J. E., 1985: Atmospheric boundary layer structure and drag coefficients over sea ice. *J. Geophys. Res.*, 90, 9029-9049.

Padman, L., M. Levine, T. Dillon, J. Morison, and R. Pinkel, 1990: Hydrography and microstructure of an Arctic cyclonic eddy. *J. Geophys. Res.*, 95, 9411-9420.

Pease, C. H., S. A. Salo, J. E. Overland, 1983: Drag measurements for first-year sea ice over a shallow sea. *J. Geophys Res.*, 88, 2853-2862.

Pollard, D., M. L. Batteen, and Y.-J. Han, 1983: Development of a simple upper-ocean and sea-ice model. *J. Phys. Oceanogr.*, 13, 754-768.

Roed, L. P., 1984: A thermodynamic coupled ice-ocean model of the marginal ice zone. *J. Phys. Oceanogr.*, 14, 1921-1929.

Ross, B., and J. E. Walsh, 1987: A comparison of simulated and observed fluctuations in summertime arctic surface albedo. *J. Geophys. Res.*, 92, 13115-13125.

Sandven, S., C. Geiger, J. A. Johannessen, O. M. Johannessen, 1987: Technical Report No. 3, CTD data report from HAKON MOSBY during winter MIZEX March-April 1987, Nansen Remote Sensing Center, Solheimsvick, Norway.

Sandven, S., and O. M. Johannessen, 1987: High-frequency internal wave observations in the marginal ice zone. *J. Geophys. Res.*, 92, 6911-6920.

Sater, J. E., A. G. Ronhoude, L. C. Van Allen, 1971: Arctic Environment and Resources. The Arctic Institute of North America, Washington D. C., 1-310.

Schmitt, R. W., 1981. Form of the temperature-salinity relationship in the central water: Evidence for double-diffusive mixing. *J. Phys. Oceanogr.*, 11, 1015-1026.

Schmitt, R. W., 1987. The Caribbean Sheets and Layers Transects (C-SALT) Program. *EOS, Trans. Amer. Geophys. Union*, 68, 57-60.

Schmitt, R. W., 1988. Mixing in a thermohaline staircase. *Small-Scale Turbulence and Mixing in the Ocean*, Nihoul and Jamart Eds., Elsevier Science Publishers, Netherlands, 435-452.

Semtner, A. J., 1987: A numerical study of sea ice and ocean circulation in the Arctic. *J. Phys. Oceanogr.*, 17, 1077-1099.

Serreze, M. C., R. G. Barry, and A. S. McLaren, 1989: Seasonal variations in sea ice motion and effects on sea ice concentration in the Canada Basin. *J. Geophys Res.*, 94, 10955-10970.

Shen, H. H., W. D. Hibler, and M. Lepparanta, 1987: The role of floe collisions in sea ice rheology. *J. Geophys. Res.*, 92, 7085-7096.

Smedstad, O. M., and L. P. Roed, 1985: A coupled ice-ocean model of ice breakup and banding in the marginal ice zone. *J. Geophys. Res.*, 90, 876-882.

Smith, D. C., A. A. Bird, and W. P. Budgell, 1988: A numerical study of mesoscale ocean eddy interaction with a marginal ice zone. *J. Geophys. Res.*, 93, 12461-12473.

Smith, S. D., R. J. Anderson, G. den Hartog, D. R. Topham, and R. G. Perkin, 1983: An investigation of a polynya in the Canadian Archipelago, 2, Structure of turbulence and sensible heat. *J. Geophys. Res.*, 88, 2900-2910.

Squire, V. A., 1984: A theoretical, laboratory, and field study of ice-coupled waves. *J. Geophys. Res.*, 89, 8069-8079.

Swift, J. H., and K. Aagaard, 1981: Seasonal transitions and water mass formation in the Iceland and Greenland seas. *Deep-Sea Res.*, 28A, 1107-1129.

Swift, J. H., and K. P. Koltermann, 1988: The origin of Norwegian Sea deep water. *J. Geophys. Res.*, 93, 3563-3569.

Thorndike, A. S., 1987: A random discontinuous model of sea ice motion. *J Geophys. Res.*, 92, 6515-6520.

Thorndike, A. S., and R. Colony, 1982: Sea ice motion in response to geostrophic winds. *J. Geophys. Res.*, 87, 5845-5852.

Thompson, N. R., J. F. Sykes, R. F. McKenna, 1988: Short-term ice motion modeling with application to the Beaufort Sea. *J. Geophys. Res.*, 93, 6819-6836.

Topham, D. R., R. G. Perkin, S. D. Smith, R. J. Anderson, and G. den Hartog, 1983: An investigation of a polynya in the Canadian Archipelago, 1, Introduction and Oceanography. *J. Geophys. Res.*, 88, 2888-2899.

Wadhams, P., 1983: A mechanism for the formation of ice edge bands. *J. Geophys. Res.*, 88, 2813-2818.

Wadhams, P., V. A. Squire, D. J. Goodman, A. M. Cowan, S. C. Moore, 1988: The attenuation rates of ocean waves in the marginal ice zone. *J . Geophys. Res.*, 93, 6799-6818.

Wakatsuchi, M., and N. Ono, 1983: Measurements of salinity and volume of brine excluded from growing sea ice. *J. Geophys. Res.*, 88, 2943-2951.

Walter, B. A., J. E. Overland, R. O. Gilmer, 1984: Air ice drag coefficients for first-year sea ice derived from aircraft measurements. *J. Geophys. Res.*, 89, 3550-3560.

Washington, W. M., A. J. Semtner, G. A. Meehl, D. J. Knight, and T. A Mayer, 1980: A general circulation experiment with a coupled atmosphere, ocean and sea ice model. *J. Phys. Oceanogr.*, 10, 1887-1908.

Welander, P., 1977: Thermal oscillations in a fluid heated from below and cooled to freezing above. *Dyn. Atmos. Oceans*, 1, 215-223.

INITIAL DISTRIBUTION LIST

		No. Copies
1.	Defense Technical Information Center Cameron Station Alexandria, VA 22304-6145	2
2.	Library, Code 52 Naval Postgraduate School Monterey, CA 93943-5002	2
3.	Chairman (Code OC/Co) Department of Oceanography Naval Postgraduate School Monterey, CA 93943-5000	1
4.	Chairman (Code MR/Hy) Department of Meteorology Naval Postgraduate School Monterey, CA 93943-5000	1
5.	Prof. R. W. Garwood (Code OC/Gd) Department of Oceanography Naval Postgraduate School Monterey, CA 93943-5000	2
6.	Prof. K. L. Davidson (Code MR/Da) Department of Meteorology Naval Postgraduate School Monterey, CA 93943-5000	1
7.	LCDR D. C. Claes, USN, Fleet Numerical Oceanography Center Monterey, CA 93943-5005	1
8.	Director Naval Oceanography Division Naval Observatory 34th and Massachusetts Avenue NW Washington, DC 20390	1
9.	Commanding Officer Naval Oceanographic Office Stennis Space Center, MS 39522-5001	1

10. Commanding Officer 1
Fleet Numerical Oceanography Center
Monterey, CA 93943-5005

11. Commanding Officer 1
Naval Oceanographic and Atmospheric
Research Laboratory
Stennis Space Center, MS 39529-5004

12. Commanding Officer 1
Naval Polar Oceanography Center, Suitland
Washington, DC 20373